UNIVERSITY OF OKLAHOMA

GRADUATE COLLEGE

SYNOPTIC AND MESOSCALE ANALYSIS OF THE 2015 SOUTHERN GREAT PLAINS FLASH PLUVIAL

A THESIS

SUBMITTED TO THE GRADUATE FACULTY

in partial fulfillment of the requirements for the

Degree of

MASTER OF SCIENCE IN METEOROLOGY

By

SARAH JEAN WUGOFSKI
Norman, Oklahoma
2019

SYNOPTIC AND MESOSCALE ANALYSIS OF THE
2015 SOUTHERN GREAT PLAINS FLASH PLUVIAL

A THESIS APPROVED FOR THE
SCHOOL OF METEOROLOGY

BY

Dr. Jeffrey B. Basara, Chair

Dr. Elinor R. Martin

Dr. Cameron Homeyer

Acknowledgments

I would like to thank all those who helped in the development of this thesis, in particular my advisor Jeff Basara for his assistance and guidance in developing this project. I would also like to thank my committee, Elinor Martin and Cameron Homeyer, for their guidance and edits. Additionally, thank you to the many amazing professors I have had in my time at both the University of Oklahoma and Florida State University. I would particularly like to thank Jason Furtado for teaching me the joys of statistics and Python.

I would also like to thank my friends and family who supported me throughout my time at the University of Oklahoma. Thank you to my parents for supporting my multiple moves 1000 miles away from home to study meteorology, and my next move another 1000 miles back to the east coast to study at Penn State. I would like to thank my many friends in Norman, including Stephanie Edwards, Ben Davis, Kevin Grempler, Hannah Wells, Sean Ernst, and Andrew Berrington. Having numerous friends in meteorology here and across the country has made enduring graduate much more fun and I cannot imagine it without all of you.

Table of Contents

List of Tables

List of Figures

Abstract

During May and June of 2015, the Southern Great Plains (SGP) of the United States experienced numerous heavy rainfall and flooding events. The immense amount of rainfall (in excess of 80 cm) over a short period had tremendous impacts on the water resources of the region, marked the end of prolonged drought, and culminated into a flash pluvial. Flash pluvials, similar to flash drought, are a short-term period of rapid transition into wetter than average conditions. Flash pluvials are marked by widespread, heavy rainfall within a region. This rainfall can lead to a regional replenishment of water resources and soil moisture, particularly in the case of 2015. The investigation of this case seeks to determine the causation of this anomalous precipitation event.

The goal of this study was to examine the traits and causes of the excessive precipitation over the SGP in May and June of 2015 including synoptic characteristics, the role of moisture transport, and the impact of Tropical Depression Bill. This was accomplished by statistically analyzing the daily precipitation with the most significant precipitation events of the flash pluvial selected for additional analysis. These cases were composited to quantify atmospheric patterns and moisture transport via Atmospheric River (AR) analysis and integrated vapor transport (IVT) to diagnose the source of moisture that led to the extreme precipitation events.

The key results included seeing an above normal number of synoptic wave events, with strong upper level low pressure systems present for the significant precipitation events. This increased wave activity combined with enhanced moisture transport from the Gulf of Mexico was a defining feature of the flash pluvial event. The interaction of the features observed in this analysis are what led to this event being highly significant. Additional features that led to the flash pluvial experiencing extreme precipitation include frequently linear storm mode and high precipitation efficiency, leading to record-breaking precipitation across the SGP. The interaction of these features at varying time scales contributed to

the SGP experiencing extreme precipitation, and by examining these features we can better understand the causation of flash pluvials and other extreme precipitation events.

Chapter 1

Introduction

During May and June of 2015, the Southern Great Plains (SGP) of the United States (Oklahoma and Texas) experienced numerous heavy rainfall events which produced in excess of 80 cm of precipitation in localized areas and widespread totals in excess of 50 cm. The excessive precipitation over a short period had tremendous impacts on the water resources of the region and marked the end of prolonged drought.

A majority of past literature on anomalously wet periods focuses on either a short time scale (flood events on the order of days) or a long time scale (pluvials on the order of months to years). This study seeks to fill a gap in the literature regarding sub seasonal periods of extreme precipitation by investigating the case study of the spring of 2015. To accomplish this, this study examines the SGP during the anomalously wet months of May and June of 2015, with the goal of identifying patterns associated with sub seasonal extreme precipitation and comparing with past work regarding longer term pluvial patterns. While it is expected to see similar atmospheric patterns and forcing as those identified in previous studies on seasonal and annual pluvials, this work seeks to determine differences in location and magnitude of these features. This study also examines case studies of specific dates within May and June of 2015, with the goal of identifying the most significant events and seeking to explain why certain dates within this event were responsible for larger portions of the extreme precipitation.

1.1 Pluvial Events

The term pluvial is associated with abundant precipitation (AMS Glossary) and is used to describe periods marked by excessive precipitation. Pluvials have been defined in many

ways across the scientific literature by precipitation anomalies, drought/precipitation indices, overall precipitation impacts, or standardized precipitation anomalies. Standardized anomalies can be used to compare the significance of events across different temporal periods and spatial domains. One metric used determine pluvial years is 10% above average annual precipitation (Christian et al. 2015; Flanagan et al. 2018). Alternatively, this can be changed to reflect the size of the spatial domain. Christian et al. (2015) also used 40% above average annual precipitation to describe pluvial months for regions on the spatial scale of the Southern Great Plains (SGP). Additionally, the Palmer Drought Severity Index (PDSI) can also be utilized; Findell and Delworth (2010) used a PDSI value of 2 to indicate pluvial conditions.

Pluvials have also been defined by impacts, largely due to resultant flooding. Many indices have been computed to represent pluvial flooding and associated flooding risk. These include hazard assessment and risk scores which incorporate parameters such as precipitation, runoff, and river levels (Szewrański et al. 2018). The overall intensity of pluvial events is less clearly defined than corresponding stages and metrics often referred to in drought studies. Instead, pluvials can be observed through a wide range of impacts including the refilling of reservoirs and flooding dangers. The recurring precipitation events in a pluvial period also have compounding impacts. For example, events early in the pluvial may fill reservoirs and rivers while later events may cause the same water bodies to overflow their banks and produce flooding.

The interannual variability of spring precipitation has been shown to be increasing for both the Northern and Southern Great Plains (Weaver et al. 2016). A better understanding of the physical processes dictating pluvials and floods is needed to enhance the understanding and to facilitate attempts at improving their predictability. In light of the changing climate, it is important to know how processes and teleconnections are changing and the impact they have on pluvials across the SGP (Weaver et al. 2016). Recent investigations into pluvial features and patterns have sought to improve the overall understanding and

predictability of these events via contributing atmospheric features at scales ranging from planetary to synoptic to mesoscale (Schubert et al. 2008; Flanagan et al. 2018).

A large-scale feature often associated with pluvial conditions is warm sea surface temperature (SST) anomalies in the Pacific Ocean (Seager et al. 2005; Schubert et al. 2008). North American climate has been shown to be quite sensitive to variations in SSTs (Findell and Delworth 2010) and numerous studies have investigated the connection between El Niño Southern Oscillation (ENSO) and anomalous precipitation and flooding events (Trenberth and Guillemot 1996; Seager et al. 2005). The dichotomy of pluvial and drought in the Central US has been tied to ENSO, with the floods of 1993 occurring during a mature El Niño and the drought of 1988 occurring during La Niña (Trenberth and Guillemot 1996). Other prior studies investigated a connection between the warming climate and rising sea surface temperatures with the strength of ENSO teleconnections, with the conclusion that warming has led to stronger teleconnections (Meehl and Teng 2007; Stevenson et al. 2011). This change in teleconnection strength is causing a change in the magnitude and location of the impacts to the SGP. As shown in Wang et al. (2015), this leads to increased late Spring precipitation. These results also agree with other studies of ENSO, that have shown Texas as a maximum in precipitation anomalies during the onset of El Niño events (Lee et al. 2014).

Modes of variability including both ENSO and Pacific Decadal Oscillation (PDO) can be associated with patterns that can enhance precipitation in the central US (Krishnamurthy et al. 2015). Research suggests that ENSO can impact the strength of the Great Plains low level jet; a stronger jet can result from La Niña conditions (cool tropical Pacific SSTs) in the spring and El Niño conditions (warm tropical Pacific SSTs) in the summer (Krishnamurthy et al. 2015). These teleconnections between features suggest that many of the synoptic and mesoscale features associated with pluvials in past studies are likely in part due to these climate patterns.

Patterns in zonal wind across the Pacific Ocean are associated with pluvial patterns. Pluvials are often associated with a southward shift of the zonal jet stream (Trenberth and Guillemot 1996; Smith et al. 2013; Weaver et al. 2016). This shift in the jet impacts the passage of synoptic waves, shifting the waveguide equatorward (Flanagan et al. 2018). Further, Rossby wave propagation from the Pacific plays a key role in forcing SGP precipitation events due to enhanced moisture transport, moisture convergence, and increased precipitation anomalies (Zhao et al. 2016).

Winds in the lower troposphere also have an important role in pluvial events, particularly in the Great Plains (Higgins et al. 1997; Ralph et al. 2005; Dong et al. 2011; Wang et al. 2015; Weaver et al. 2016). The Great Plains low-level jet (LLJ) supplies the SGP with warm, moist air from the Gulf of Mexico and is key to enhanced precipitation and pluvials in the United States (Higgins et al. 1997; Dong et al. 2011; Wang et al. 2015; Weaver et al. 2016; Zhao et al. 2016). Further, the interaction of the LLJ with other factors such as moisture convergence has been shown to be impactful during pluvial and flood events (Schubert et al. 2008; Dong et al. 2011; Smith et al. 2013). (Higgins et al. 1997; Ralph et al. 2005; Dong et al. 2011; Wang et al. 2015; Weaver et al. 2016)

Finally, many other large-scale patterns play a role in pluvial events including cut-off lows and blocking patterns that have been observed during extreme precipitation events (Zhao et al. 2016). Additionally, within the SGP cyclones interact with the gulf moisture and LLJ, and as such, wet years see enhanced cyclone activity and dry years see suppressed cyclone activity (Dong et al. 2011). Further, persistent low pressure systems in the southwestern United States can induce instability and lead to precipitation and convective storms (Nieto et al. 2005; Flanagan et al. 2018).

Ultimately, the interwoven of the SST patterns, ENSO, subtropical jet, low level jet, and synoptic disturbances can be associated with Great Plains pluvial events. Identifying these known patterns associated with pluvial events in the 2015 case study will confirm the role of these features in sub seasonal events.

1.2 Flash Pluvial Definition

The definition of flash pluvial is rooted in the definition of flash drought. Flash drought is a term that was utilized to describe the unusually rapid intensification of certain droughts events (Svoboda et al. 2002). More recently, flash drought events were defined by Otkin et al. (2017) as rapid onset drought events lasting multiple weeks. Droughts and pluvials both occur on varied temporal scales from weeks to years, and impact a wide range of spatial domains (Otkin et al. 2017). The temporal and spatial size of these events can dictate the impacts on water resources, agriculture, and society. This variety in events makes defining a flash event more complex, as the significance of an event can be defined based on multiple parameters and impacts. Two major characteristics of flash events are the rate of intensification and the duration, with the prior being emphasized in Otkin et al. (2017) as a characteristic defining feature. As Otkin et al. (2017) established the need to define these events based upon rate of intensification, the defining of flash pluvial should mirror this definition and emphasize the rapid onset of wetter than average conditions. As such, a flash pluvial can be defined as a period of rapid transition into wetter than average conditions at a sub-seasonal time scale. Further, flash pluvial events are a subset of pluvials and can lead to a longer term pluvial or transition back to normal or dry conditions. These flash pluvial events can lead to and enhance flooding on multiple spatial and temporal scales.

An objective definition for flash pluvial can be constructed from previous criteria used to define pluvials. The criteria for defining a pluvial month or year can vary widely between studies. Flanagan et al. (2018) defined a pluvial year such that the calendar-year total precipitation is 10% greater than the climatological annual total precipitation. Findell and Delworth (2010) defined a pluvial month as one with 80% or more above the average precipitation for the month. The Findell and Delworth (2010) definition was also adapted in Christian et al. (2015), being applied to small spatial domains (Oklahoma climate divisions, regions that are on the order of 200 km long and wide). This definition has been adapted for

different spatial domains, with 40% above average rainfall being utilized for domains such as the SGP (Christian et al. 2015). These past definitions vary with temporal and spatial scales, commonly assessed across a domain to determine the significance of the event. In light of the sub seasonal time scale on the order of 4-8 weeks, referencing a past pluvial definition for pluvial months is a fair comparison. For this reason, regions with greater than 40% above average precipitation across a sub seasonal period on the order of 4-8 weeks may be designated as flash pluvials.

1.3 Significance of Flooding and Pluvial Events to Society

One of the most significant threats to life and property is flooding; flooding events are responsible for a large percentage of total losses caused by natural hazards (Federal Interagency Floodplain Management Task Force 1992). Excessive precipitation often brings the threat of both river flooding and flash flooding, and it is expected that for the remainder of twenty-first century, we will see a higher frequency and greater magnitude of high intensity rainfall events (IPCC 2013). This will, in turn, increase the potential frequency and magnitude of flooding events. For this reason, the study and predictability of these events is of growing significance.

Flooding is defined by the National Weather Services (NWS) as high flow, overflow, or inundation by water that can pose a threat to lives and property (NWS 2006). There are three types of flooding: flash, river, and coastal (French and Holt 1989). The two most relevant to the Southern Great Plains (SGP) are flash and river flooding. Flash flooding is defined as a flood that develops within 6 hours of the original cause, often rainfall from thunderstorms with intense rainfall across a small area (NWS 2006). The occurrence of flash floods is dependent on a combination of hydrological and topographical factors (Jessup and DeGaetano 2008). River flooding occurs when river levels rise such that they overflow their banks. These floods are categorized as minor, moderate, or major based upon the inundation of roadways and structures, as well as public threats/impacts (NWS

2006). A large portion of the SGP is prone to flooding from excessive precipitation events; the topography and numerous rivers lead to vulnerability to flash and river flooding (Smith et al. 2000; Ashley and Ashley 2008).

Flash flooding is complex as it is impacted by numerous natural and human influenced factors such as rainfall rate and duration, soil type and moisture, topography, and land use (Trenberth and Guillemot 1996; Szewrański et al. 2018). Rainfall intensity and antecedent soil moisture are two of the most significant factors in flash flooding (Martínez-Mena et al. 1998; Castillo et al. 2003). Increasing urbanization and the rise in concentration of property and infrastructure impact the pathways that rainwater may take, and lead to increased flooding (Szewrański et al. 2018). During pluvial periods, the soil is often saturated by previous rainfall events, making following events more favorable for flash flooding. In addition, antecedent soil moisture can lead to local evaporation and water recycling, impacting and increasing precipitation furthering the risk of flash flood vulnerability (Trenberth and Guillemot 1996; Dirmeyer et al. 2009).

Flooding is both one of the most deadly and one of the most costly natural disasters as it ranks first in weather related causes of property damage in the US, and second in weather related causes of death worldwide (Rauber et al. 2005). Ashley and Ashley (2008) found that an average of 97.6 fatalities per year and a median of 81 fatalities per year occur due to flooding. In the United States, most flooding fatalities, of all types, occur within the warm season (May through September) with a maximum in June (Ashley and Ashley 2008). This is attributed to (1) increased convective thunderstorms throughout the eastern and central portions of the US and (2) tropical cyclones during late summer (Changnon 2001; Ashley et al. 2003; Ashley and Ashley 2008). In particular, Texas yielded the highest number of fatalities due to flooding from 1959 through 2005 (Ashley and Ashley 2008). One factor contributing to this is the topography of the Balcones Escarpment whereby precipitation events require less rainfall and runoff to reach similar peak river discharges as needed to flood other regions (Ashley and Ashley 2008).

Beyond the dangers and costs of flooding, the SGP are home to a large agricultural industry dependent on the weather and climate conditions for planting and harvesting. Agricultural land use in the SGP has been increasing since the late nineteenth century, with nearly half of the region becoming cropland by the 1920s (Gutmann et al. 2005; Caruthers 2017). In the Great Plains, approximately 70% of land is designated for agriculture land use (Karl et al. 2009). Given the large agricultural industry, precipitation is a critical asset to agricultural producers. Further, the timing between the climatological peaks of precipitation and temperature can greatly impact crop and livestock production (Flanagan et al. 2018). While dry precipitation extremes have significant impacts on agriculture, excess precipitation can have consequences as well (Cook et al. 2011; Pederson et al. 2012). Pluvial periods have been attributed to setting unrealistic exceptions for future water availability for both agriculture and consumption (Cook et al. 2011; Pederson et al. 2012).

1.4 Impacts of the 2015 Warm Season

The 2015 warm season yielded excessive precipitation, with many instances of flooding (Wang et al. 2015). This was accompanied by numerous mesoscale convective systems (MCSs), clusters of thunderstorms producing a large area of precipitation, on the order of 100 km or more (Anderson and Arritt 2001; Houze Jr. 2004). Flash flooding is often associated with squall lines and MCSs (Doswell et al. 1996; Rauber et al. 2005) and previous studies have tied the number of MCSs to the total annual rainfall, drought, and pluvial events (Fritsch et al. 1986; Anderson and Arritt 1998, 2001; Ashley et al. 2003; Haberlie and Ashley 2018). On average, the Great Plains can attribute 8% to 18% of their warm season precipitation come from MCSs (Ashley et al. 2003; Haberlie and Ashley 2018). In extreme cases, the Central Plains have been shown to have as much as 40% of their warm season precipitation due to MCSs (Ashley et al. 2003; Haberlie and Ashley 2018).

Flooding had a devastating impact during 2015 and spanning the calendar year, 15 fatalities occurred in Oklahoma and 48 fatalities occurred in Texas due to flooding (NOAA

National Weather Service Analyze Forecast and Support Office 2015). Flash flooding was the most costly weather hazard of the year (NOAA National Weather Service Analyze Forecast and Support Office 2015) and one event alone, May 23-26 in Oklahoma and Texas, cost $2.7 billion in flood damages along with 31 fatalities across four days (NOAA National Centers for Environmental Information (NCEI) 2015).

However, the precipitation event during the 2015 warm season was also critical to the water resources of the SGP. As shown in Figure 1.1, on April 28 prior to the extreme precipitation, portions of Oklahoma and Texas were experiencing exceptional drought (USDM; Svoboda et al. 2002). As the event progressed, the drought monitor (Fig. 1.2) illustrates the depletion of drought conditions with only small portions of Oklahoma and Texas abnormally dry by May 16. In the first week of the excessive precipitation (May 5-12), a 2-class improvement in southwest Oklahoma occurred. This deterioration of the drought over a one month period (Fig. 1.3) shows the significance of the flash pluvial as significant precipitation following a drought is important for the recovery of water resources (Christian et al. 2015).

1.5 Study Purpose

The purpose of this study is to complete a comprehensive analysis of the 2015 flash pluvial using a range of data sources spanning from in situ observations to reanalyses. An investigation of this event will help to fill in the literature on events at a sub seasonal time scale and compare the similarities and differences between this rapid transition into pluvial conditions with past pluvial events. Specifically, the objectives of the study are:

1. To establish the significance of the extreme precipitation that occurred during May and June of 2015

2. To determine the most significant events within this period that contributed to the flash pluvial

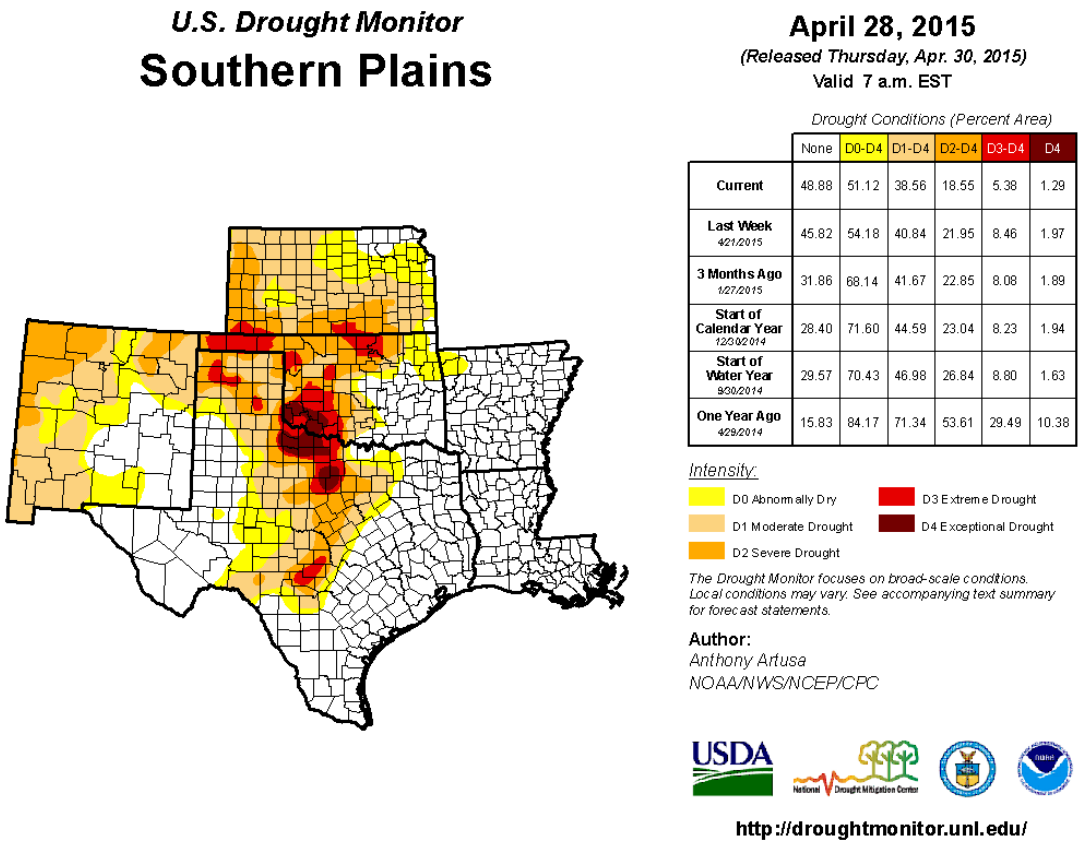

Figure 1.1: Weeks before the onset of the flash pluvial, the Southern Great Plains saw widespread areas of drought. Moderate to severe drought is widespread across Oklahoma and north and central Texas. The strongest drought is shown over the Oklahoma panhandle, and southwest Oklahoma/northern Texas.

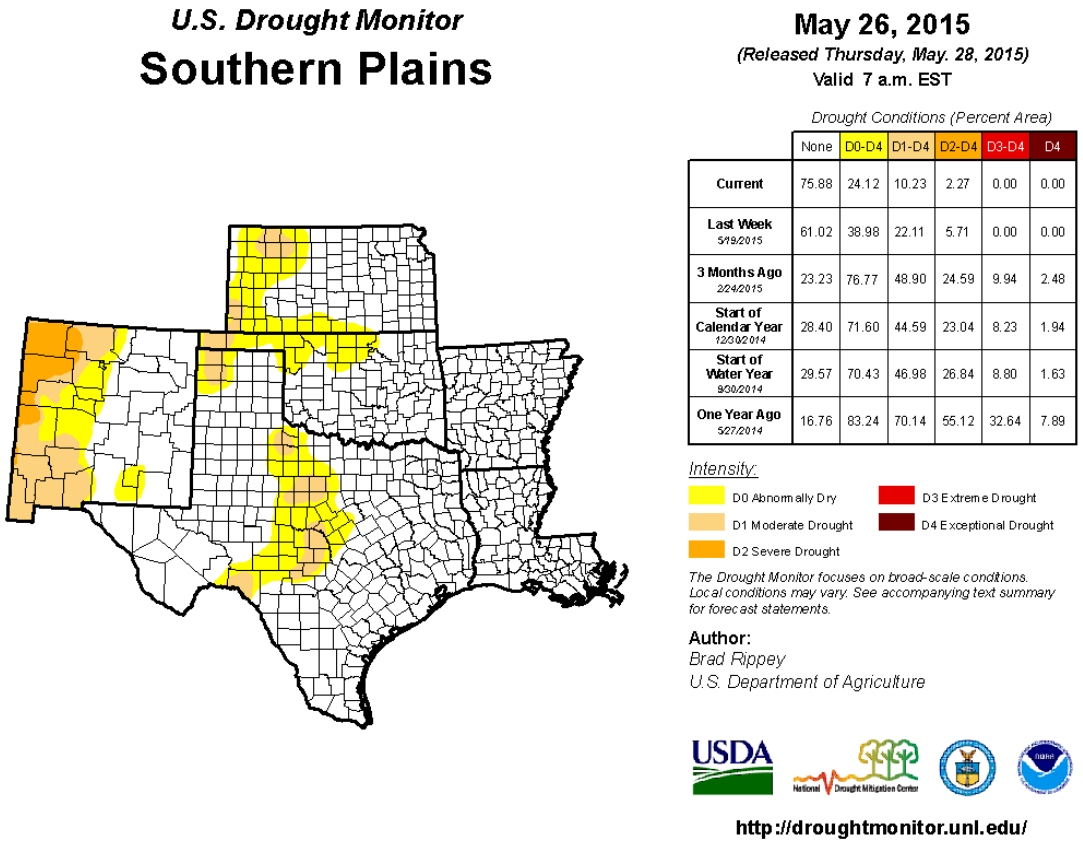

Figure 1.2: Three weeks into the flash pluvial, the previous drought in the Southern Great Plains was diminished to moderate drought and below. The remaining drought is located in northern Oklahoma and the Oklahoma panhandle, as well as central Texas.

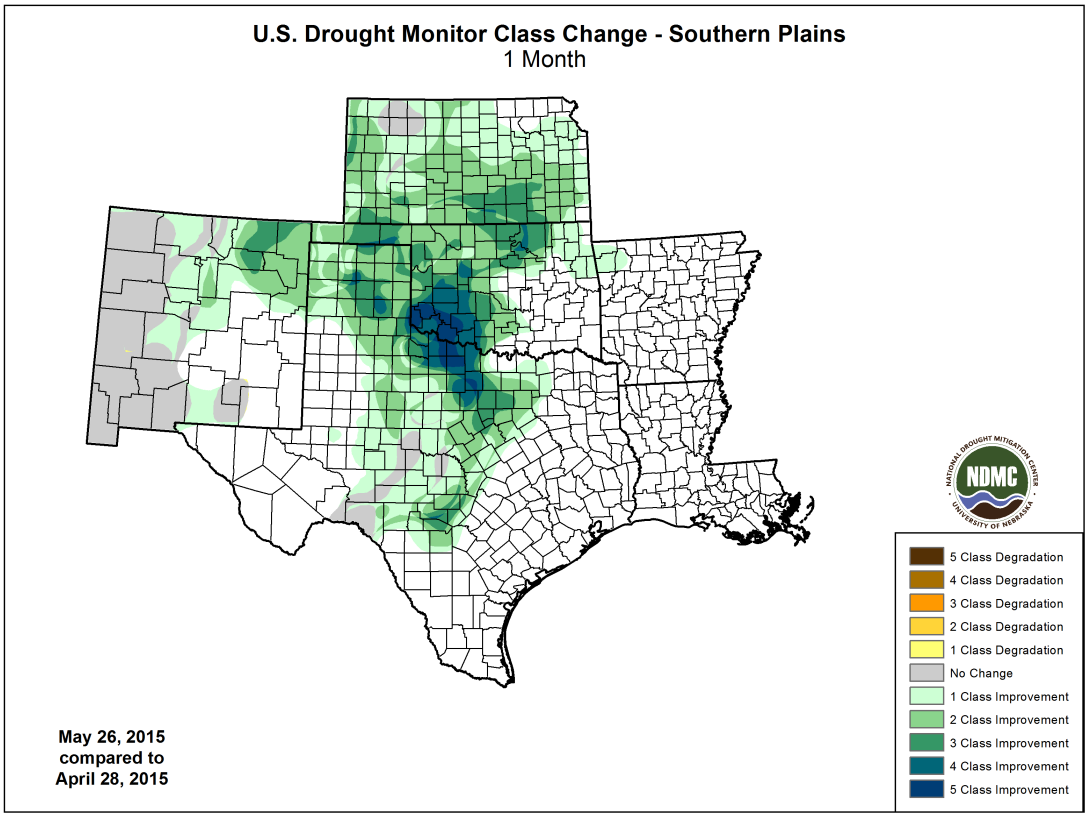

Figure 1.3: In the first month of the flash pluvial, there is widespread improvement to the previous drought conditions. Improvement is maximized in southwestern Oklahoma, where drought was previously at the exceptional stage (D4).

3. To establish large scale patterns during the flash pluvial, contributing to the excessive precipitation

4. To establish mesoscale features during the flash pluvial, contributing to the excessive precipitation

Chapter 2

Data and Methods

2.1 Data

To examine the traits of the 2015 flash pluvial event, numerous datasets were utilized spanning in situ observations to reanalyses. These datasets include the Parameter-elevation Regressions on Independent Slopes Model (PRISM), the Oklahoma Mesonet, ERA-Interim, the North American Regional Reanalysis (NARR), GridRad radar data, and radiosondes launched by the National Weather Service.

2.1.1 PRISM

The PRISM precipitation data (PRISM Climate Group) was incorporated to evaluate the extreme precipitation across the spatial domain. The PRISM dataset has a horizontal resolution of 4 km and a temporal resolution of one day. It uses a blend of climatological and statistical concepts and local regression techniques to quantify precipitation accumulation using point data (Daly et al. 1994; Daly 2006). PRISM grids stations that record precipitation measurements and accounts for orographic information in the estimation of precipitation on the 4 km grid spacing (Daly et al. 1994). The PRISM methodology was compared to other geostatistical interpolation methods and was shown by Daly et al. (1994) to accurately depict precipitation.

2.1.2 Oklahoma Mesonet

The Oklahoma Mesonet operates over 110 surface observing stations that collect 5 minute in situ observations (Brock et al. 1994; McPherson et al. 2007). The Oklahoma Mesonet

uses a 30.5 cm diameter tipping-bucket rain gauge, with a resolution of 0.25 mm (McPherson et al. 2007). The temporal resolution of Oklahoma Mesonet data makes it desirable for investigation of individual days. This dataset was used to generate time series of precipitation for several case studies in Oklahoma.

2.1.3 Soundings

Upper air data was obtained through the University of Wyoming sounding archives. This data is from the National Weather Service (NWS) radiosonde launches at 96 sites in the contiguous U.S., twice daily, at 0000 UTC and 1200 UTC (NWS 2010). From this upper air data, precipitable water (PWAT) was of particular interest. PWAT was compared to the Storm Prediction Center (SPC) sounding climatology (Storm Prediction Center 2015). This climatology is compresses of historical sounding data available internally at SPC (Storm Prediction Center 2015). The climatology is filtered remove extreme and likely erroneous outliers (Storm Prediction Center 2015). Moving averages of variables from this climatology represent a 91 day moving average, chosen to smooth data across a seasonal period (Storm Prediction Center 2015).

2.1.4 Radar

Radar data was used to examine the convective systems producing precipitation throughout the flash pluvial. The GridRad radar data used in this study were obtained from the NCAR Research Data Archive (`https://rda.ucar.edu/datasets/ds841.0/`) with observations from the NEXRAD WSR-88D radar network operated by the National Weather Service (NWS). This dataset provides hourly, three dimensional, high resolution analysis of radar reflectivity across the SGP domain. The GridRad radar data is quality controlled (Bowman and Homeyer 2017). has a spatial resolution of 0.02^{o} longitude x 0.02^{o} latitude x 1 km altitude and temporal resolution of 1 hour (Bowman and Homeyer 2017). Plots of

the radar data were generated using the Interactive Data Language (IDL) GridRad Viewer software developed by Dr. Cameron R. Homeyer at The University of Oklahoma.

2.1.5 ERA-Interim

The primary reanalysis used to investigate synoptic scale atmospheric patterns is ERA-Interim (Dee et al. 2011), which has a 0.75^{o} x 0.75^{o} longitude-latitude resolution and a temporal resolution of 6 hours. This reanalysis dataset includes a four-dimensional variational data assimilation (4D-Var) that adjusts for biases in satellite observations to avoid overestimation of precipitation previously seen in the ERA-40 reanalysis (Dee et al. 2011; Sun et al. 2018). ERA-Interim reanalysis is produced by the European Centre for Medium-Range Weather Forecasts (ECMWF), which models the coupled components of the atmosphere, land surface, and ocean waves (Dee et al. 2011). Because this dataset is a global reanalysis, it is used for investigation of large scale features that require observing across the northern hemisphere.

2.1.6 NARR

The NARR, produced by the National Center for Atmospheric Prediction (NCEP), is an atmospheric and land surface hydrology dataset for North America (Mesinger et al. 2006). The NARR dataset is a high spatial and temporal resolution reanalysis, with a spatial resolution of 0.3^{o} x 0.3^{o} (32km) and a temporal resolution of 3 hours (Mesinger et al. 2006). The NARR uses the NCEP Eta model and data assimilation system (Black 1988; Janjić 1994; Mesinger et al. 2006) and a high quality data assimilation of precipitation observations, leading to more accurate precipitation and less room for error in model forecast precipitation (Mesinger et al. 2006). This also provides a more accurate forcing of the land-surface model, and as such NARR can be used to improve analysis of land hydrology and land-surface interactions (Mesinger et al. 2006). NARR has a smaller spatial resolution

than ERA-Interim, and thus is desirable for use in the smaller scale analyses. This dataset was utilized to quantify features including precipitation efficiency and soil moisture.

2.2 Domain

The 2015 flash pluvial impacted the Southern Great Plains (SGP), and in particular, Oklahoma and Texas. Thus, the study domain focused on the SGP and spans 30-37^{o} N and 103-94^{o} W (Figure 2.1). Additionally, the temporal domain spans the months of May and June of 2015, with specific focus from 5 May – 19 June which began with the first major precipitation event of the flash pluvial and ended with precipitation and impacts associated with Tropical Depression (TD) Bill.

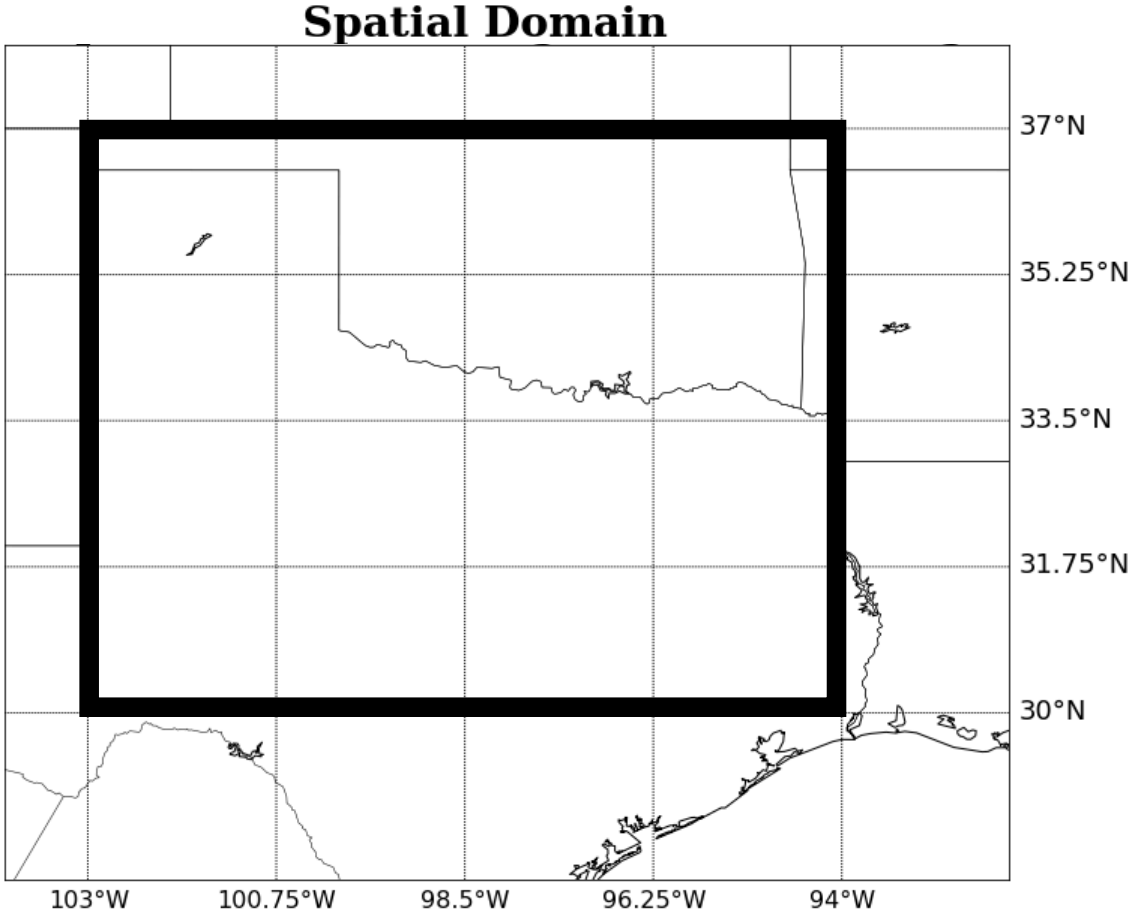

Figure 2.1: The spatial domain used for analysis of precipitation.

2.3 Methods

2.3.1 Significance Methods

It was critical to determine and examine the most significant precipitation events of the flash pluvial. To determine these events, a 30-year period of PRISM data was analyzed (1986-2015) and precipitation anomalies were computed and standardized via:

$$k = (x - \mu)/\sigma \tag{2.1}$$

where k is the standardized anomaly of precipitation, x is the actual precipitation, μ is the 30-year mean of daily precipitation, and σ is the 30 year standard deviation of daily precipitation. Next, a spatial average of the domain was computed to form a composite time series. From this time series, all dates within the 30-year period exceeding the 95th and 90th percentiles were quantified to determine (1) the most significant dates of the 30-year period and (2) those within 2015. Additionally, the dates within 2015 were compared to the dates of when TD Bill impacted the region to specifically extract that unique event. The inclusion of TD Bill within the dates obtained via this methodology induces a need to examine the dates as two separate sets: all significant dates and non-tropical dates. To investigate these phenomena separately, any date after 14 June is designated tropically influenced to do the temporal proximity with the development of Bill in the Gulf of Mexico (NHC).

Additionally, the methodology was repeated and performed upon 16 equally sized grid boxes (1.75^{o} latitude x 2.25^{o} longitude) within the domain to determine whether the significant events were representative of the full domain versus smaller spatial sections. These grid boxes can be observed in Figure 2.1), indicated by the latitude and longitude lines.

2.3.2 Synoptic Wave Event Methods

Previous studies (Dong et al. 2011; Flanagan et al. 2019) have linked the frequency of synoptic wave events with pluvial years; enhanced cyclone activity is expected during periods

of enhanced precipitation. Dong et al. (2011) noted that during excessive precipitation in the SGP during 2007, an active synoptic pattern marked by numerous shortwave troughs moving across the lee of the Rocky Mountains was present. As mentioned in Dong et al. (2011), this active synoptic pattern is associated with rising motion and convective development critical to excessive precipitation. This active pattern was quantified in (Flanagan et al. 2019), which developed a climatology of synoptic wave events in pluvial and drought years for the SGP. The climatology developed by (Flanagan et al. 2019) extends from 1926-2010 and uses ERA-20th Century reanalysis data. This near century long climatology can be used to compare the wave activity across different years and provide a comparison to the synoptic wave frequency in 2015.

Thus, to quantify the synoptic activity during the flash pluvial event, the frequency of synoptic waves was investigated for 2015. The methodology for this investigation was modified from the methodology of (Flanagan et al. 2019) and determined synoptic wave event events via geopotential height and relative vorticity. As such, ERA-Interim 850 hPa relative vorticity and 500 hPa geopotential height at 0000 UTC were analyzed over the southwestern United States in a domain spanning 20^{o}-40^{o}N and 130^{o}-10^{o}W. This domain was determined by (Flanagan et al. 2019) to be consistent with anomalous synoptic signals in pluvial patterns in the SGP noted in Flanagan et al. (2018). Both relative vorticity and geopotential height were processed with a 10-day, high pass filter and the standardized anomalies were computed for each grid point. Three criteria were then applied to determine the synoptic wave events:

- The spatial domain of investigation must have a mean geopotential height anomaly of less than -0.5 standard deviations
- There must be at least one grid point having a value of less than -3.5 standard deviations
- The relative vorticity anomaly must have at least one grid point with a value greater than 3.5 standard deviations

These single grid point criteria correspond to the 15th percentile value for geopotential height anomaly and vorticity anomaly for each single grid point.

2.3.3 Composite Analysis Methods

The daily ERA-interim atmospheric fields (geopotential height, specific humidity, zonal wind (u), meridional wind (v), 2 meter temperature, and surface pressure) at 0000 UTC were composited for the study period consistent with previous studies that allow comparison with atmospheric soundings (Flanagan et al. 2018). Anomalies of these fields are quantified by removing the 20-year mean (1989-2008) and subsequently standardized with respect to the 20-year standard deviation (see Equation (2.1)). These variables were also used to compute moisture flux, as well as integrated vapor transport (IVT).

Multiple significance thresholds for dates (see Section 2.3.1) were investigated for composite analysis. For comparison to climatological normals, the 20 year mean of May-June is plotted for each variable. Additionally, the 5 May - 18 June 2015 composite mean of each variable is shown for comparison to the climatological normals. The standardized anomaly of each variable is composited for both the full temporal domain of the flash pluvial (5 May - 18 June) and for the 95th percentile significant precipitation dates. Composites of the 90th percentile non-tropical significant precipitation dates were also compared, but are not shown because of the close similarities with the 95th percentile composites.

Significance testing was completed on the criteria composites to determine whether they are significantly different from the full period composite. This was done with Monte Carlo simulations (Metropolis and Ulam 1949; Wilks 2006); 1000 random samples were taken of the total composite field and compared to the significant precipitation date composite to quantify statistical significance stippled at the 0.05 significance level on associated plots.

2.3.4 Integrated Vapor Transport and Atmospheric River Methods

Atmospheric rivers (ARs) are elongated, synoptic jets of water vapor that account for a majority of poleward water vapor transport in midlatitudes (Zhu and Newell 1998; Guan and Waliser 2015). These features are critical in weather and hydrology and when intersecting land are often associated with enhanced precipitation.

To diagnose moisture transport during the study period, integrated vapor transport (IVT) and atmospheric rivers (ARs) were investigated via derived fields from the ERA-Interim reanalysis computed via:

$$IVT = -\frac{1}{g}\int_{1000}^{250}(q * \vec{V_H})dp \tag{2.2}$$

where g is the acceleration due to gravity, q is the specific humidity (kg kg^{-1}), V_H is the horizontal wind, and dp is the differential of pressure. This is computed between the levels of 1000 hPa to 250 hPa, as a majority (approximately 75%) of vapor transport occurs in the lower 2.5 km of the atmosphere (Ralph et al. 2005; Lorente-Plazas et al. 2018).

To identify AR events, a method developed by Guan and Waliser (2015) and Guan et al. (2017) was employed: the algorithm uses an 85th percentile threshold of 6 hourly ERA-Interim IVT. An AR must have length exceeding 2000 km and a length to width ratio greater than 2. Further, this AR detection algorithm was used due to its consistency utilizing ERA-Interim data as well as associated benefits of using an IVT-based detection over integrated water vapor (IWV; Guan and Waliser 2015).

2.3.5 Precipitation Efficiency Methods

In addressing the ingredients of the heavy precipitation seen during the flash pluvial, precipitation efficiency contributes to the relationship between rainfall rate, input water flux, and how efficiently a storm produces rain accounting for reevaporation of rain and local moistening (Sui et al. 2007). Studies have investigated precipitation efficiency estimation in combination with flash flood events, as high rainfall rates are often associated with flash

flooding (Doswell et al. 1996; Market et al. 2003). Precipitation efficiency impacts the precipitation rate and storm total precipitation, and the prediction of these generally elevated efficiencies can be beneficial to prediction of flash floods (Doswell et al. 1996; Market et al. 2003).

Throughout past investigations of precipitation efficiency, the approach to computing a value has varied. There are slight variations in definition and computation, varying from methods that are bound to 0-100% to others that can range from 0 to infinity (Sui et al. 2007; Market et al. 2003). A basic definition, used in Market et al. (2003), states that precipitation efficiency is the ratio of precipitation to ingested moisture. For the purposes of this investigation, the ratio between observed precipitation and precipitable water was used. In the interest of preserving the accuracy of the precipitation data, this was computed with PRISM precipitation and NARR precipitable water. The two datasets are transformed to the same grid spacing (32 km x 32 km), and precipitation efficiency was then computed, via:

$$PE = \frac{rainfall}{PWAT} \tag{2.3}$$

where PWAT is total precipitable water.

Chapter 3

Results

3.1 Significance Results

The majority of the May-June precipitation fell between 5 May 2015 and 19 June 2015. During these 46 days, a widespread portion of Oklahoma and parts of northern Texas saw greater than 50 cm of rainfall (Fig. 3.1a). On average during this period, the entire study domain yielded positive precipitation anomalies (Fig. 3.1b). These anomalies were greatest in the Texas panhandle and along the Red River in Oklahoma and Texas.

To better capture the variation in precipitation across this period, both the precipitation accumulation and precipitation anomalies are plotted in Figure 3.2 by 15-16 day periods. Nearly one half of Oklahoma experienced over 17 cm of precipitation in 15 days, from May 5 through May 20. Additionally, a large section of the Texas panhandle and parts of northern and central Texas received over 17 cm of rain. During the second period (May 21 through June 5) a very similar region of enhanced precipitation occurred across the southern half of Oklahoma. This time period also included a greater area of extreme precipitation in north and central Texas, particularly surrounding the Dallas-Fort Worth metropolitan area. It was also during this period that one of the most impactful flooding events occurred in Texas, marked by numerous river and flash floods and water rescues during Memorial Day weekend. The third period (June 6 - June 19) displayed a very different pattern and was largely dominated by Tropical Depression Bill (TD Bill). The precipitation maxima was located on the Oklahoma-Texas border on the Red River and was colocated with the regions that experienced excessive precipitation in the previous 30 days. As such, the rainfall associated with these later events fell onto already saturated soil which impacted flash flood occurrence (Martínez-Mena et al. 1998; Castillo et al. 2003).

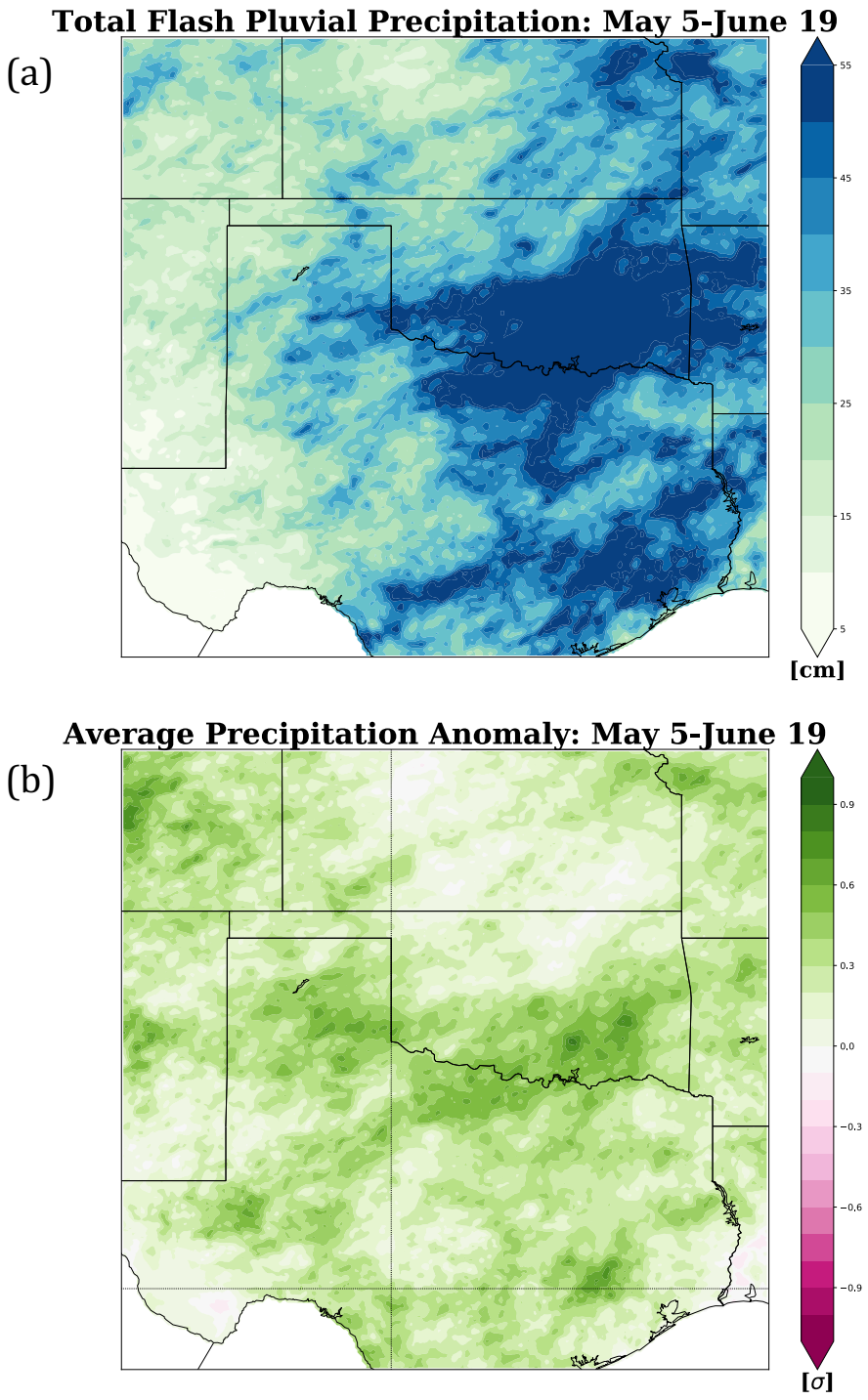

Figure 3.1: (a) Precipitation accumulation from May 5 through June 19 2015. (b) Standardized anomalies of precipitation, averaged from May 5 through June 19 2015.

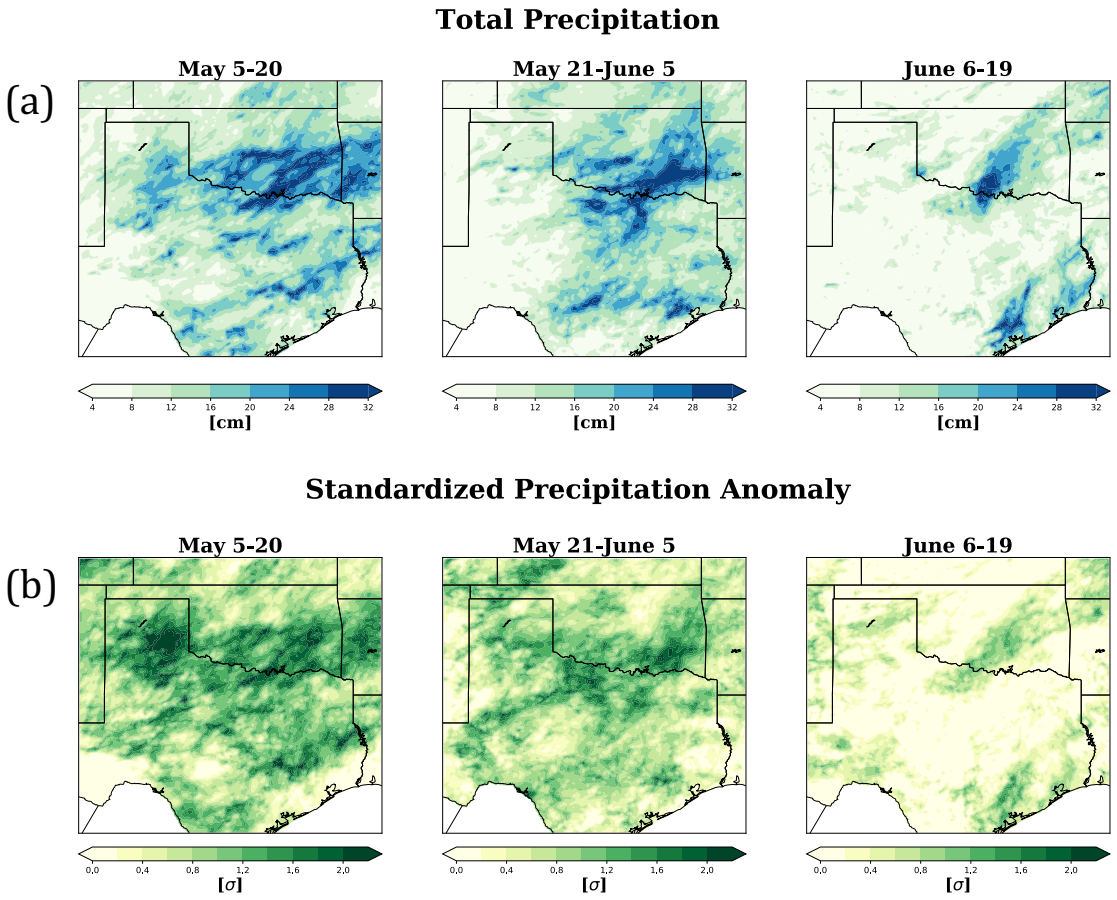

Figure 3.2: (a) Precipitation accumulation during the three sub-periods of the flash pluvial. (b) Average standardized anomaly of precipitation during the three sub-periods of the flash pluvial.

In terms of precipitation anomalies, the first period of the flash pluvial event exhibited the greatest statistical significance whereby a majority of the Texas panhandle averaged one standard deviation greater than normal rainfall during this time. Precipitation remained anomalous during the middle 15 days with widespread anomalies in excess of 0.7 standard deviations. The latter 16 days, largely representative of TD Bill, yielded a much weaker overall anomaly pattern. To fully capture the anomalous precipitation experienced during that event, the precipitation totals and anomalies are displayed in Figure 3.3. The part of Bill's path along which it slowly passed over the Red River and central Oklahoma experienced as much as 30 cm in only four days. In some localized areas, Bill was responsible for approximately one third of the total flash pluvial precipitation. Many parts of Oklahoma and Texas within Bill's path experienced over 2 standard deviations above normal precipitation from the event.

Beyond the precipitation data, the significance of the flash pluvial can be seen in changes to soil moisture; Figure 3.4 shows the spatially averaged soil moisture across the SGP domain, with data from the NARR. Four depths of liquid volumetric soil moisture are plotted: 0, 10, 40, and 100 cm. Due to the higher variably in shallow depths of soil moisture during the growing season, the seasonal to sub-seasonal nature of the event is best observed at the 40 and 100 cm depths. The 40 cm soil moisture captures the dry periods both before and after the flash pluvial whereby at beginning of May, the 40 cm soil moisture shows a steady increase with an intermittent decrease between the end of May and T.D. Bill in mid-June. This is echoed at the shallower soil moistures, but with less variability between precipitation events. The deepest soil moisture, at 100 cm, shows less variability with a slow, but steady increase in the values across the flash pluvial and the eradication of the much drier conditions seen in soil moisture before the flash pluvial.

Next, the individual days were investigated for significance. In a comparison to the 30-years climatology, 10 days within the flash pluvial exceeded the 95th percentile criteria, explained in Section 2.3. These dates are shown in Table 3.1. When the criteria was shifted

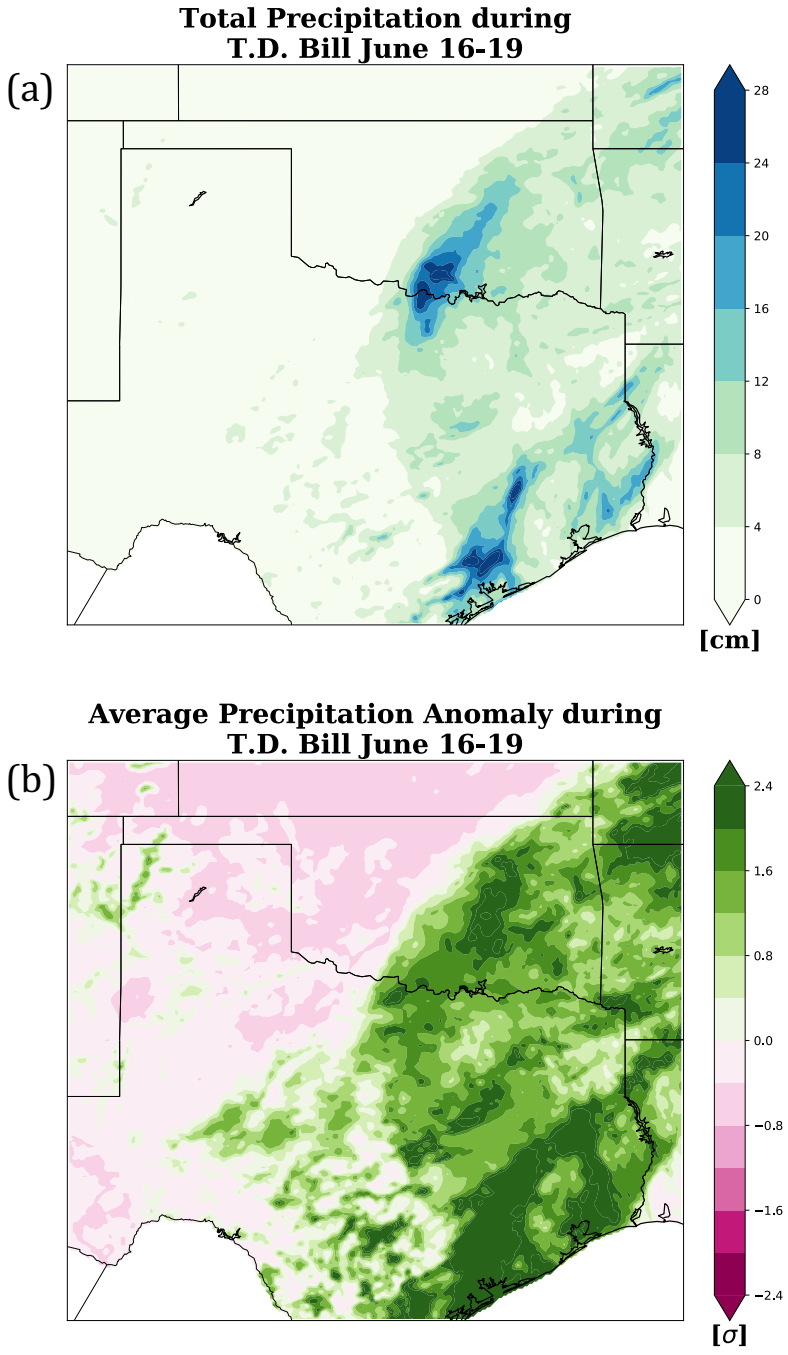

Figure 3.3: (a) Accumulated precipitation during June 16-19, due to Tropical Depression Bill. (b) Mean standardized anomaly of precipitation during the period of June 16-19, due to Tropical Depression Bill.

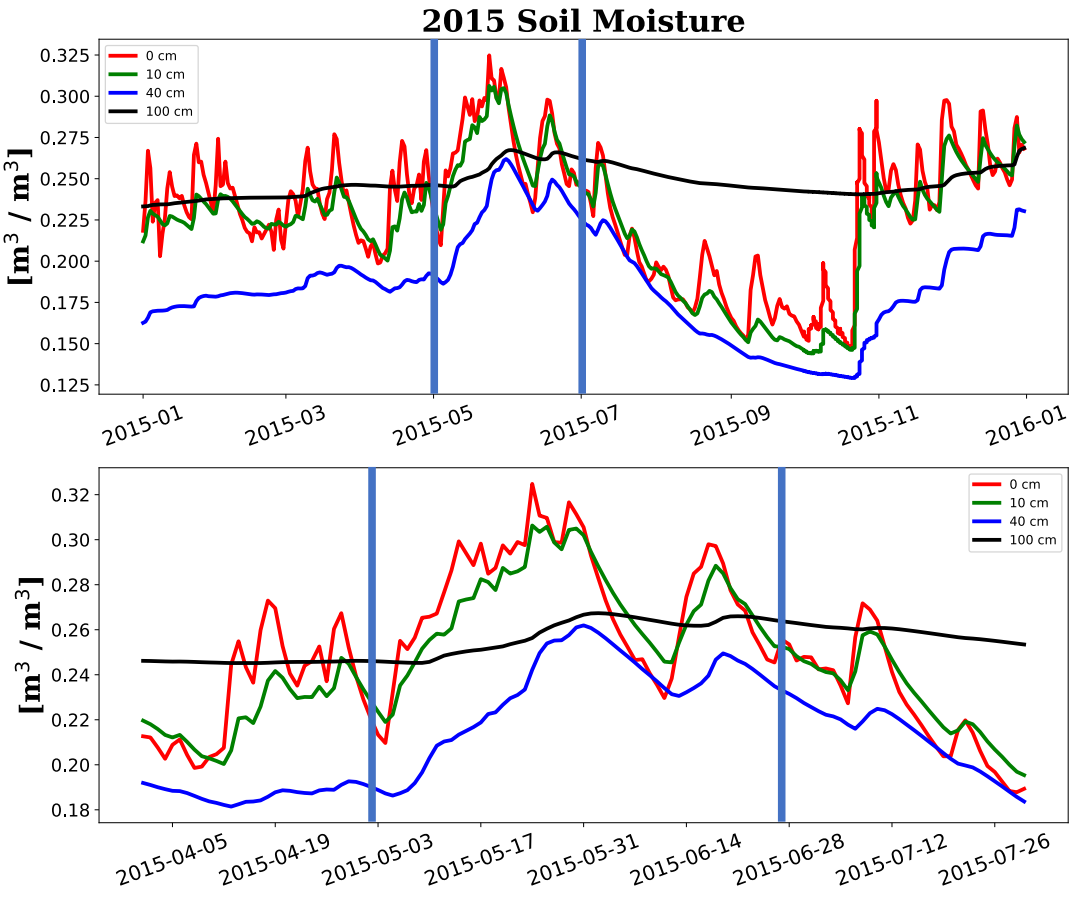

Figure 3.4: Evolution of the mean soil moisture in the Southern Great Plains during 2015, from the NARR. The top panel represents the entire year of 2015, while the bottom panel highlights April through July. May and June are highlighted between the vertical blue bars.

to the 90th percentile, 6 additional dates exceed the criteria, seen in Table 3.2. The three most significant dates, in order, were May 24th, May 29th, and May 14th. These top three events occurred in the first four weeks of the flash pluvial.

Table 3.1: List of significant precipitation days at the 95th percentile criteria

May 6 2015	May 20 2015
May 9 2015	May 24 2015
May 11 2015	May 26 2015
May 14 2015	May 29 2015
May 17 2015	June 13 2015

Table 3.2: List of significant precipitation days at the 90th percentile criteria.

May 6 2015	May 22 2015
May 8 2015	May 24 2015
May 9 2015	May 26 2015
May 10 2015	May 29 2015
May 11 2015	June 13 2015
May 14 2015	June 15 2015
May 17 2015	June 17 2015
May 20 2015	June 18 2015

To examine the robustness of this significance criteria and the impacts of the significant dates, the same criteria was repeated for smaller subregions. This investigation determined that the significant dates for the subregions were nearly the same dates with minor exceptions for localized events. For each of the sixteen 1.75^{o}x2.25^{o} grid boxes (seen in Fig. 2.1),

the number of significant precipitation dates was plotted with the results of this test for the 95th percentile displayed in Figure 3.5. All subregions experienced at least four days exceeding the 95th percentile criteria for that subregion. The most frequent dates seen in the subregions were the same dates indicated by the analysis of the entire domain as a whole. This was repeated with the 90th percentile, non-tropical criteria, which is plotted in Figure 3.6. The subregions each experienced between six and sixteen significant precipitation days at this nontropical criteria. The regions with the most frequent days exceeding the 90th percentile were located in the along the Red River, the Texas panhandle, and western Texas. During the five-day period impacted by TD Bill, all regions saw between two and five days exceeding the 90th percentile.

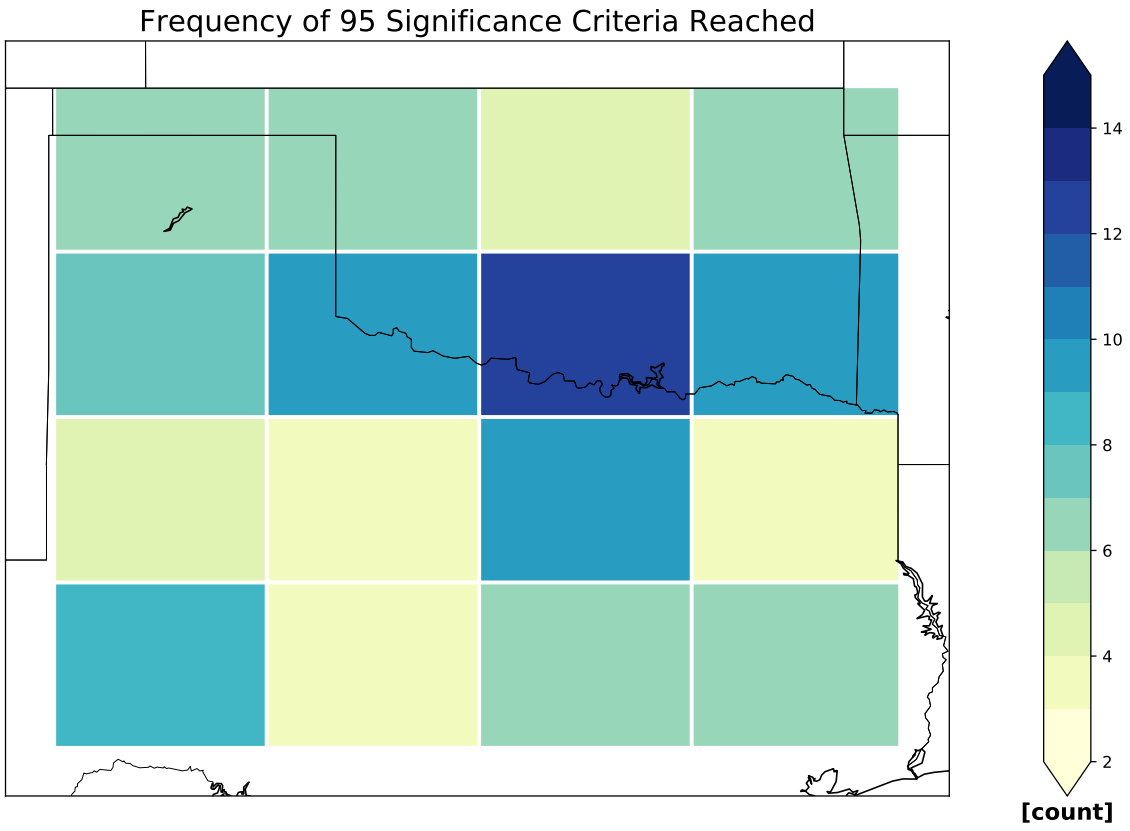

Figure 3.5: Frequency of each region meeting the 95th percentile criteria.

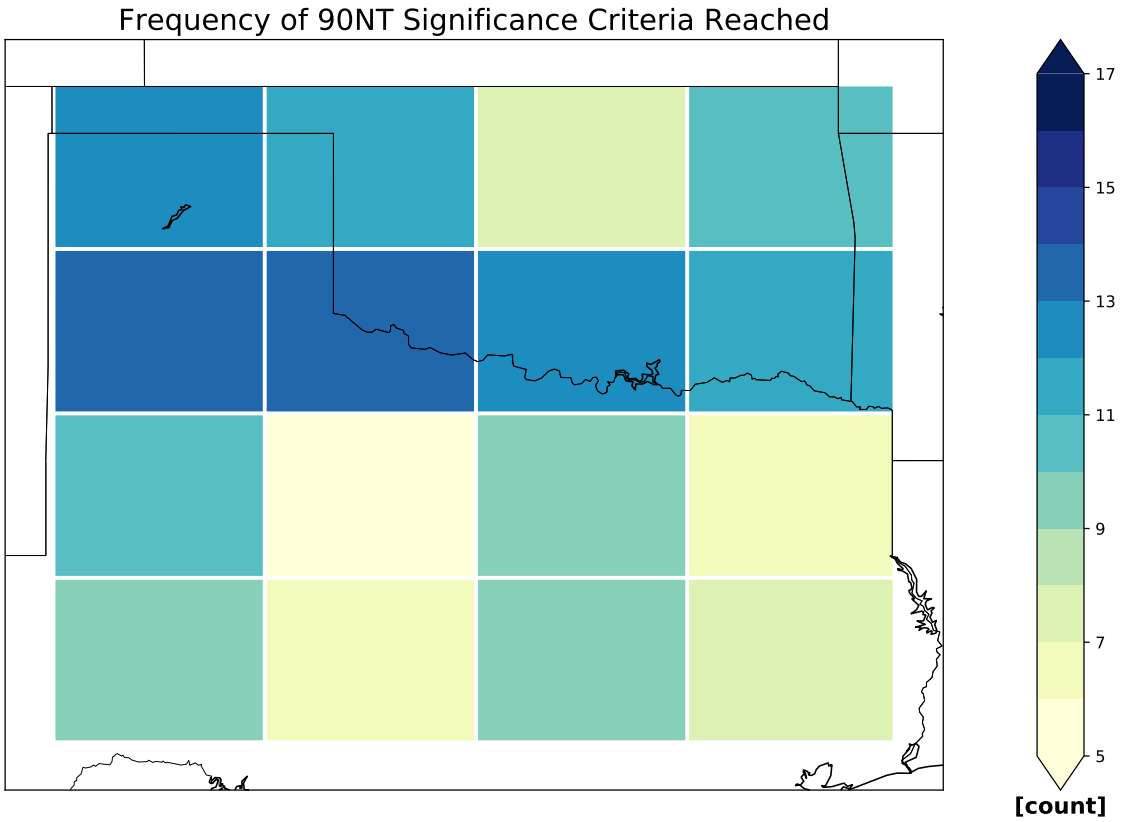

Figure 3.6: Frequency of each region meeting the 90th percentile criteria, excluding T.D. Bill.

In order to investigate the significance of this event in the context of past definitions of pluvials, the percent above normal precipitation was computed (Fig. 3.7). Previous studies have used the criteria of 40% and 80% above normal precipitation, and such those contours are bolded in Figure 3.7. The SGP received over 40% above normal precipitation across most of the spatial domain. A wide region across the Red River as well as the Texas panhandle received over 80% above normal precipitation. Parts of the Red River exceed this criteria greatly, with an area as high as 200% above normal precipitation. By these previously used criteria, it can be said that the period of May-June 2015 meets the criteria of a pluvial.

3.2 Synoptic Wave Event Results

2015 was characterized by a greater than normal number of synoptic wave events. According to the synoptic wave climatology of Flanagan et al. (2019), the mean annual synoptic wave count for the SGP is 51.5 and the mean May-June synoptic wave count of 5.8. Because drought preceded the flash pluvial period during the late spring, 2015 yielded only a slightly above average number of waves (58) from an annual perspective. There were notably few events in February, August, November, and December (Fig. 3.8). However, May and June yielded a combined 15 synoptic wave events which exceeding the prior maximum of 13 in 1963; nine events occurred during May and six occurred during June. The dates of the synoptic wave events are listed in Table 3.3. In order to facilitate comparison with the significant precipitation dates that may be linked to these wave events, a list of all significant precipitation dates and synoptic wave events can be seen in Table 3.4.

In examining the climatology of synoptic wave events (Fig. 3.9), several years appear to have a similar amount of wave events as 2015. One surprisingly analogous year to 2015 was 1988. While 1988 yielded fewer events May-June (11) and annually (54), it had 20.37% of wave events in May-June which was the closest ratio to the 25.86% observed in 2015. This year, 1988, was surprising given it is a drought year. However, (Trenberth and

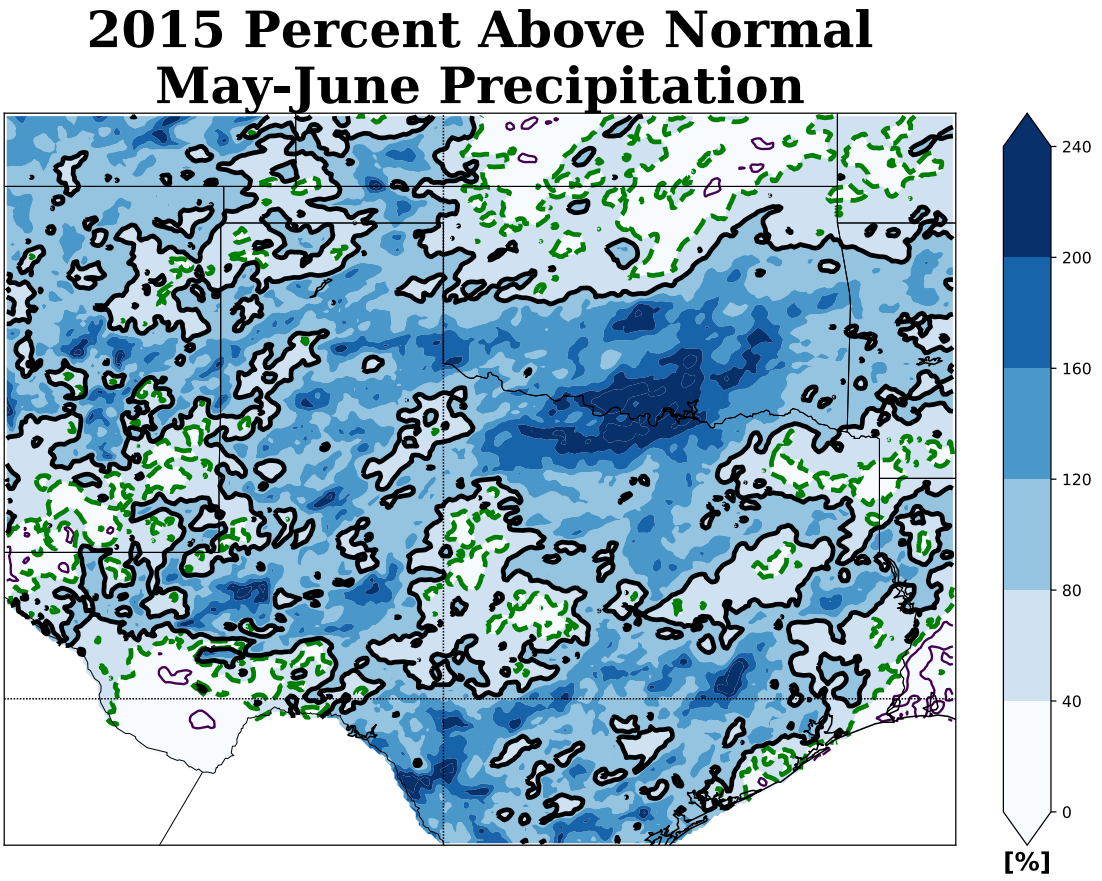

Figure 3.7: Percent above normal precipitation for the period of May-June 2015. The black solid contour indicates 80% above normal. The dashed green contour indicates 40% above normal. These contours are indicative of previous criteria of pluvial periods.

Guillemot 1996) noted that 1988 was synoptically active, but the storm track was too far north to tap into deep moisture and hence the drought pattern developed versus a pluvial pattern. Trenberth and Guillemot (1996) also examined the extremely wet year, 1993, in comparison to the 1988 drought; 1993 yielded 59 annual synoptic wave events by the Flanagan et al. (2019) methodology, comparable to both 1988 and 2015.

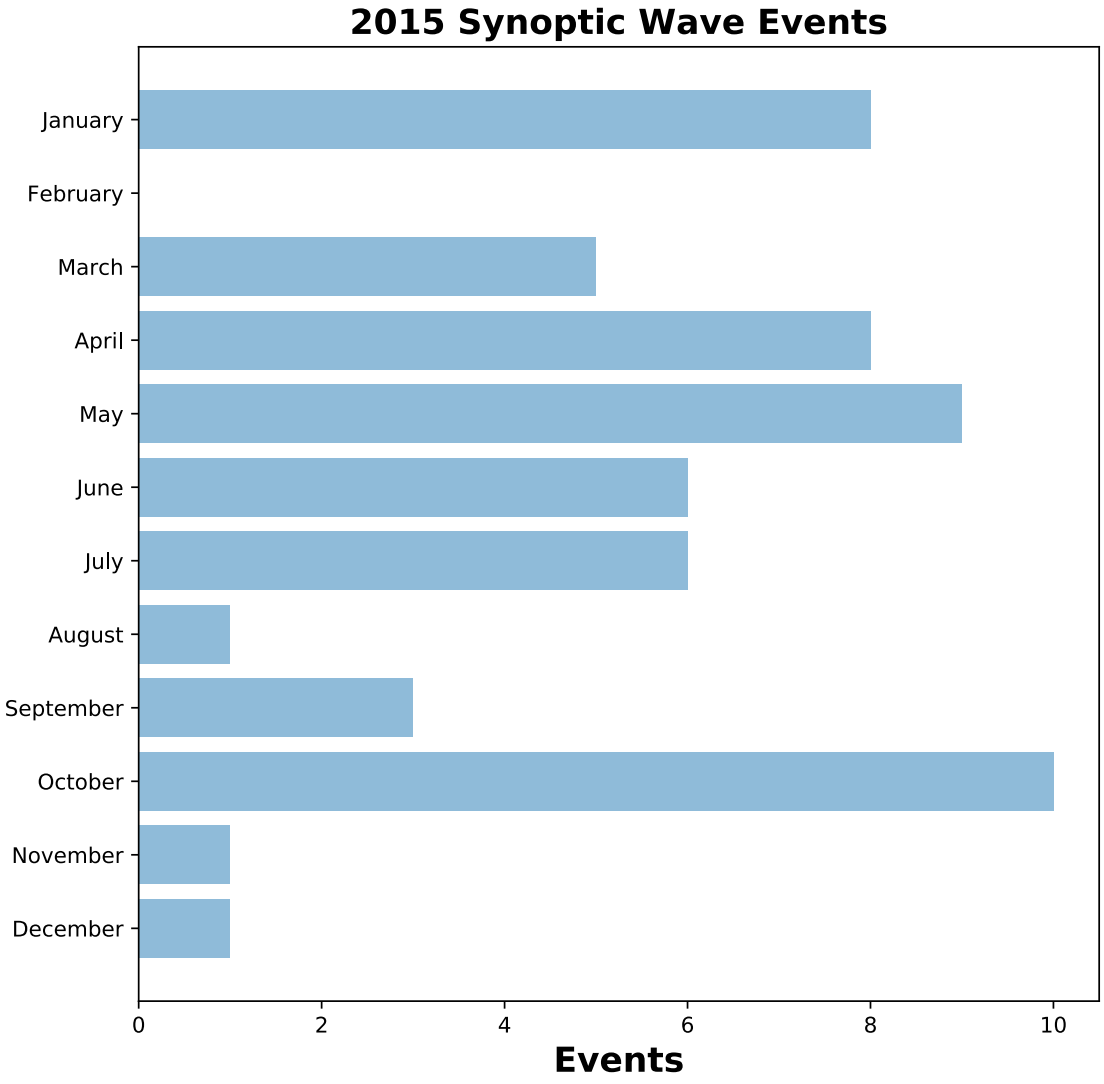

Figure 3.8: Synoptic wave events in 2015 by month.

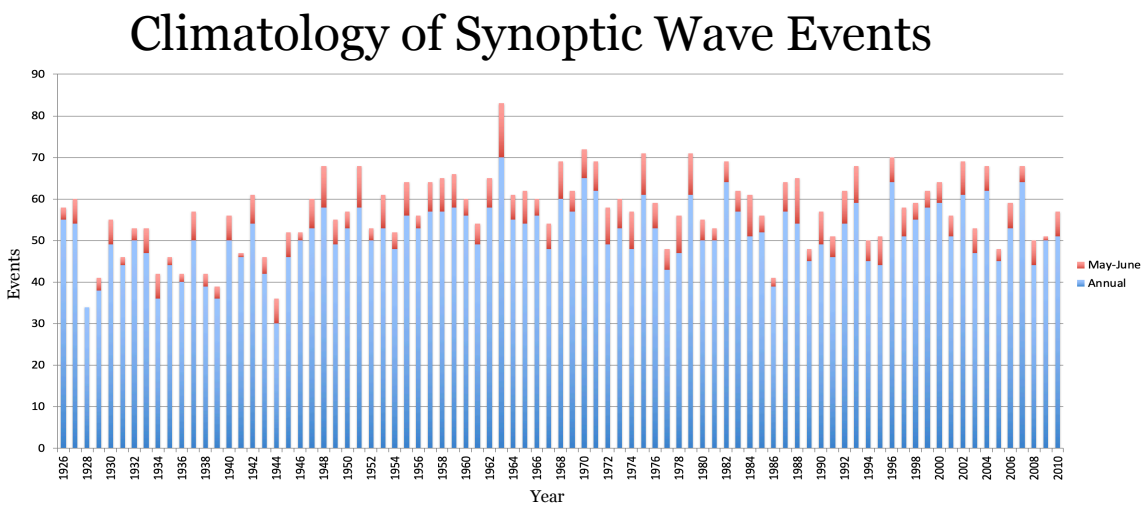

Figure 3.9: Climatology of synoptic wave events. Figure courtesy of Paul Flanagan (Flanagan et al. 2019)

3.3 Composite Analysis Results

To investigate both the overall persisting conditions during the flash pluvial and the conditions specific to the significant precipitation events within the flash pluvial, several approaches were taken. For comparison to normal conditions, the 20 year May-June average of each variable is plotted and compared with a composite of the mean atmospheric conditions during the 95th percentile criteria days. Composites of anomalies of atmospheric anomalies were created for (1) May 5 - June 19 and (2) the days meeting the 95th percentile criteria. The 95th percentile criteria does not contain any days of TD Bill.

3.3.1 Mean Conditions During the Flash Pluvial

Before assessing the anomalies observed in the flash pluvial event composites, it is important to address the mean conditions from which these anomalies were derived. The average, climatological conditions in May-June display two jet streams at 250 hPa: the polar jet and the subtropical jet. In the climatological mean (Fig. 3.10a), the polar jet has a greater magnitude and is directed across the Pacific Ocean towards the northwestern United States,

Table 3.3: List of days in May and June of 2015 with synoptic wave events.

May 1 2015	May 19 2015
May 3 2015	June 8 2015
May 4 2015	June 9 2015
May 8 2015	June 10 2015
May 9 2015	June 27 2015
May 10 2015	June 28 2015
May 15 2015	June 29 2015
May 17 2015	

while the subtropical jet has a lesser magnitude and extends into northern Mexico. The mean conditions during the 2015 event illustrate these jets, but display greatly different magnitude (Fig. 3.10b). Both jet streams appear stronger than climatology, and the subtropical jet displays a maximum in wind over Baja California. When considering 250 hPa meridional wind, climatologically there is no strong feature in Figure 3.11a. In contrast, when compositing the 95th percentile days of May-June 2015, a strong southerly feature is present over the central United States (Fig. 3.11b). Upper level geopotential heights, plotted at 500 hPa, show generally zonal flow with isohypses following along meridians (Fig. 3.12a). When examining the composite of 95th percentile days, a wave pattern emerges and shows a trough over the western US and a ridge over the eastern US (Fig. 3.12b). This figures also indicates an area over northwestern Canada with an area of locally higher heights. This is a feature associated with El Niño, as mentioned in Yeh et al. (2018).

Low level meridional winds, at 925 hPa, climatologically display a southerly wind extending from the Gulf of Mexico to the central US (Fig. 3.13a). When examining the 95th percentile dates, this low level jet is much stronger, with a magnitude in excess of 10 kt in the composites (Fig. 3.13b). In terms of meridional moisture flux (the product of specific

Table 3.4: List of significant precipitation days at the 95th and 90th percentile criteria. Any dates that coincide with synoptic wave events are indicated.

Date	95th Percentile day	90th Percentile day	Synoptic Wave Event
May 1 2015	-	-	x
May 3 2015	-	-	x
May 4 2015	-	-	x
May 6 2015	x	-	-
May 8 2015	-	x	x
May 9 2015	x	-	x
May 10 2015	-	x	x
May 11 2015	x	-	-
May 14 2015	x	-	-
May 15 2015	-	-	x
May 17 2015	x	-	x
May 19 2015	-	-	x
May 20 2015	x	-	-
May 22 2015		x	-
May 24 2015	x	-	-
May 26 2015	x	-	-
May 29 2015	x	-	-
June 8 2015	-	-	x
June 9 2015	-	-	x
June 10 2015	-	-	x
June 13 2015	x	-	-
June 15 2015	-	x	-
June 17 2015	-	x	-
June 18 2015	-	x	-
June 27 2015	-	-	x
June 28 2015	-	-	x
June 29 2015	-	-	x

humidity and meridional wind, v'q'), climatologically the SGP receives positive moisture flux from the Gulf of Mexico (Fig. 3.14a). In the case of the 95th percentile days, this moisture flux is much stronger and extends over a larger region of the SGP and Mississippi valley (Fig. 3.14b). Climatologically, the months of May and June have generally lower surface pressure over the western half of the US and higher pressure over the Pacific (Fig. 3.15a). Surface pressure patterns for the 95th percentile days illustrate similar features, but with more clearly defined areas of high pressure over the Pacific, Atlantic, and northern Canada (Fig. 3.15b). The 2-meter temperature across the US in the May-June climatology shows a general pattern of temperature decreasing with latitude and altitude around regions with mountainous terrain (Fig. 3.16a). In comparison, the composite of 2-meter temperature for the 95th percentile days shows a colder airmass over the high plains, west of the SGP (Fig. 3.16b).

3.3.2 Overall Patterns

Several anomalous features were observed in the composite analysis. First, the wind patterns yielded a distinct subtropical jet displaced slightly southward with much greater strength via composites of 250 hPa zonal wind. This feature is displayed in Figure 3.17a, with the zonal jet extending into Baja California. Additionally, the 250 hPa meridional wind was anomalously strong over the central U.S., with its greatest strength over Oklahoma and Kansas (Fig. 3.18a). A plot of the total wind vector anomalies displayed these same features (Fig. 3.19a), while also exhibiting cyclonic curvature over the Pacific corresponding to the location of another anomalous pattern observed at 500 hPa: a low in geopotential heights (Fig. 3.20a).

Nearer to the surface, 925 hPa meridional winds were anomalously strong extending from the Gulf of Mexico into the central to southeastern United States (Fig. 3.21a). The specific humidity (q) across the central United States was anomalously high with a maxima located west of the SGP in the high plains of Colorado and New Mexico (Fig. 3.22 a).

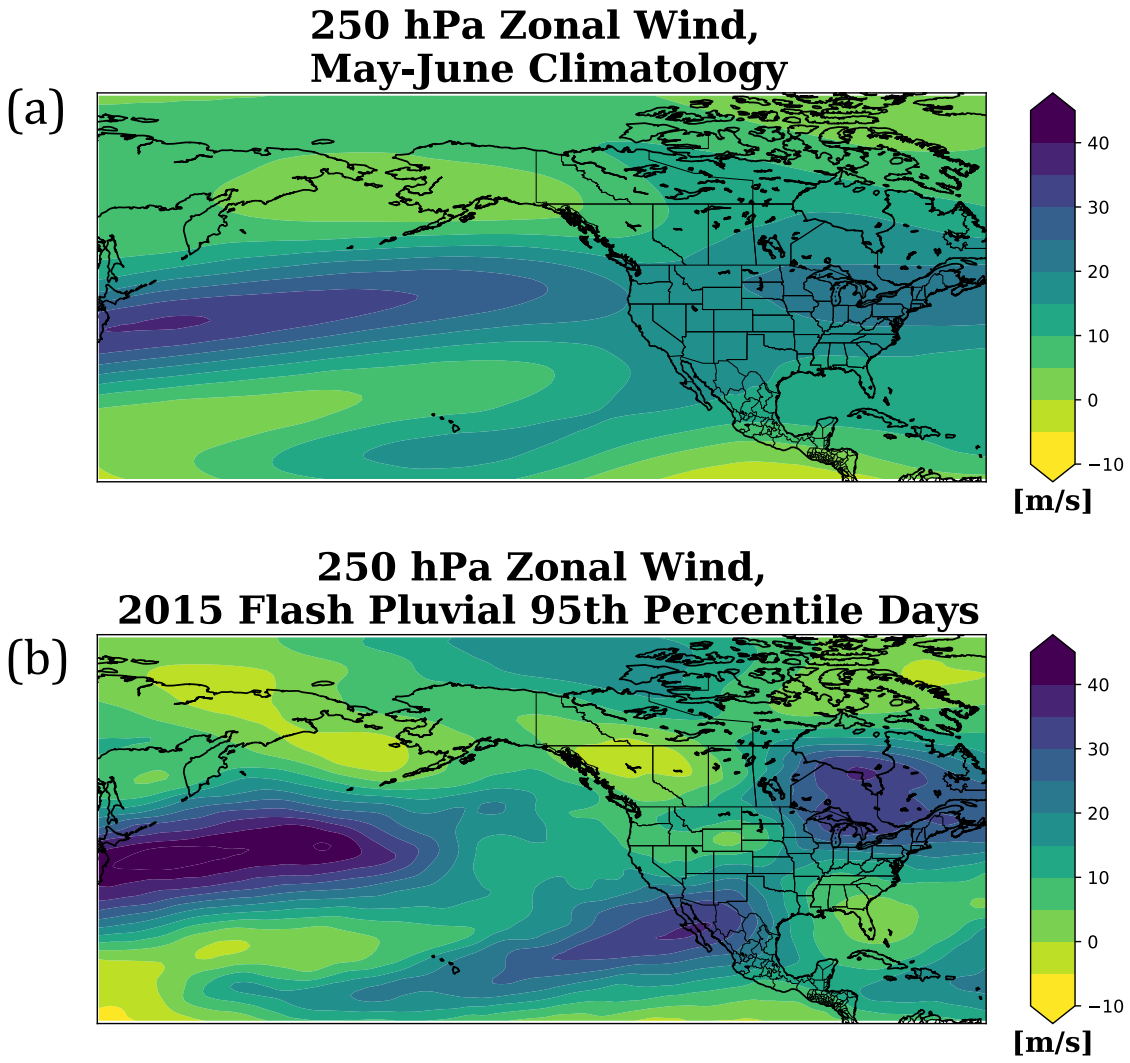

Figure 3.10: (a) Mean 250 hPa zonal wind for May-June (b) Composite of 250 hPa zonal wind for days exceeding the 95th percentile significance criteria.

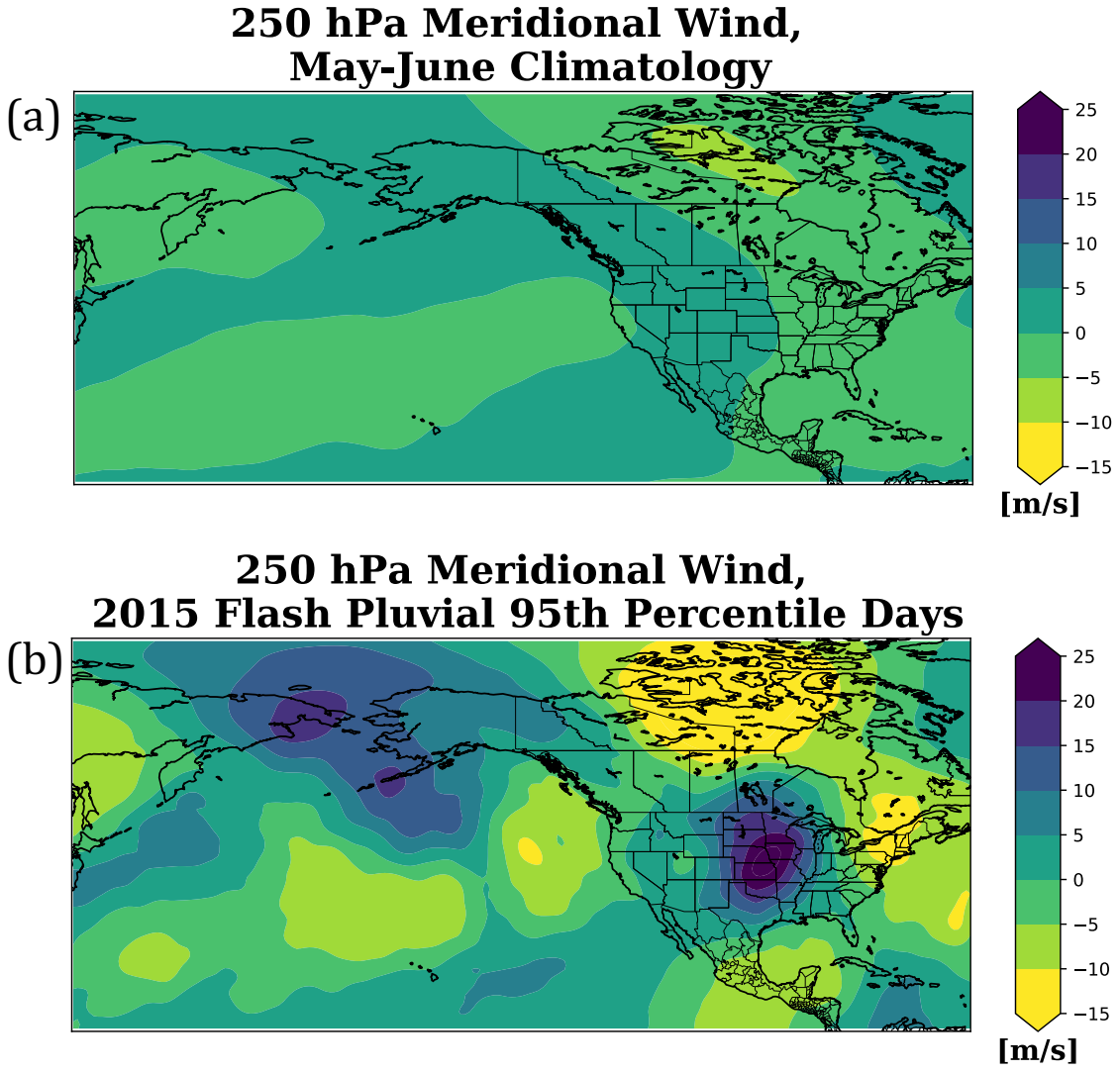

Figure 3.11: (a) Mean 250 hPa meridional wind for May-June (b) Composite of 250 hPa meridional wind for days exceeding the 95th percentile significance criteria.

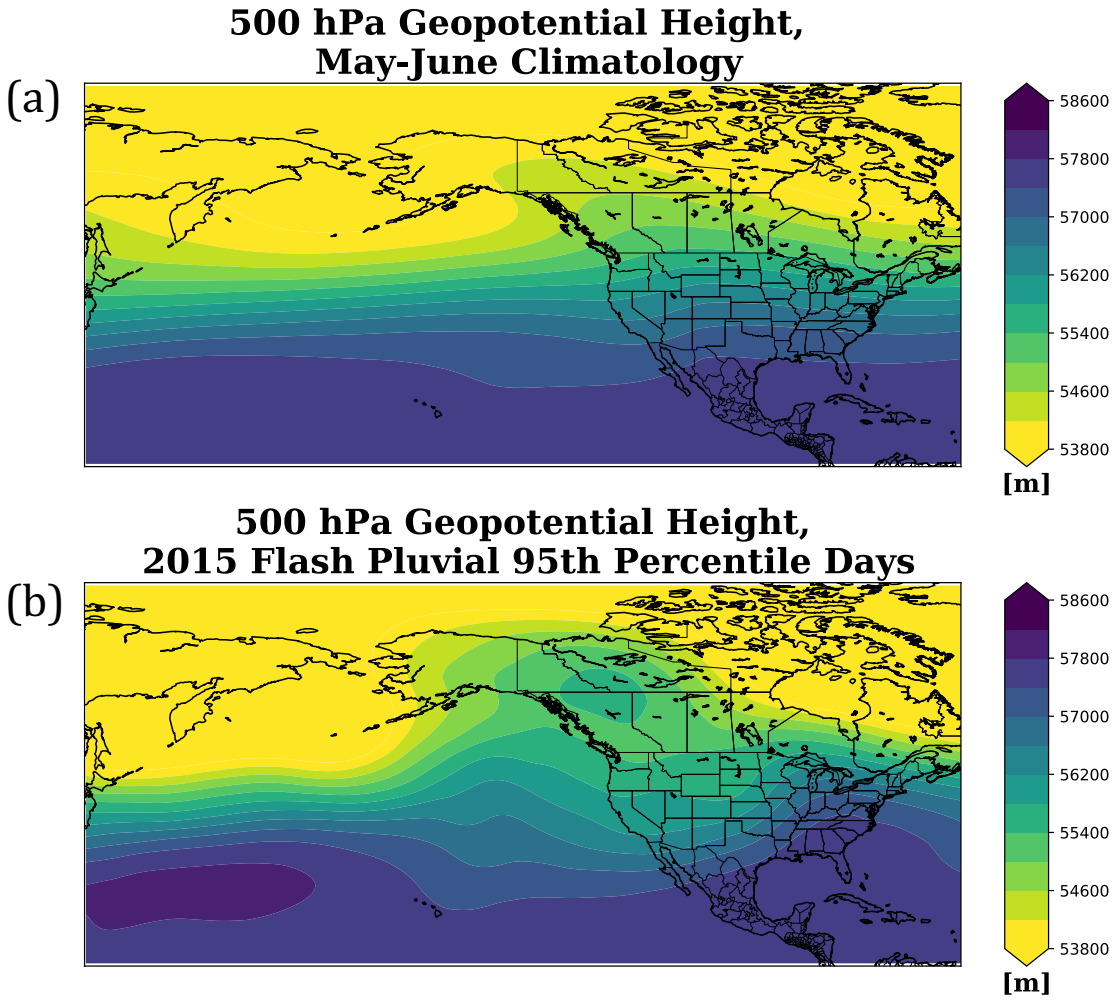

Figure 3.12: (a) Mean 500 hPa geopotential height for May-June (b) Composite of 500 hPa geopotential height for days exceeding the 95th percentile significance criteria.

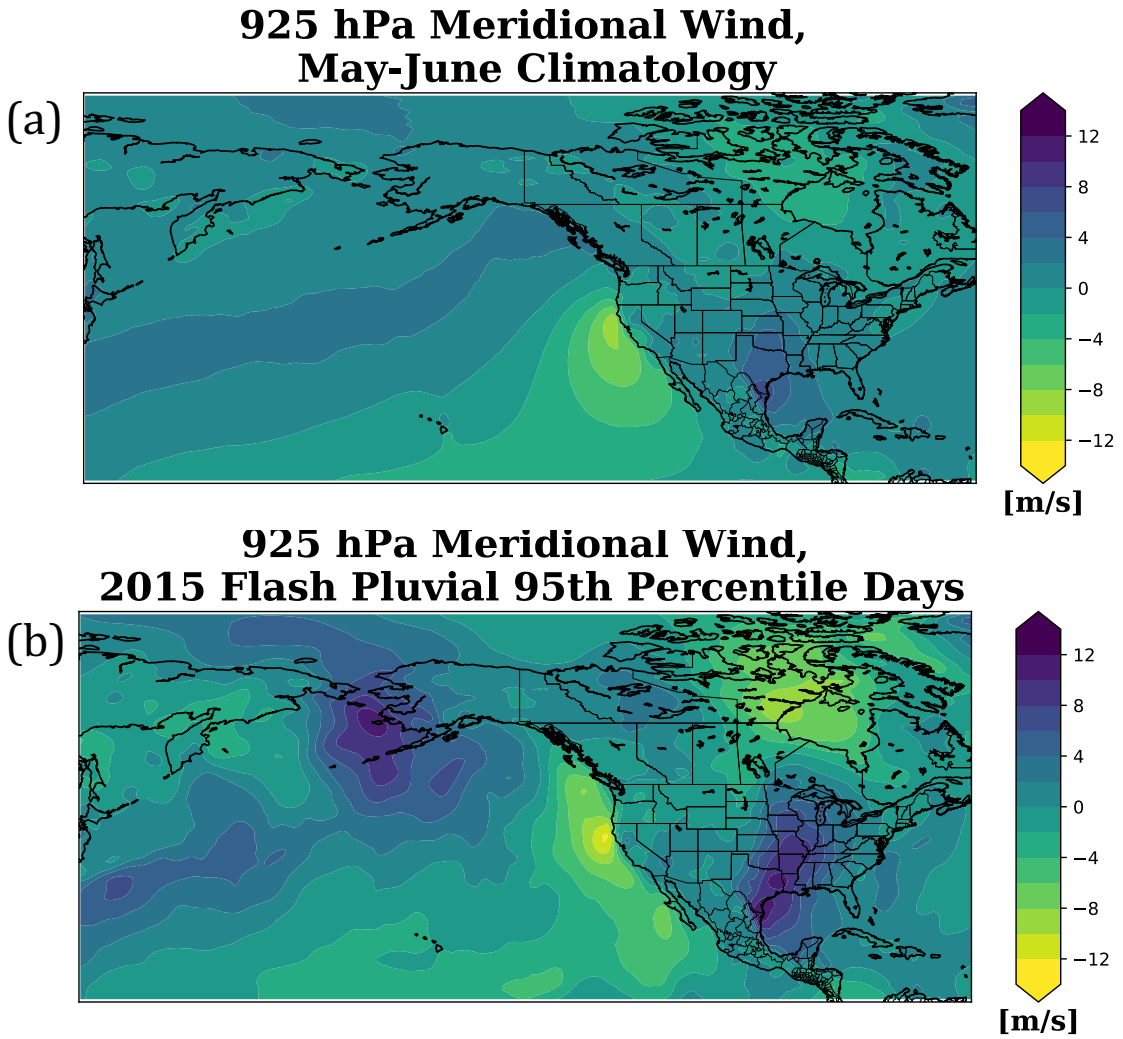

Figure 3.13: (a) Mean 925 hPa meridional wind for May-June (b) Composite of 925 hPa meridional wind for days exceeding the 95th percentile significance criteria.

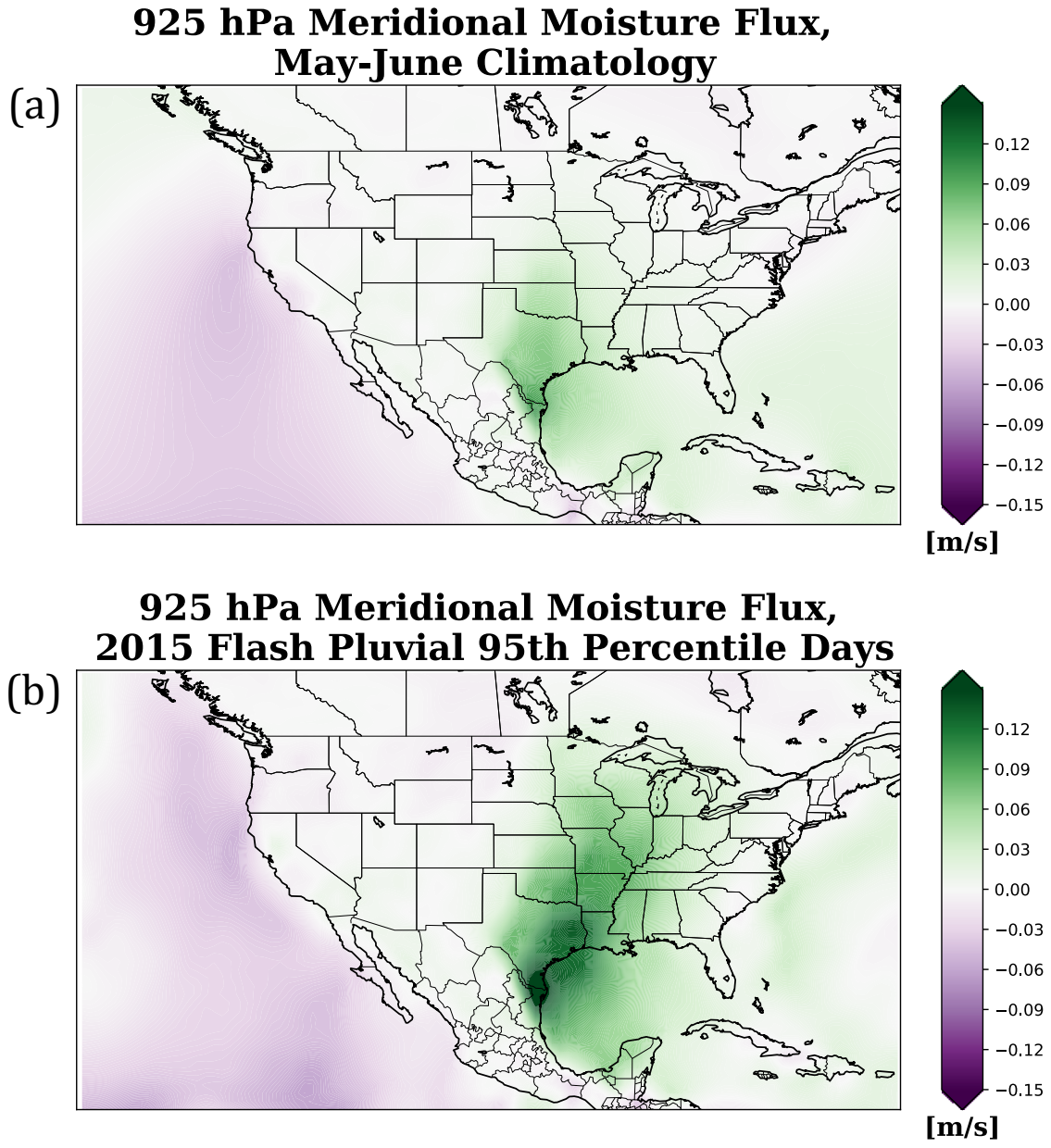

Figure 3.14: (a) Mean 925 hPa meridional moisture flux for May-June (b) Composite of 925 hPa meridional moisture flux for days exceeding the 95th percentile significance criteria.

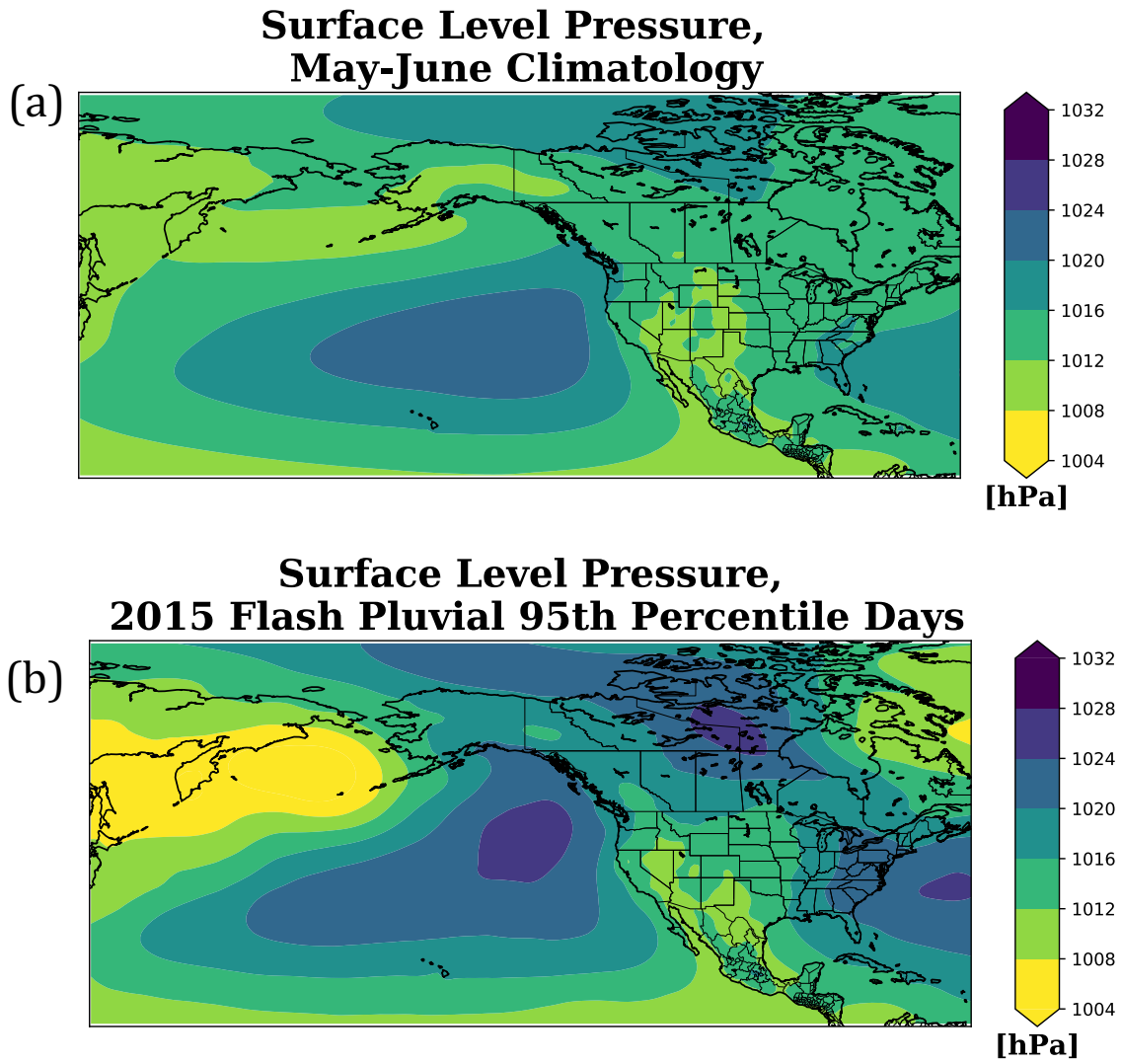

Figure 3.15: (a) Mean surface level pressure for May-June (b) Composite of surface level pressure for days exceeding the 95th percentile significance criteria.

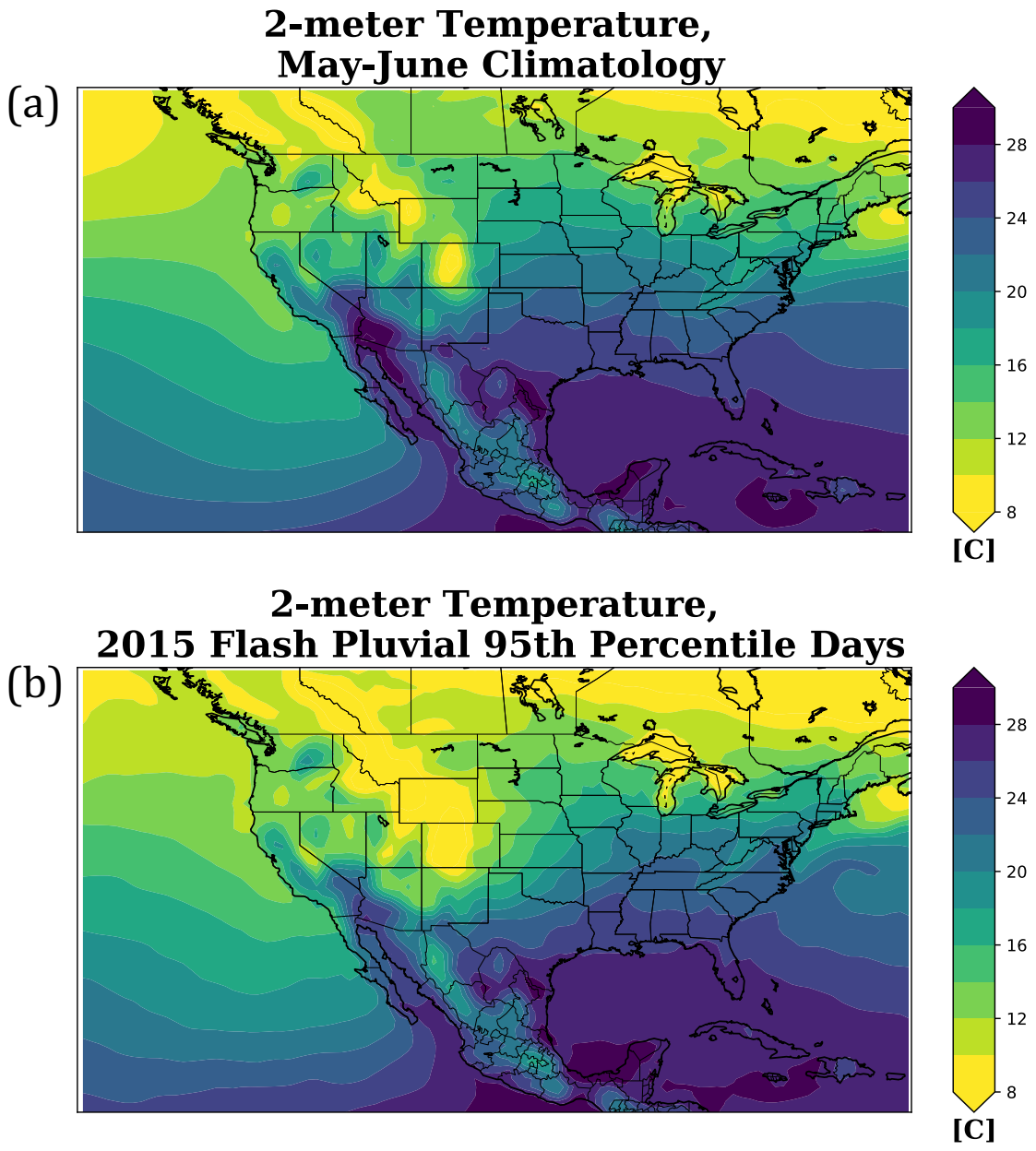

Figure 3.16: (a) Mean 2-meter temperature for May-June (b) Composite of 2-meter temperature for days exceeding the 95th percentile significance criteria.

Specific humidity and meridional wind were combined to compute the meridional moisture flux (v'q') which yielded the greatest anomaly across the western SGP and Kansas (Fig. 3.23a). Two surface variables, surface-level pressure and two-meter temperature, were also investigated. The surface pressure composite did not reveal any consistent anomalies, but rather showed a general slightly positive anomaly across most of the continental U.S (Fig. 3.24a). This anomaly was stronger in the eastern US. Additionally, temperature anomalies yielded a gradient of temperature across the SGP with colder anomalies to the west and warmer anomalies to the east (Fig. 3.25a).

3.3.3 Patterns for Significant Precipitation Days

Composites conditions of only the significant precipitation days yield many of the same features, but at a much greater magnitude. Beginning aloft with the zonal wind composite, the same strong subtropical jet is observed in Figure 3.17b. Two differences between the original and criteria composites stand out: (1) a stronger wind anomaly and (2) the shape of the anomalous wind pattern is oriented from southwest to northeast from Hawaii to central Texas. The upper level meridional winds, shown in Figure 3.18b, again show a similar pattern with a greater magnitude in the wind anomaly. Both of these features are depicted in the total wind vector anomalies in Figure 3.19b, but the combination of the zonal and meridional components helps to illustrate the westward component of the meridional winds off the Gulf of Mexico. The total wind plot also displays two significant synoptic features: a cyclone over the the eastern Pacific ocean and an anticyclone over the northeastern US. Geopotential height anomalies at 500 hPa confirm these two features (Fig. 3.20b), displaying both the low over the Pacific and high over the eastern US, but also a strong, anomalous low over the southwestern US and a driving force for dynamic ascent over the SGP.

Near the surface, the low level winds displayed a similar pattern to the overall composites, but with greater magnitudes. For example, the magnitude of the wind anomaly in the low level jet in Figure 3.21b exceeds one standard deviation extending through Louisiana

and eastern Texas. The criteria composite of specific humidity, seen in Figure 3.22b, still displays anomalous dry air over the southeastern U.S., but the pattern over the SGP shows a maximum in specific humidity over east-central Texas and southern Texas. Additionally, the meridional moisture flux, seen in Figure 3.23b, exhibits a similar pattern to the specific humidity whereby the maximum in moisture flux was located over western Texas, but the majority of the SGP domain experienced an anomaly of 0.8 or more standard deviations.

At the surface, the composite of surface pressure shown in Figure 3.24b yielded a very different pattern than the full period composites. In the composite of significant precipitation days, a surface low pressure anomaly was centered over southern Texas and the Mexico border, with a general negative anomaly extending through most of Texas, into New Mexico. This is accompanied by surface high pressure anomalies on both the west over the eastern Pacific and Baja California and over the entire eastern US. The two-meter temperature anomalies also display a significant difference from the entire period with a strong anomalously cold air mass located over the area northwestern of the SGP and a much warmer anomalous airmass to the east (Fig. 3.25b).

3.4 Integrated Vapor Transport and Atmospheric River Results

To address moisture transport across all levels of the atmosphere, integrated vapor transport (IVT) was investigated to determine the source of moisture. Further, in conjunction with IVT, atmospheric river (AR) events during the flash pluvial period were investigated. Daily IVT and AR events were investigated for each of the significant precipitation events specified by the significant precipitation day criteria (Fig. 3.26). It was found that the events did not all include AR events, but rather some events included AR activity while others did not; May 6th and 9th exhibited atmospheric rivers in the proximity of the SGP and Gulf of Mexico while May 24th, the most significant day of the flash pluvial, did not include an AR.

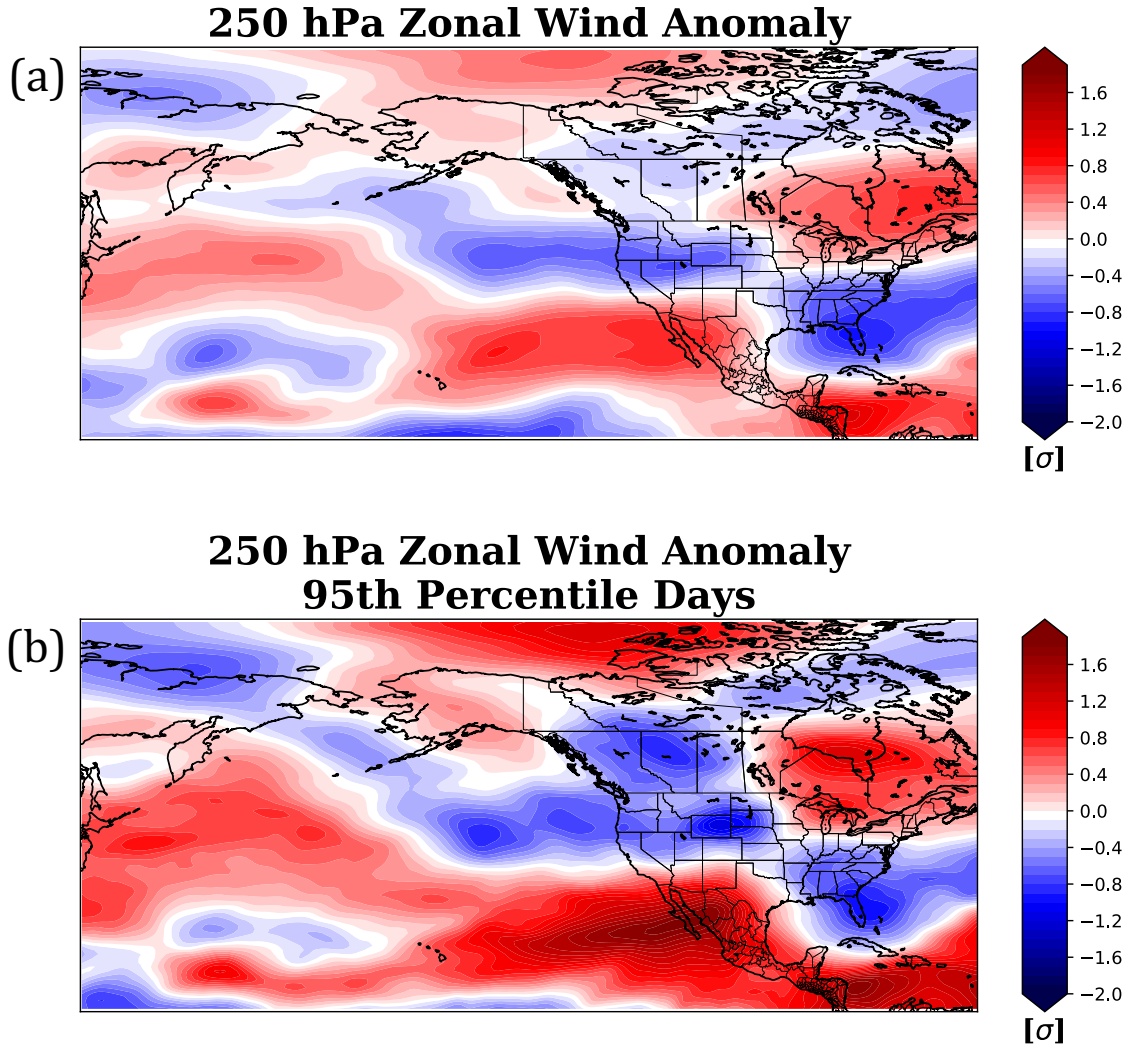

Figure 3.17: (a) Composite of 250 hPa zonal wind anomaly for 5 May-19 June (b) Composite of 250 hPa zonal wind anomaly for days exceeding the 95th percentile significance criteria.

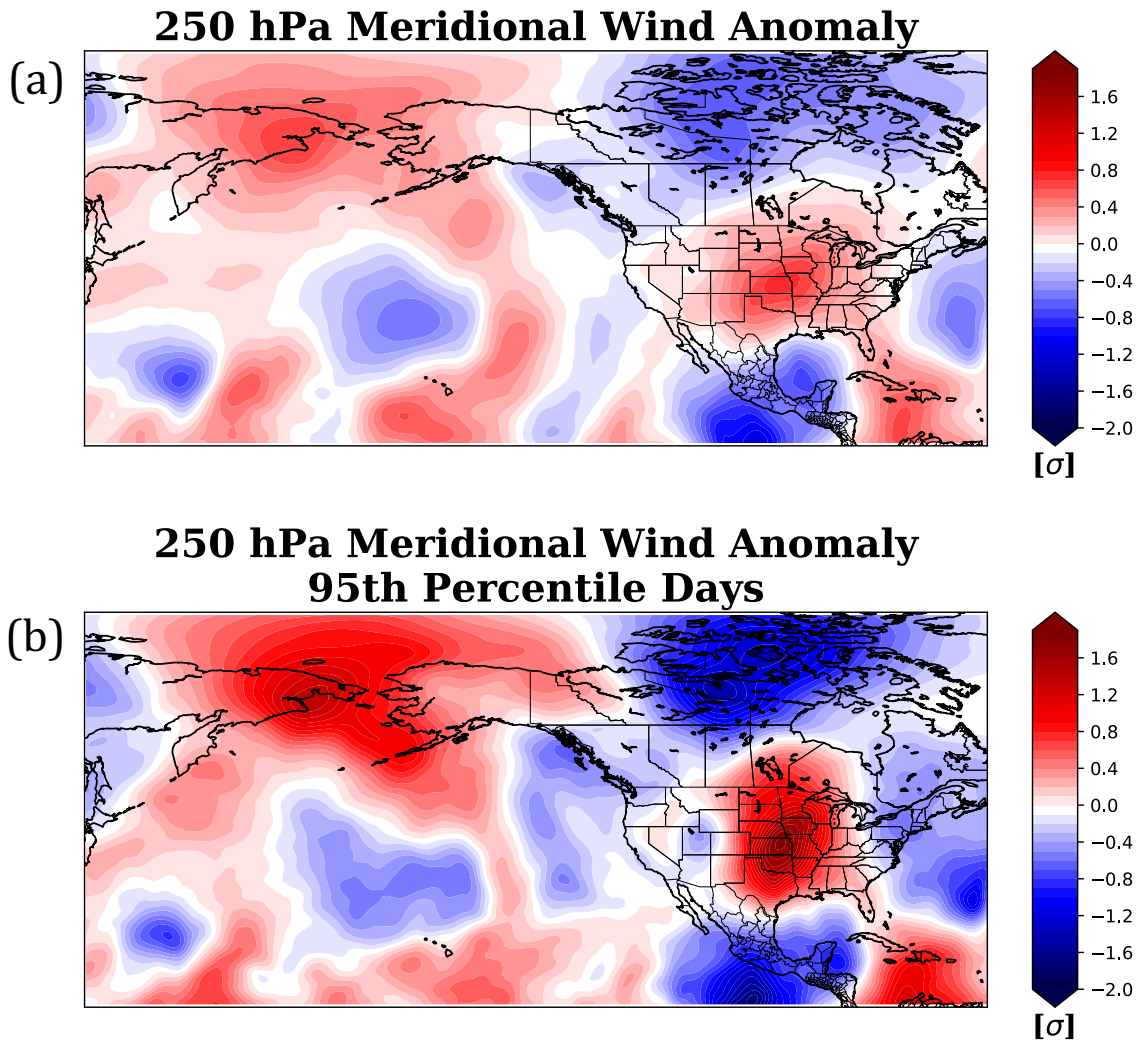

Figure 3.18: (a) Composite of 250 hPa meridional wind anomaly for 5 May-19 June (b) Composite of 250 hPa meridional wind anomaly for days exceeding the 95th percentile significance criteria.

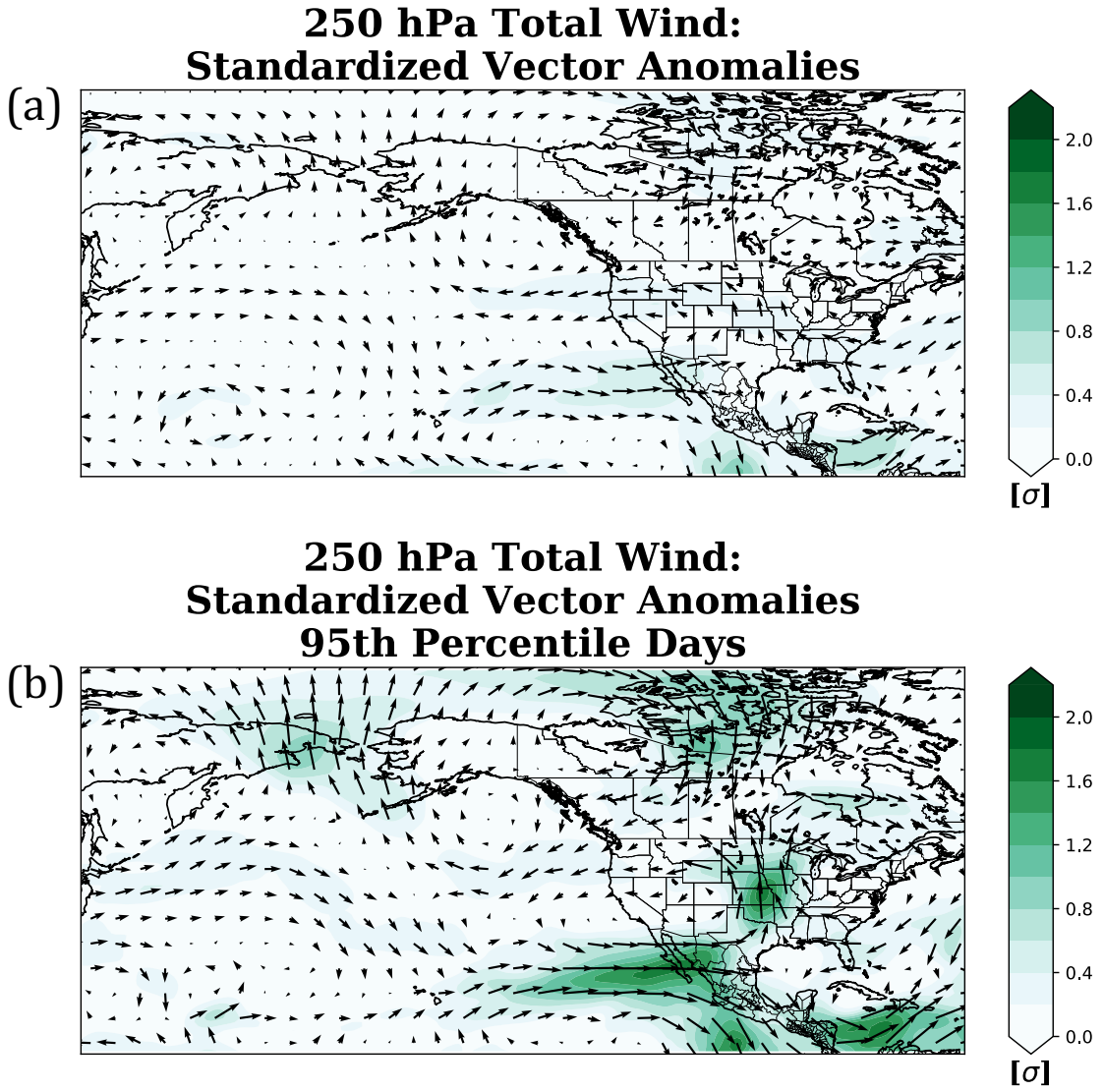

Figure 3.19: (a) Composite of 250 hPa total wind anomaly for 5 May-19 June (b) Composite of 250 hPa total wind anomaly for days exceeding the 95th percentile significance criteria.

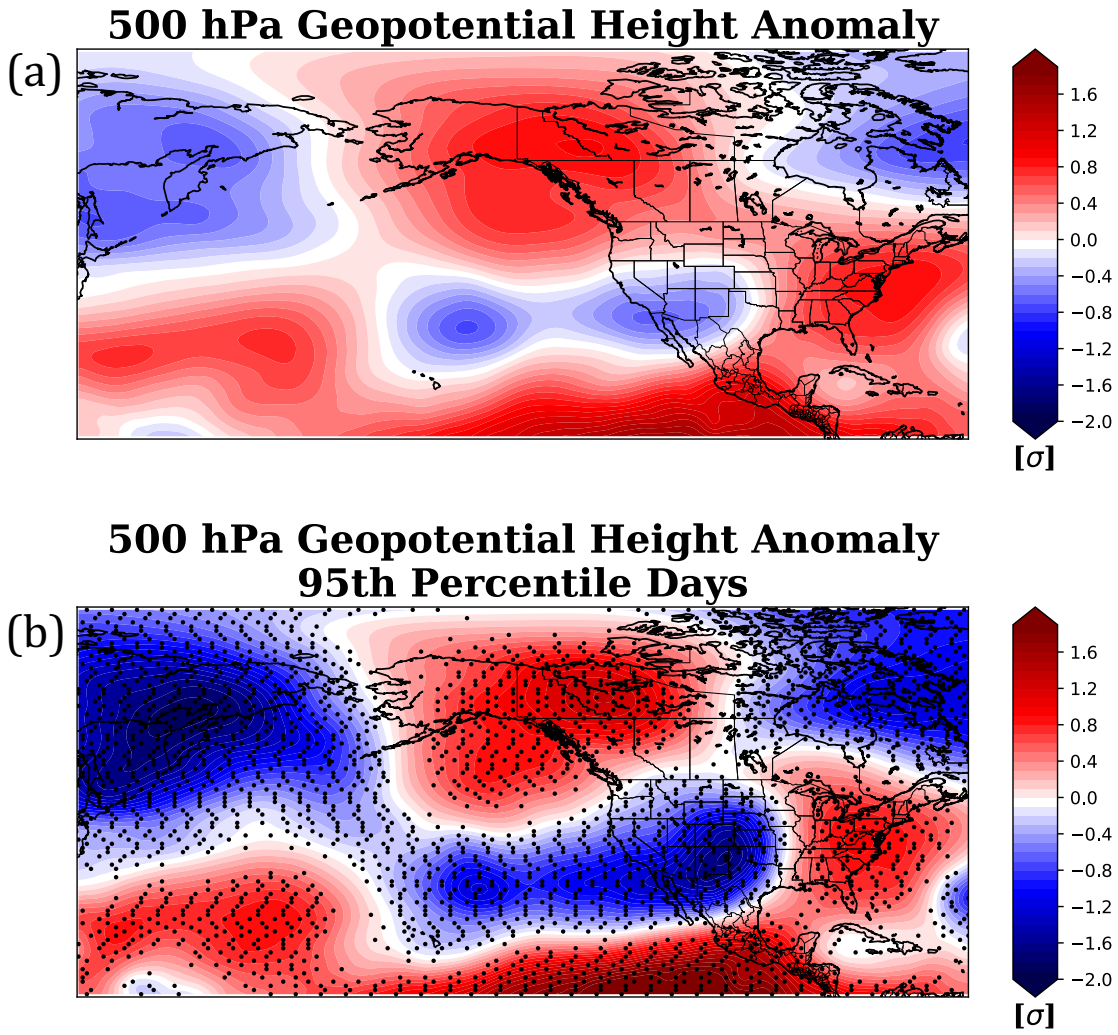

Figure 3.20: (a) Composite of 500 hPa geopotential height anomaly for 5 May-19 June (b) Composite of 500 hPa geopotential height anomaly for days exceeding the 95th percentile significance criteria.

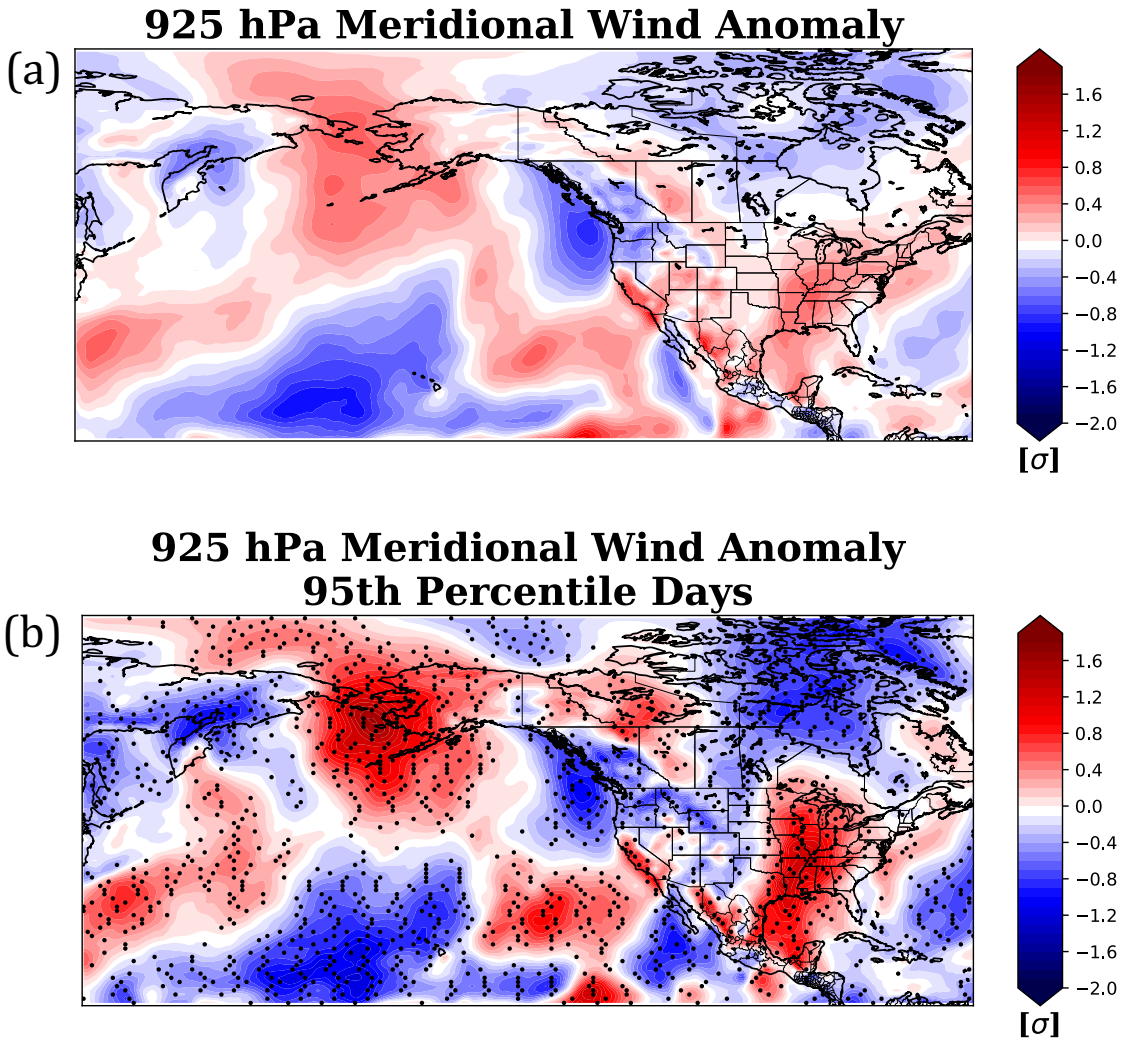

Figure 3.21: (a) Composite of 925 hPa meridional wind anomaly for 5 May-19 June (b) Composite of 925 hPa meridional wind anomaly for days exceeding the 95th percentile significance criteria.

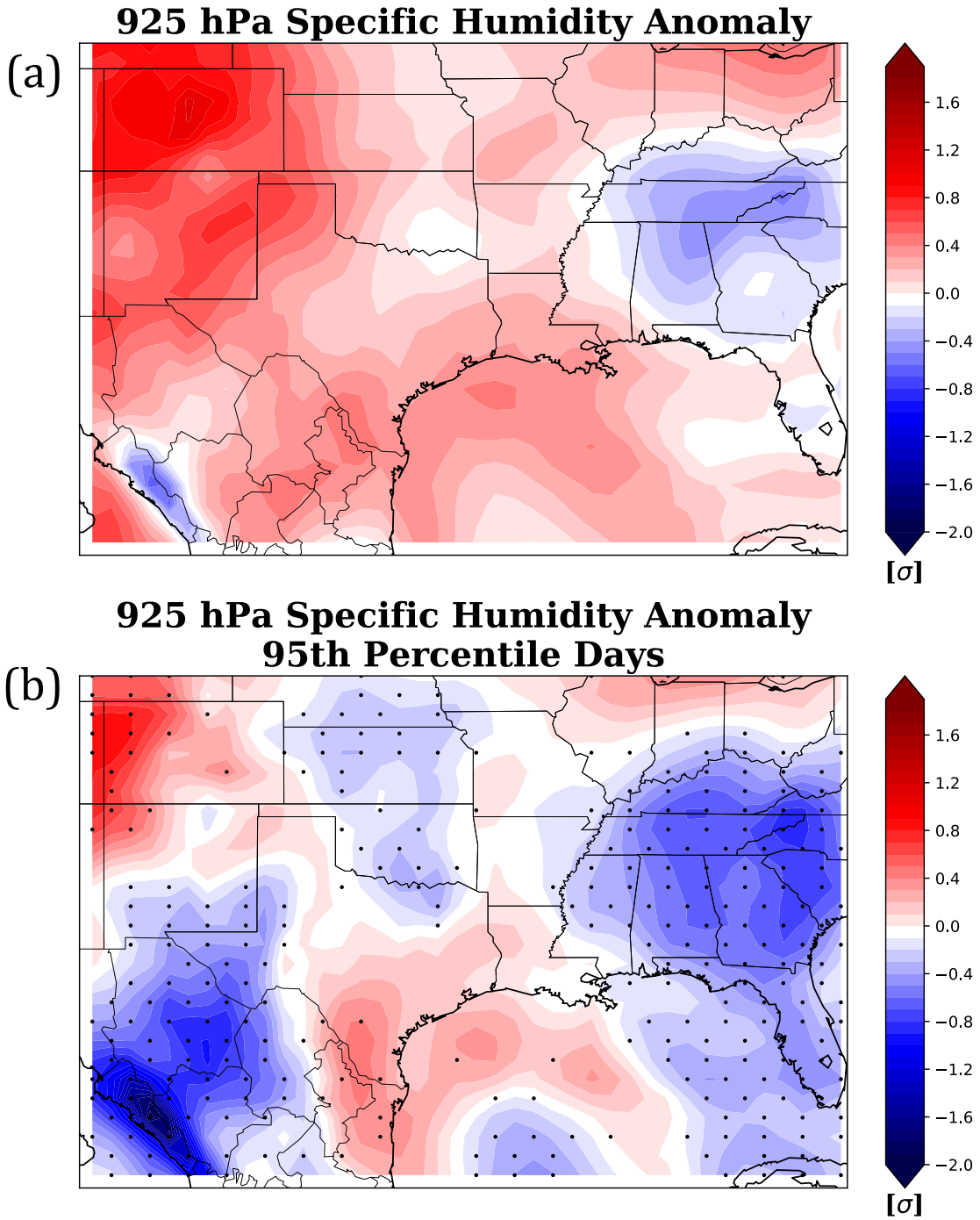

Figure 3.22: (a) Composite of 925 hPa specific humidity anomaly for 5 May-19 June (b) Composite of 925 hPa specific humidity anomaly for days exceeding the 95th percentile significance criteria.

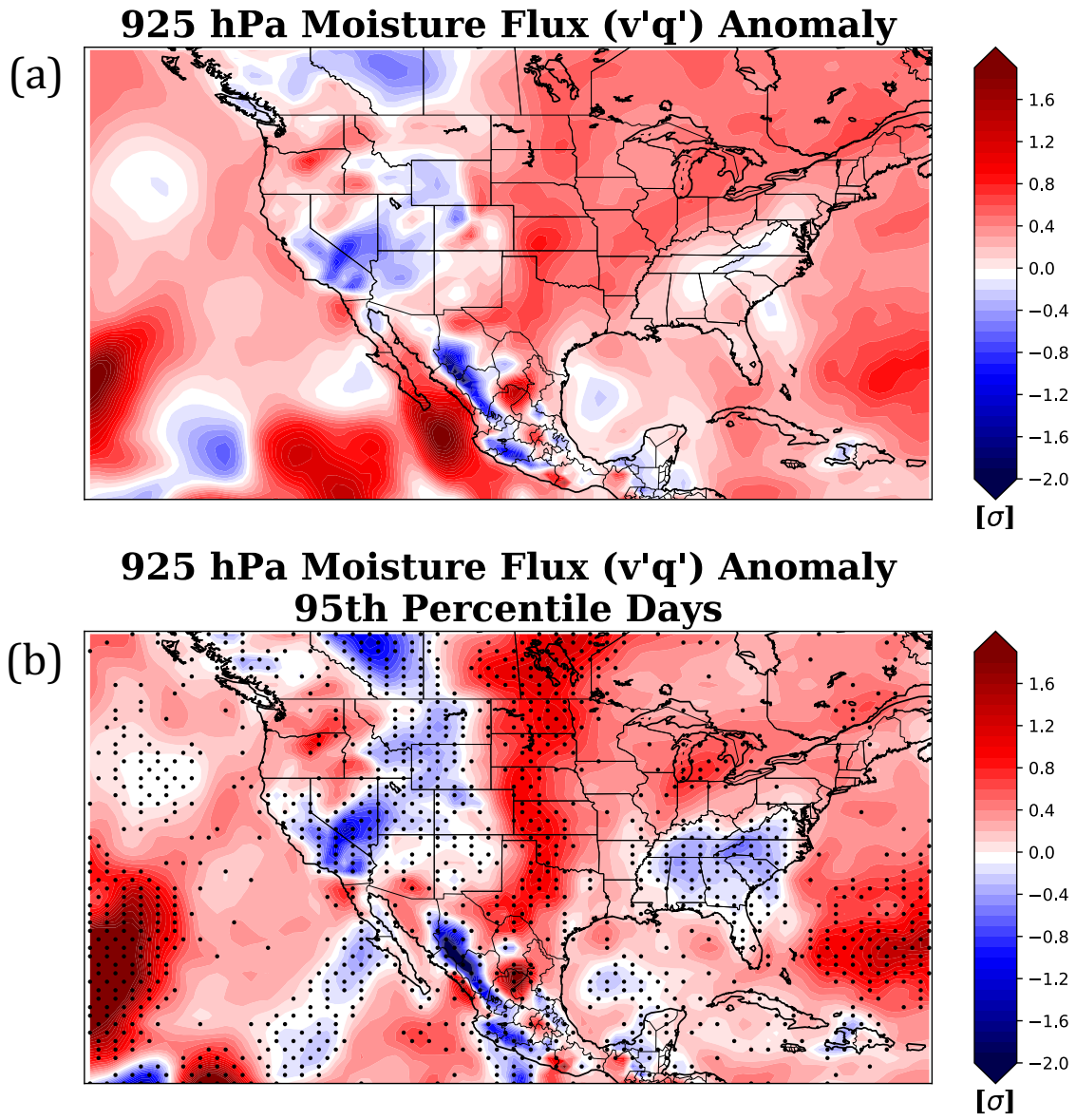

Figure 3.23: (a) Composite of 925 hPa moisture flux anomaly for 5 May-19 June (b) Composite of 925 hPa moisture flux anomaly for days exceeding the 95th percentile significance criteria.

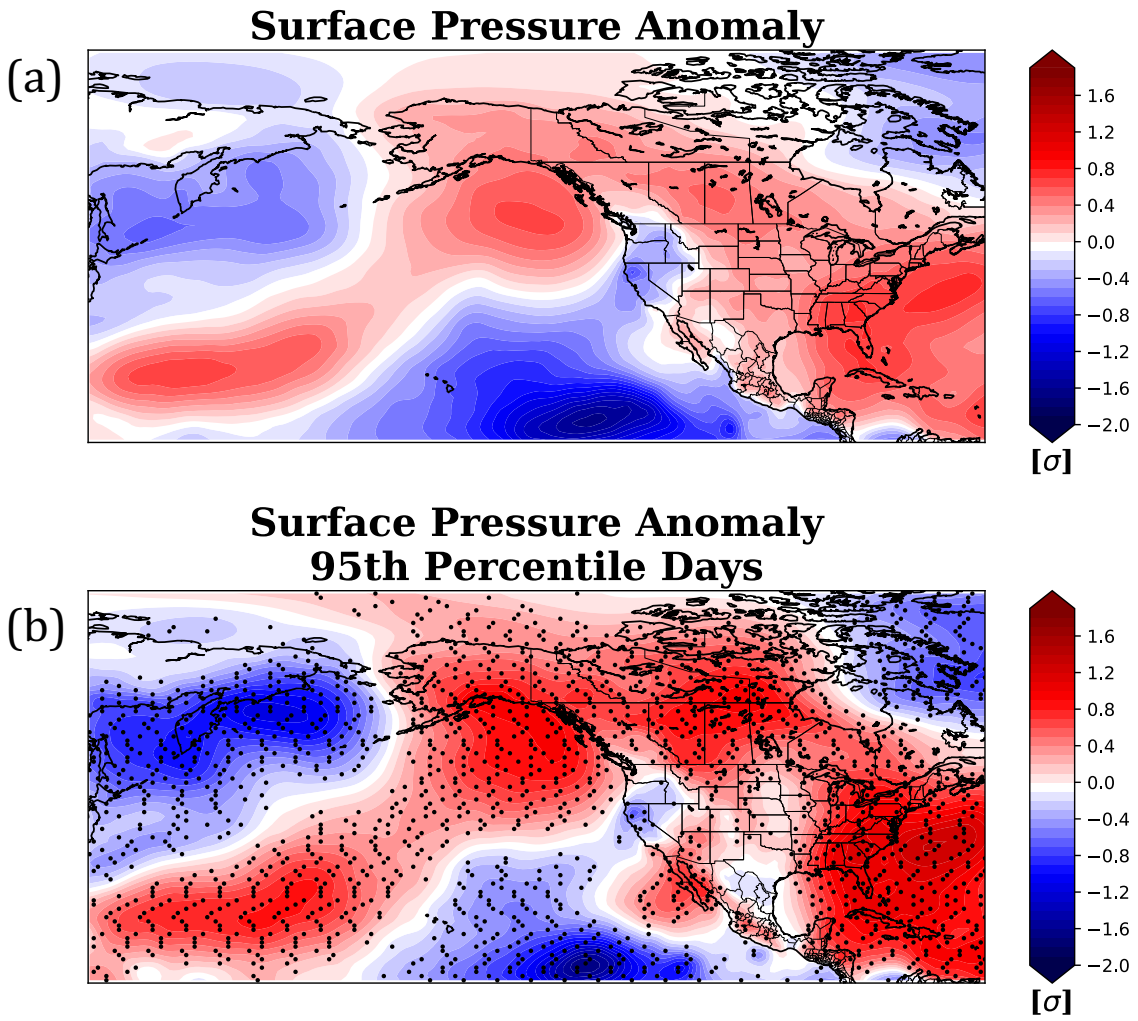

Figure 3.24: (a) Composite of surface level pressure anomaly for 5 May-19 June (b) Composite of surface level pressure anomaly for days exceeding the 95th percentile significance criteria.

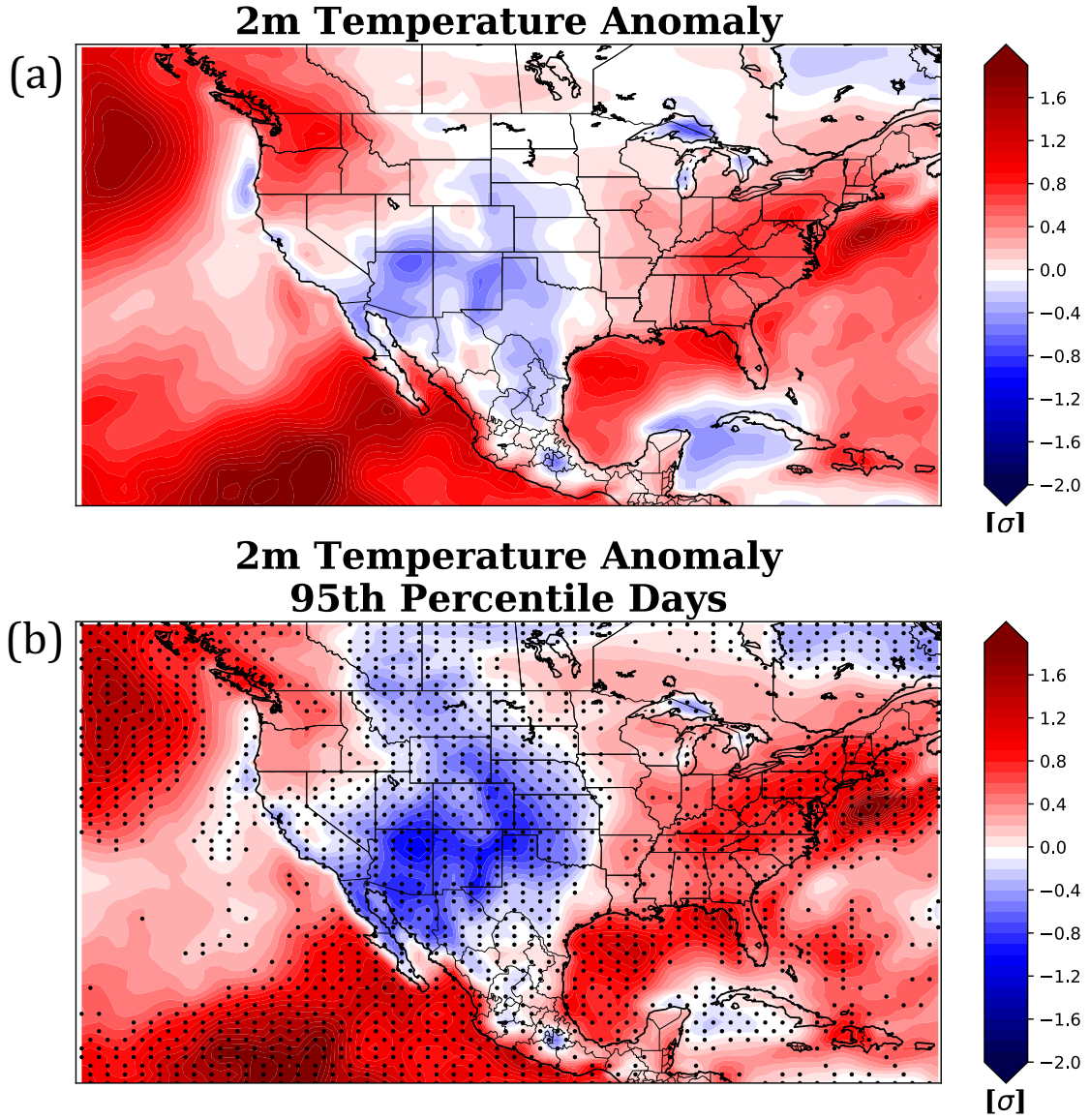

Figure 3.25: (a) Composite of 2-meter temperature anomaly for 5 May-19 June (b) Composite of 2-meter temperature anomaly for days exceeding the 95th percentile significance criteria.

While not all events included a defined AR, the events included a defined pattern in IVT. As such, it was generally seen that there was a maximum in IVT over land along the gulf coast extending into the SGP and lower Mississippi River Valley. This is illustrated in the composite IVT (Fig. 3.27), which shows a clear maximum along the Texas coast, extending into the Red River region. To diagnose moisture transport in the Pacific and Gulf of Mexico, a composite of IVT throughout the entire temporal domain was created (Fig. 3.28). This composite shows a similar pattern to the criteria composite, but with weaker magnitudes.

IVT was examined for six of the significant precipitation cases, shown in Figure 3.29. The pattern observed in the composite of IVT (Fig. 3.27) of enhanced IVT off the Gulf of Mexico can be observed in each of these cases, with varying strength. This pattern is stronger in 6, 9, 24 May and 13 June, and weak in 14 and 29 May. An interesting second feature in the case studies is an area of elevated IVT along the coast of South Carolina on 9 May; this is an artifact resulting from tropical storm Ana occurring concurrently with the significant precipitation over the SGP in early May.

Atmospheric rivers were investigated for the entire 46 day period of May 5th - June 18th of 2015. Throughout this time, 17 days included AR events impacting SGP. Of these events, 11 showed ARs over the Gulf of Mexico, and 8 showed ARs over the eastern Pacific Ocean, converging on the SGP. Two of these events showed AR activity over both the Gulf of Mexico and Pacific Ocean. While this implies that the anomalous moisture in the SGP was impacted by moisture transport from both the Pacific and Gulf of Mexico, the dates of the Gulf AR events corresponded more with the significant rainfall events. The only significant event that did not include either a Gulf AR or a Pacific AR was the May 24th event; a Pacific AR was present the day before the event.

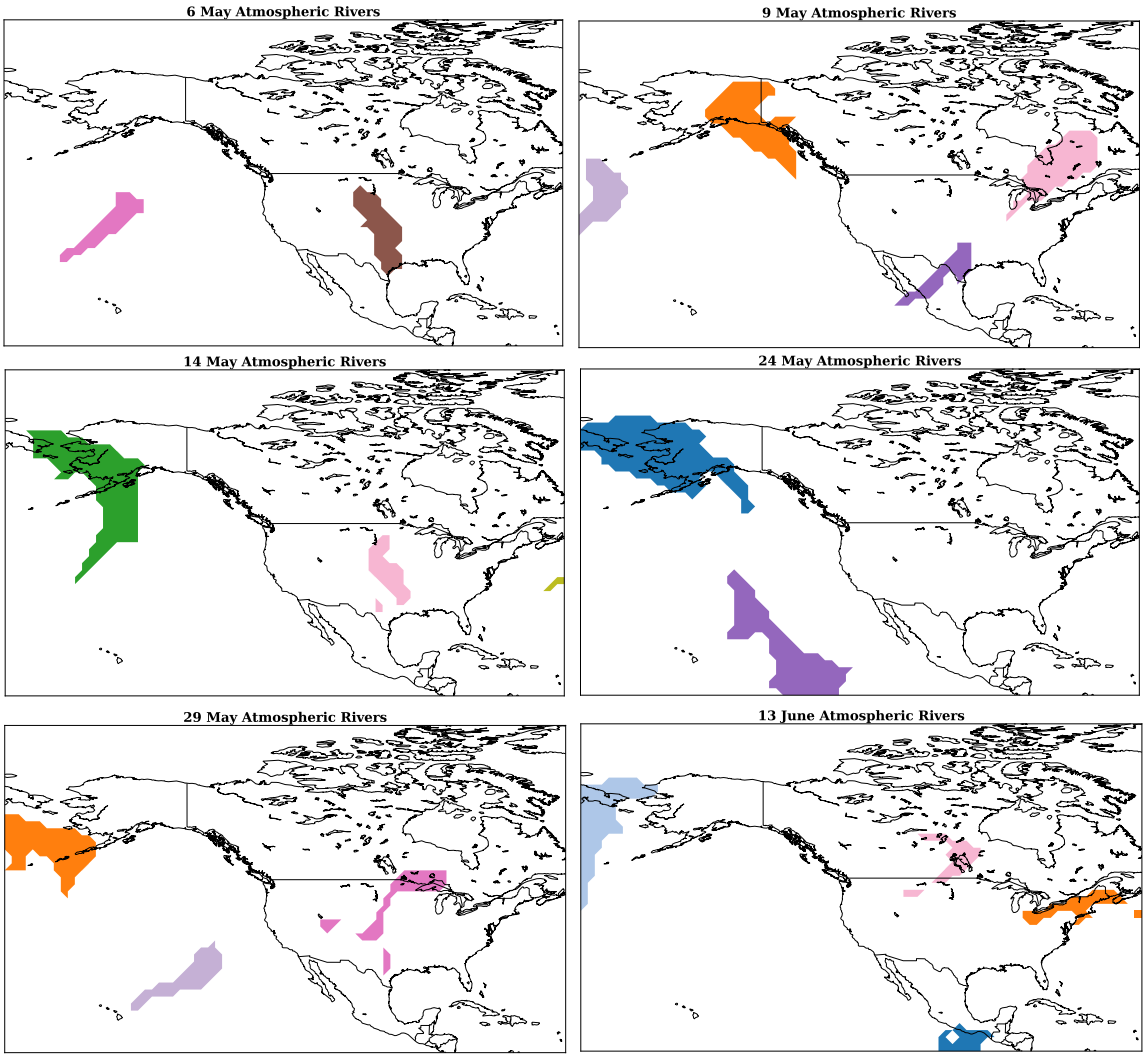

Figure 3.26: Atmospheric rivers detected by the Guan and Waliser (2015); Guan et al. (2017) detection algorithm, displayed for 6, 9, 14, 24, 29 May and 13 June.

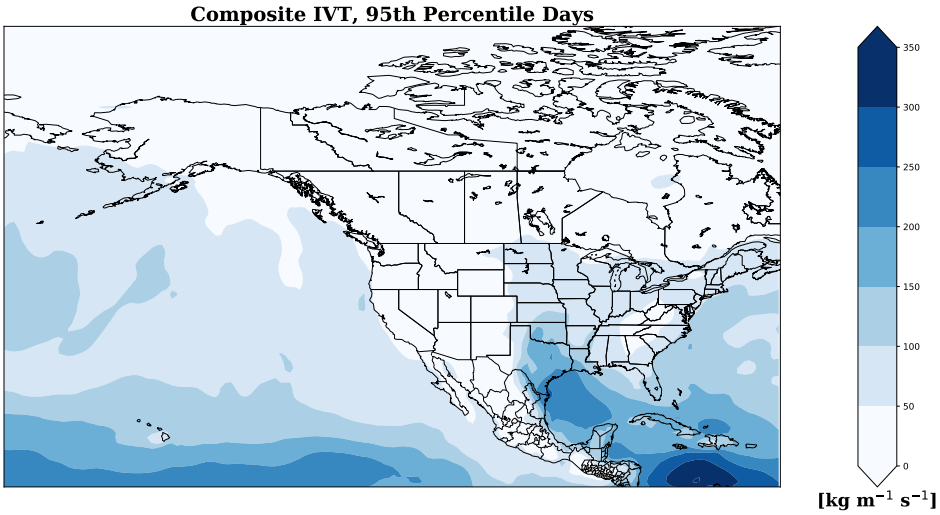

Figure 3.27: Composite of integrated vapor transport for days exceeding the 95th percentile significance criteria.

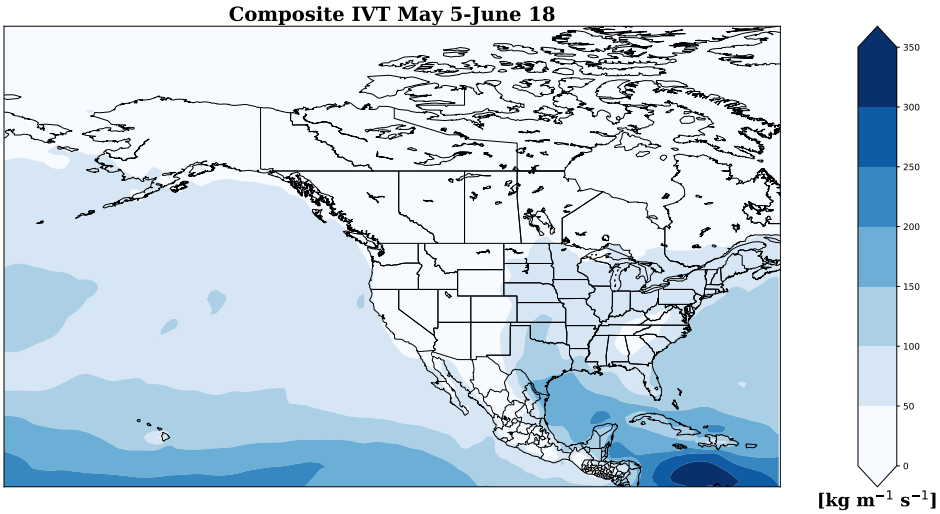

Figure 3.28: Composite of integrated vapor transport for 5 May-19 June.

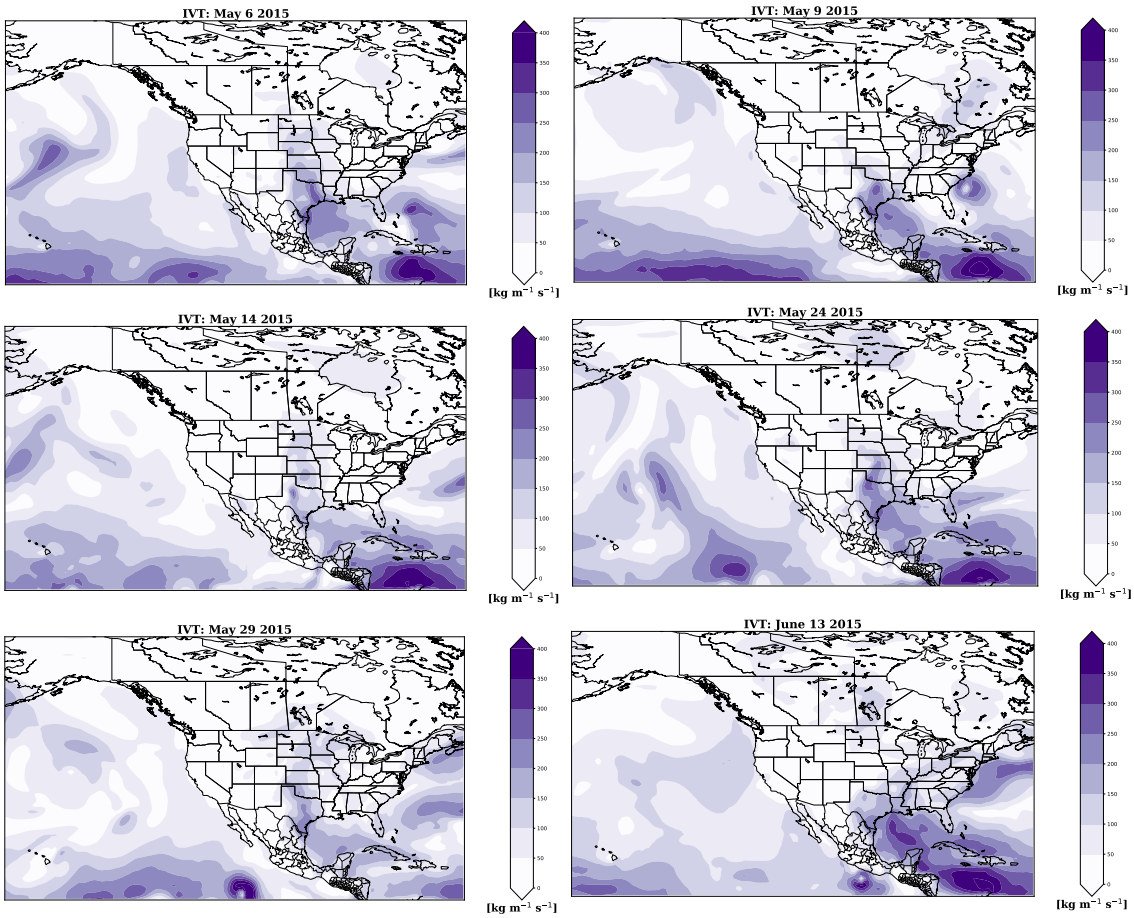

Figure 3.29: Integrated water vapor transport displayed for 6, 9, 14, 24, 29 May and 13 June.

3.5 Precipitation Efficiency Results

A composite of precipitation efficiency was computed for the 95th percentile significant precipitation dates (Fig. 3.30) and for the 90th percentile non-tropical significant precipitation dates (Fig. 3.31). A composite mean of the significant precipitation dates yielded relatively low precipitation efficiencies compared to individual cases, with a large region of precipitation efficiency exceeding 105% across and north of the Red River, extending through the TX panhandle and central to southern Oklahoma. This is due to the varied spatial extent of the significant precipitation dates. Despite the spatial variation of the cases, the composite highlights southern Oklahoma and the Red River as an area that saw repeated days with large precipitation efficiency. This region was colocated with the maximum in precipitation for the flash pluvial. Seeing this colocation implies that the extreme precipitation was the highly efficiently precipitation. It is challenging to determine a definition of normal precipitation efficiency due to a variety of computation methods in previous work (Doswell et al. 1996; Market et al. 2003; Sui et al. 2007). A theoretical definition of 100% efficiency is that all available moisture is rained out, and any value above 100% is indicative of additional moisture flux contributing to elevated precipitation efficiency. For this reason, this investigation focuses largely on where, relative to each day, the precipitation was most efficient.

Precipitation efficiency is also plotted for several of the 95th percentile, non-tropically forced, significant precipitation dates in Figure 3.32. The plotted cases are elaborated on in Section 3.6. Most significant cases saw localized areas of precipitation efficiency exceeding 250%. Two dates have smaller regions of high precipitation efficiency, with more widespread low precipitation efficiency: 14 May and 29 May. These two days saw more widespread precipitation efficiency around 140% or lower. May 6, 9, and 24 each saw several maxima of precipitation efficiency up to 300%. These were located along the storm tracks for each day, and nearly colocated with the precipitation maxima for each day. Some variations were seen in these precipitation efficiency maxima and precipitation maxima, in

part due to the coarser gridding used for computing precipitation efficiency. One case in particular, May 9, saw the most efficient precipitation not being colocated with the greatest precipitation for the day. This demonstrates that the relationship between extreme precipitation and efficient precipitation is complex and indirect. While several cases illustrated the variables being paired, more factors have a role in causing the extreme precipitation.

Precipitation efficiency was plotted for TD Bill in Figure 3.33. In the period of June 17-18, Bill made its way north across Texas and then was nearly stationary over the Red River. For June 17, relatively low precipitation efficiency was computed along the path northward. There was a maximum of precipitation efficiency on the coastline near where Bill made landfall on Matagorda Island (NHC, `https://www.nhc.noaa.gov/data/tcr/AL022015_Bill.pdf`). The relatively low precipitation efficiency, approximately 120% throughout central TX accompanied the weakening of Bill. The precipitation efficiency signature changed June 18, as the precipitation associated with Bill became greater as it reached Oklahoma border. While Bill did not reintensify in winds or via a drop in pressure, it maintained tropical appearance with more efficient precipitation than the previous day and a large region along the Red River experienced precipitation efficiency in excess of 450%. Further, a broad area stretched between the Dallas-Fort Worth metropolitan area to the Oklahoma City metropolitan with over 200% precipitation efficiency. This highly efficient precipitation fell onto a part of the flash pluvial domain that already was a spatial maximum in rainfall from earlier in the season.

3.6 Significant Case Studies

In order to investigate the observed conditions and features that occur during the flash pluvial event, several of the top precipitation events were selected for further investigation. Some of the most significant non-tropical cases are 6 May, 9 May, 14 May, 24 May, 29 May, and 13 June. The first five of these cases were selected for being five most significant dates, and 13 June was included due to its temporal separation from the other significant

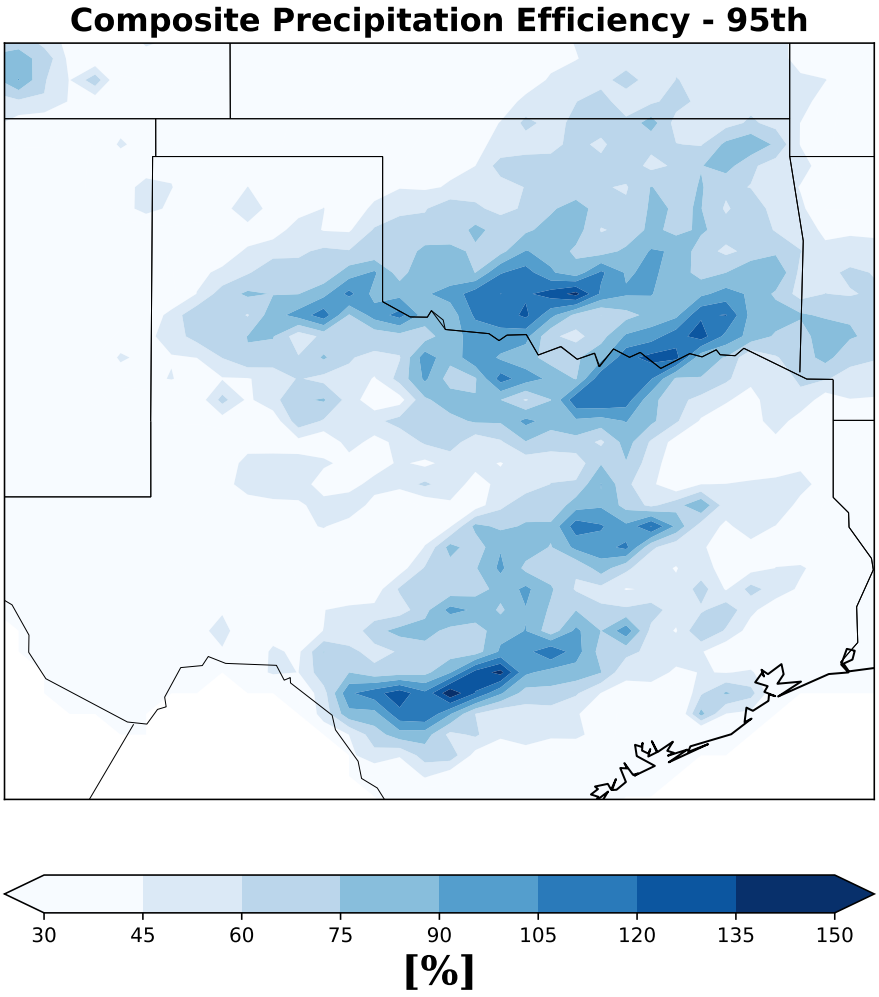

Figure 3.30: Composite of precipitation efficiency for days exceeding the 95th percentile significance criteria.

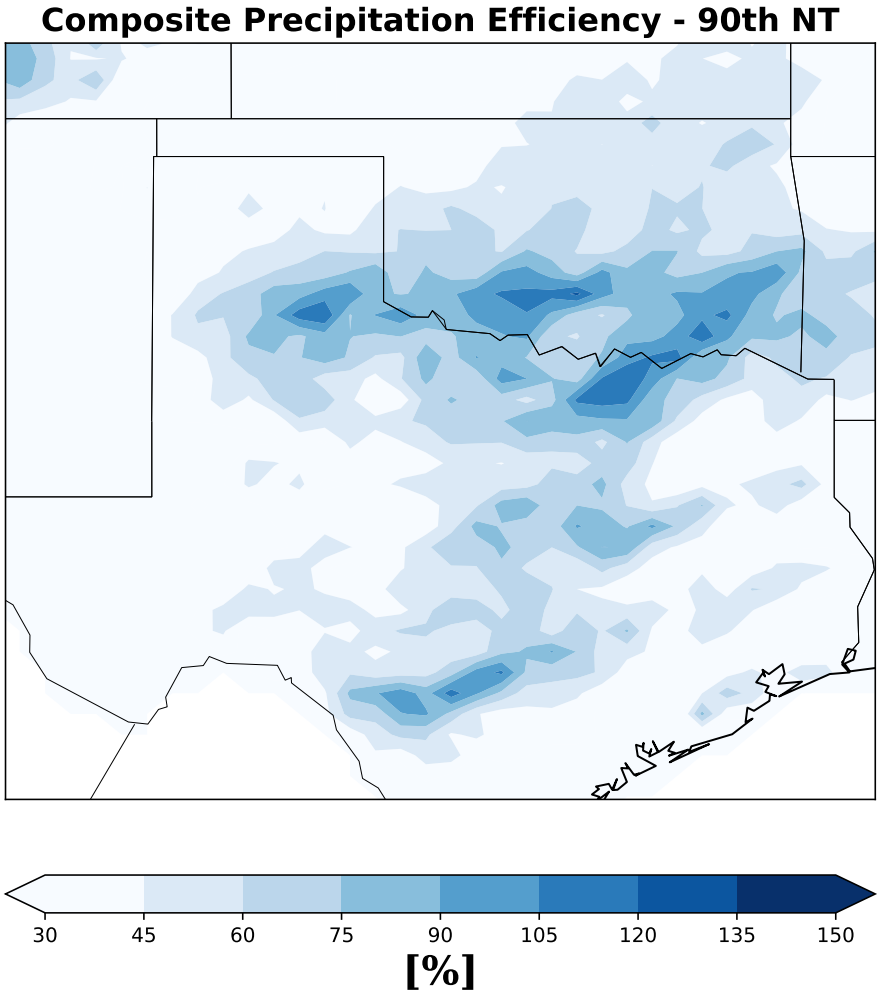

Figure 3.31: Composite of precipitation efficiency for days exceeding the 90th percentile, nontropical significance criteria.

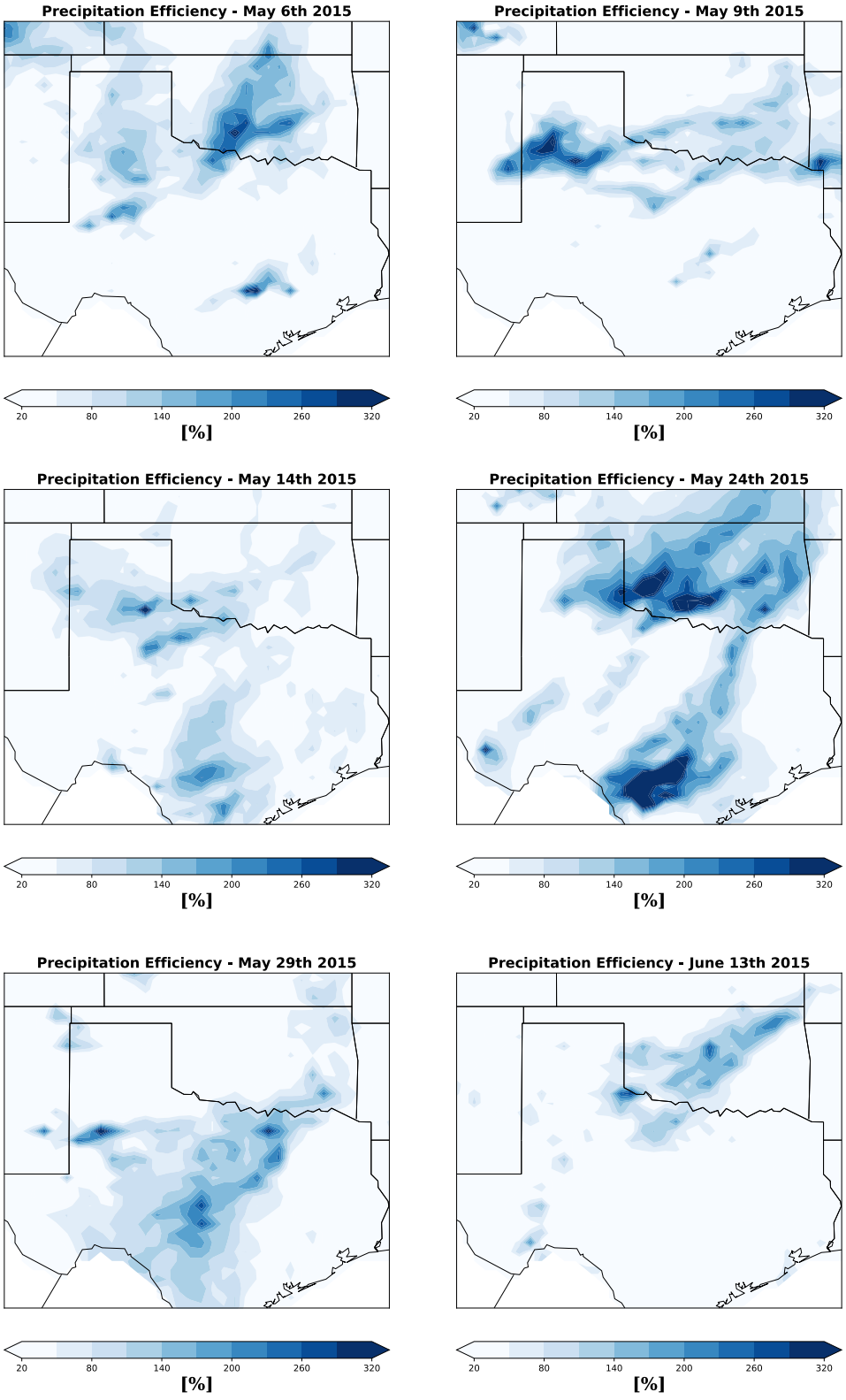

Figure 3.32: Precipitation efficiency displayed for 6, 9, 14, 24, 29 May and 13 June.

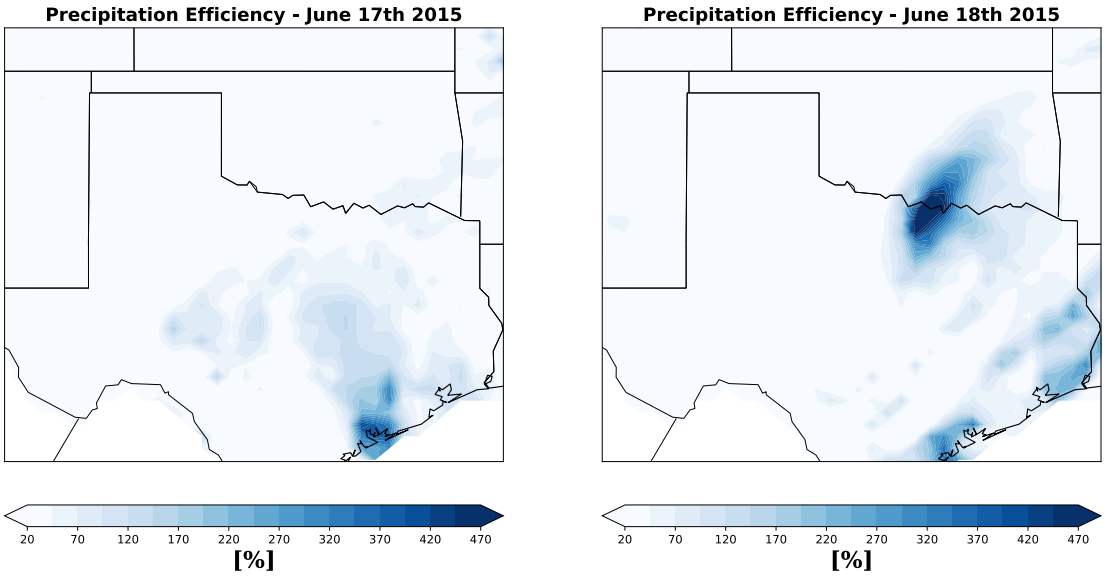

Figure 3.33: Precipitation efficiency plotted for 17-18 June, while TD Bill was over Texas and Oklahoma.

cases. There were two weeks between 13 June and the other cases that were significant at the 95th percentile level. These cases, as well as T.D. Bill, are investigated as case studies.

3.6.1 6 May 2015

The fourth most significant precipitation event in the flash pluvial event was 6 May 2015, with a broad area of Oklahoma and the Texas panhandle being impacted. A large part of central Oklahoma and the area near Austin TX saw over 6 cm of rainfall (Fig. 3.34a). The Texas panhandle saw widespread areas exceeding 3 cm of rainfall, with small areas up to 5 cm. This led to the Texas panhandle having broad areas exceeding 4 standard deviations (Fig. 3.34b), similar to the large precipitation anomalies over central OK and Austin, TX. A time series of the precipitation occurring in Medicine Park, OK and Okemah, OK (MEDI and OKEM Mesonet sites) shows over 8 cm falling in the afternoon to overnight hours (Fig. 3.35).

The atmospheric sounding launched from Norman, OK (OUN) at 0000 UTC on 6 May 2015 (Fig. 3.36) measured precipitable water of 39.25 mm (1.55 in) which exceeded the

daily maximum moving average displayed in the Storm Prediction Center (SPC) sounding climatology.

The Weather Prediction Center (WPC) surface analysis 0000 UTC 6 May displayed a surface low pressure in southeast New Mexico, as well as a surface low pressure system in eastern Colorado, associated with frontal boundaries (Fig. 3.37a). A radar image shortly after this analysis, Figure 3.37b, shows two broad areas of precipitation at 0200 UTC. There was a line of storms moving across the Texas panhandle, as well as a broad region of precipitation across central Oklahoma.

3.6.2 9 May 2015

The fifth most significant precipitation day in the flash pluvial event is 9 May 2015. This day saw impacts across Oklahoma and northern Texas (Fig. 3.38a). Many areas experienced between 3 to 7 cm of rain in a single day. Daily precipitation anomalies exceeded four standard deviations in many areas (Fig. 3.38b). A time series of the precipitation occurring in Oklahoma City, OK (OKCE Mesonet site) shows over 10 cm falling between 0000UTC and 0400 UTC (Fig. 3.39).

The atmospheric sounding launched from Norman, OK (OUN) at 00 UTC on 9 May 2015 and was timed very closely with the occurrence of the storm (Fig. 3.40). It measured precipitable water of 41.96 mm (1.65 in), which exceeds the daily maximum moving average displayed in the Storm Prediction Center (SPC) sounding climatology.

The 12 UTC 8 May 2015 WPC surface analysis (Fig. 3.41a) shows a surface low pressure system in central Colorado. Additionally, it shows a dry line set up west of the SGP along eastern New Mexico as well as a cold front set up on the northern side of the domain, extending through the Texas panhandle and northern Oklahoma. These features provided the force for lifting and storm initiation ahead of the linear MCS that produced the prolific rainfall (MCS seen in Fig. 3.41b). Following the strong line of storms, towards

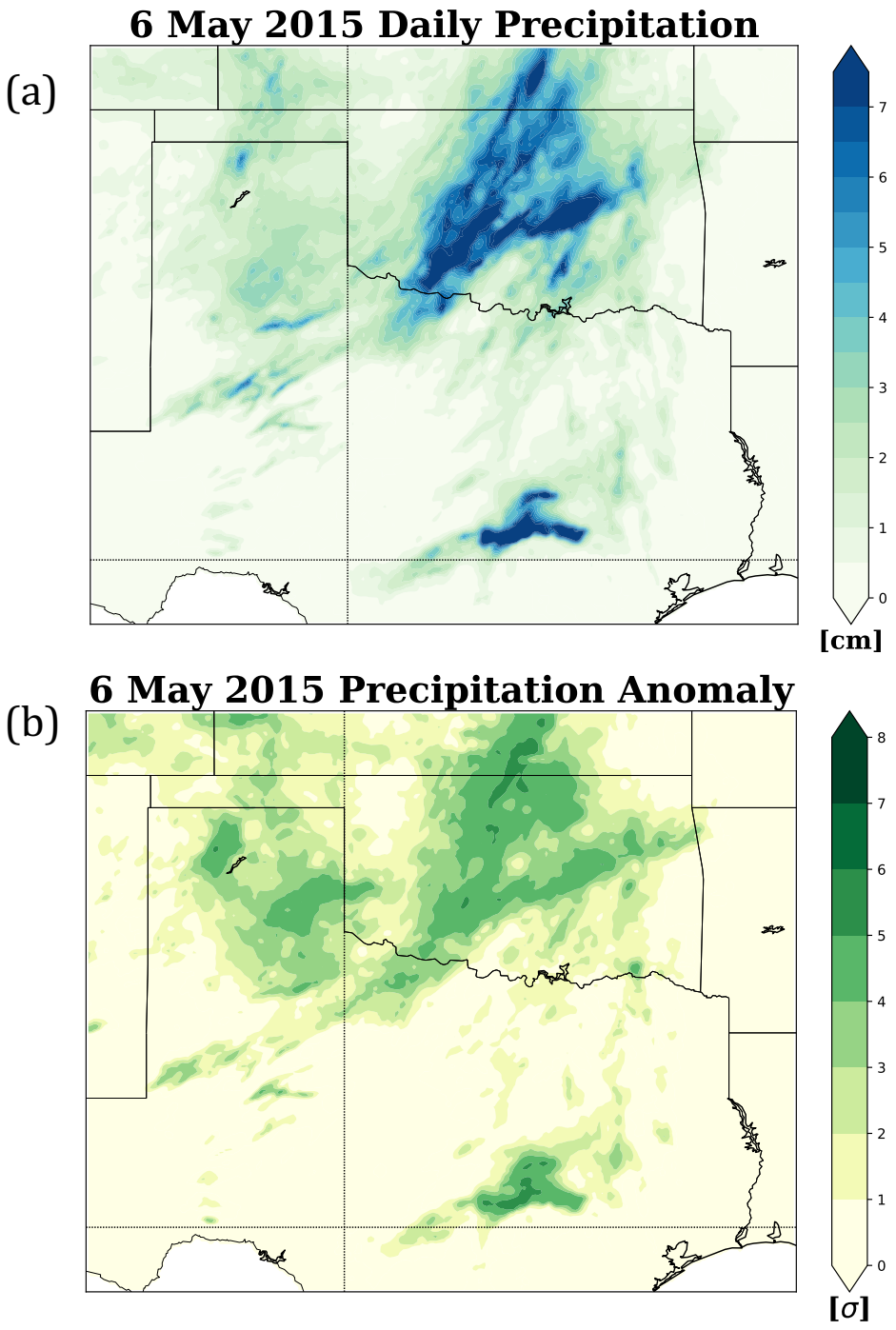

Figure 3.34: (a) The daily precipitation on 6 May 2015. (b) The daily precipitation anomaly on 6 May 2015.

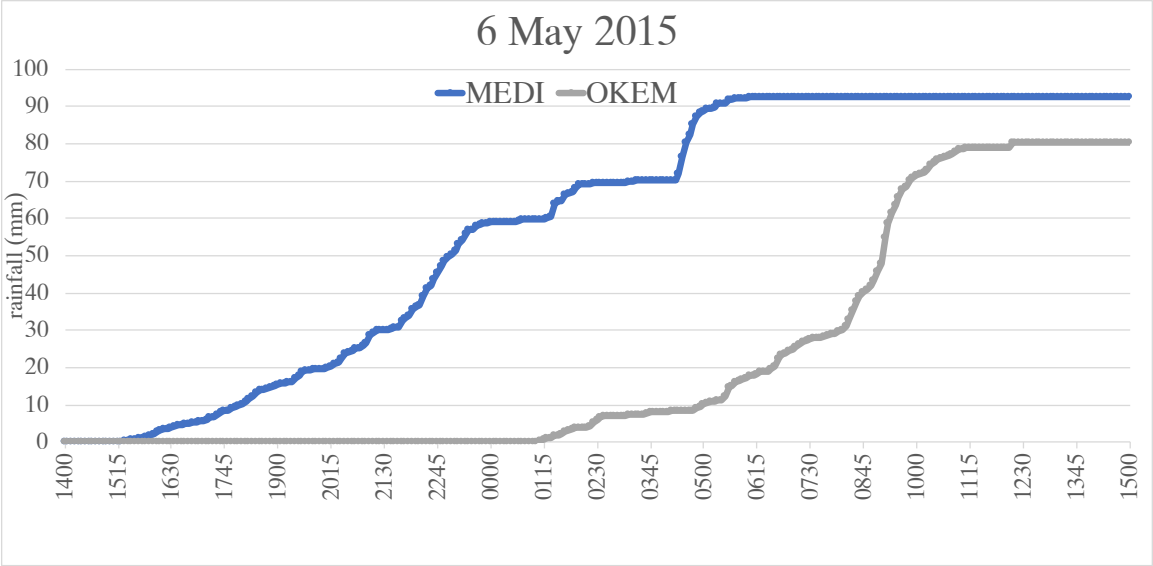

Figure 3.35: 5-6 May time series of precipitation at the MEDI and OKEM Mesonet sites.

the end of 9 May (20 UTC onwards), several discrete storms initiated and also contributed to the precipitation for the day.

3.6.3 14 May 2015

The third most significant precipitation day in the event was 14 May 2015. The most significant precipitation fell along storm tracks extending from the Texas panhandle into central Oklahoma, as well as in southern Texas. These regions saw up to 7 cm locally, with more widespread areas of 3 cm extending across the domain (Fig. 3.42a). This corresponds to precipitation anomalies exceeding 4 standard deviations in the Texas panhandle and central/southern Texas (Fig. 3.42b).

The 0000 UTC 14 May sounding taken in Norman, OK (OUN) was launched concurrently with precipitation in the area, measuring 37.43 mm (1.47 in) precipitable water (Fig. 3.43). This exceeds the daily 90% moving average displayed in the SPC sounding climatology. The 0000 UTC WPC surface analysis shows a surface low over the Texas panhandle, associated with a warm front that stretches across Texas, just south of the Red

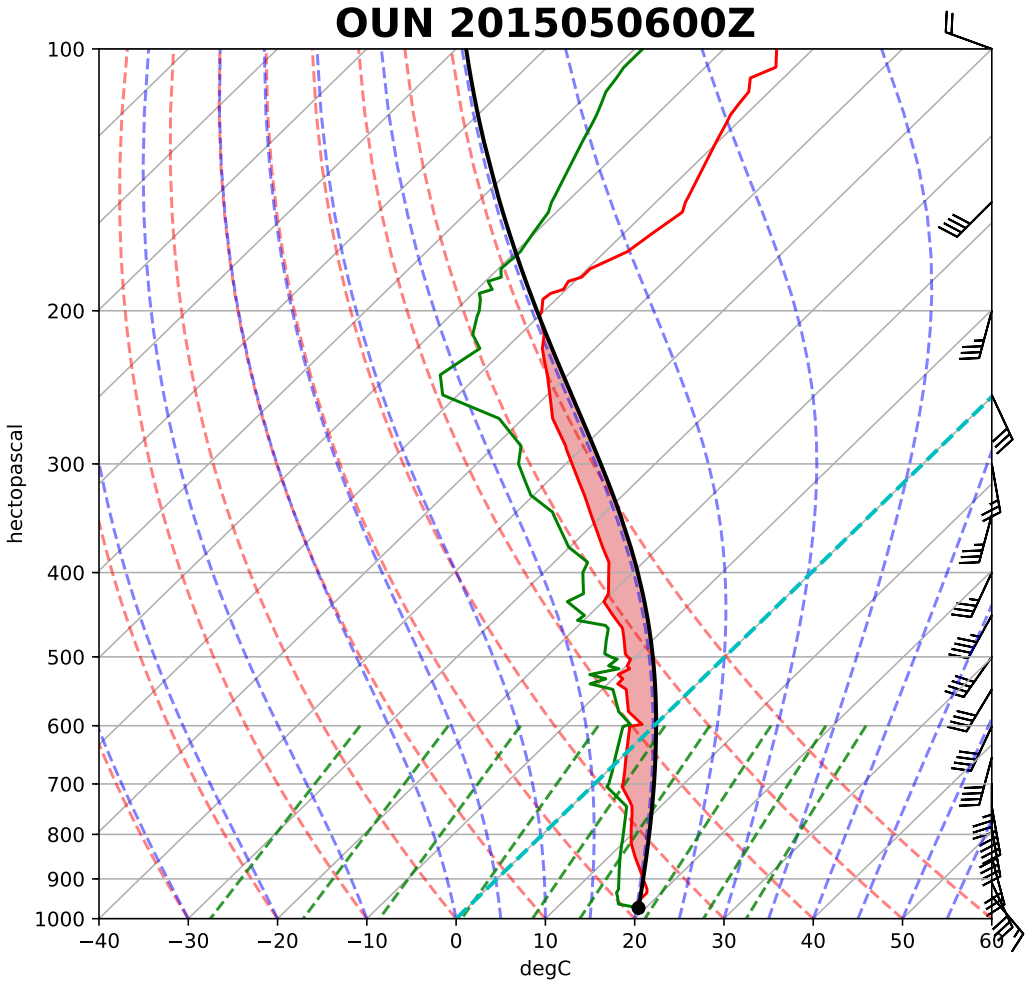

Figure 3.36: 2015050600Z OUN Sounding

(a)

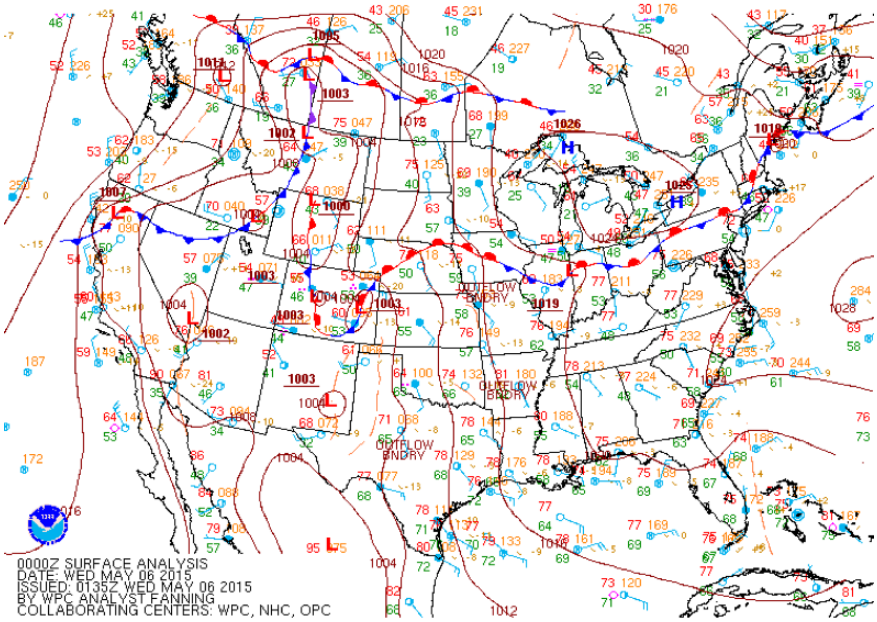

(b)

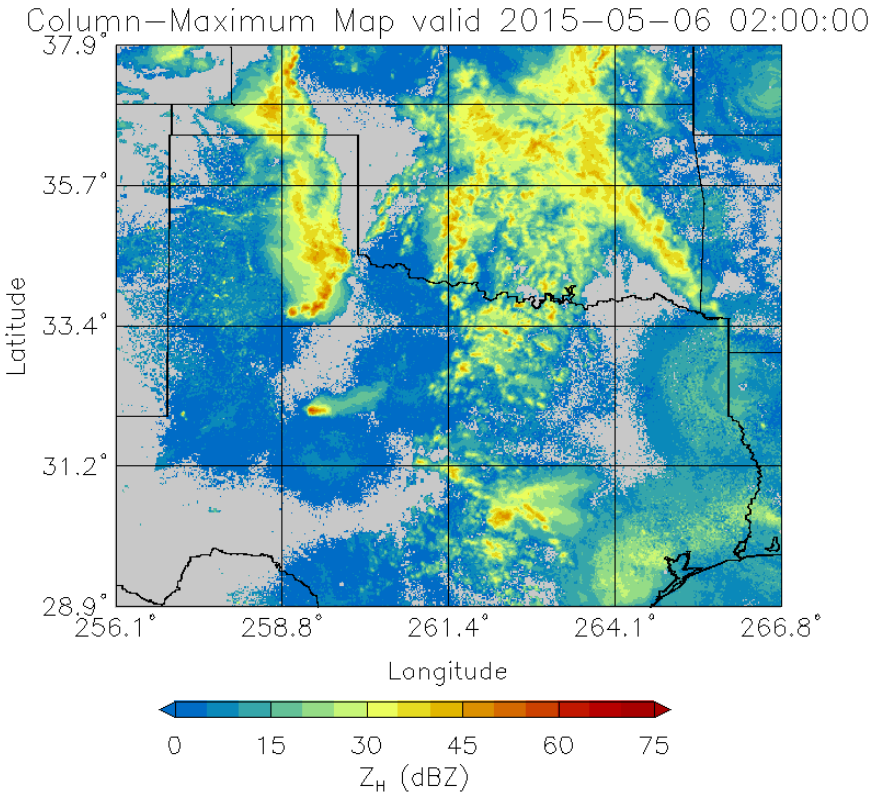

Figure 3.37: (a) 00 UTC WPC surface analysis on 6 May 2015. (b) Radar observations at 0200 UTC 6 May 2015.

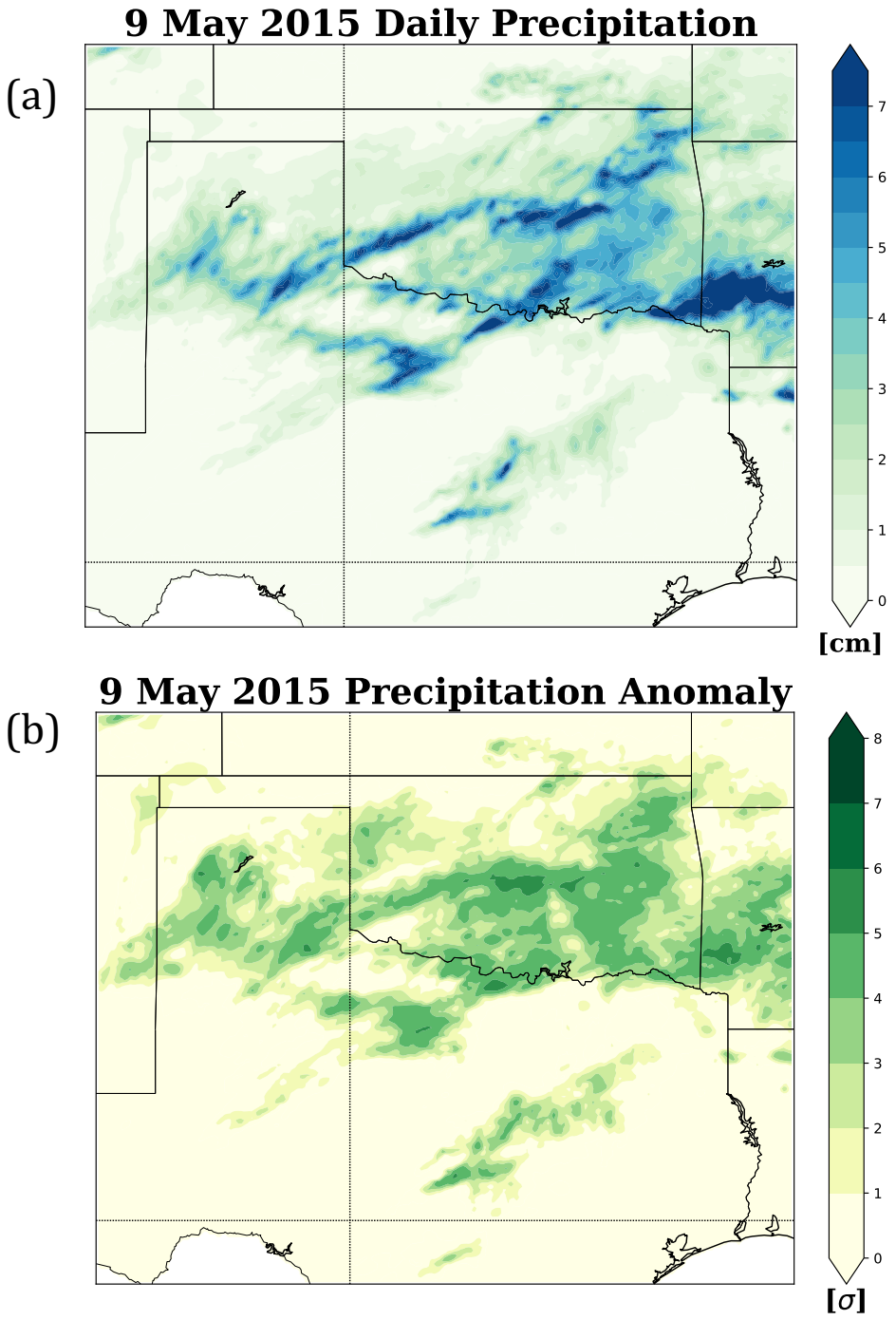

Figure 3.38: (a) The daily precipitation on 9 May 2015. (b) The daily precipitation anomaly on 9 May 2015.

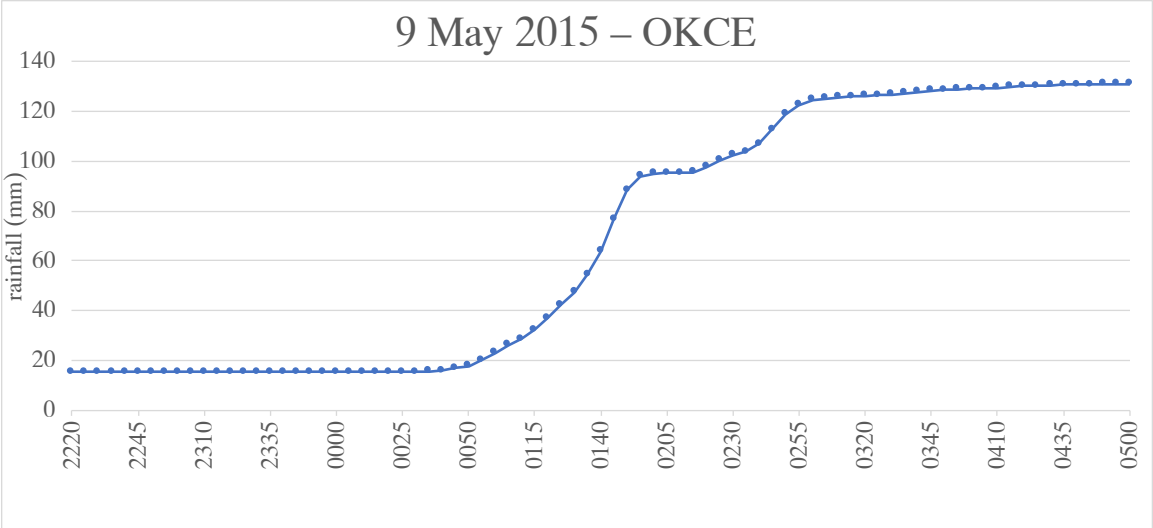

Figure 3.39: 8-9 May time series of precipitation at the OKCE Mesonet site.

River (Fig. 3.44a). This frontal system helps to provide dynamic forcing for the precipitation event. The 0200 UTC radar image shows a broad region of precipitation moving across northern and eastern Oklahoma, as well as some discrete and interacting cells along the Oklahoma-Texas border (Fig. 3.44b).

3.6.4 24 May 2015

The most significant precipitation day in the flash pluvial event was 24 May 2015 with two main regions impacted across Oklahoma and southern Texas. In the north, a large area of Oklahoma experienced over 6 cm of precipitation (Fig. 3.45a) while in the south, near the San Antonio metropolitan area 6 to 12 cm of rain occurred; these daily precipitation anomalies exceeded 4 standard deviations (Fig. 3.45b).

Atmospheric conditions for this event were primed for a major precipitation event. The 24 May sounding taken in Norman, OK (OUN) at 0000 UTC is shown in Fig. (Fig. 3.46). The conditions yielded surface based CAPE of 1312 J/kg and precipitable water observed of 44.48 mm (1.75 in) which exceeds the daily maximum moving average displayed in the SPC sounding climatology. Further, the WPC surface analysis at 0000 UTC (Fig. 3.47a)

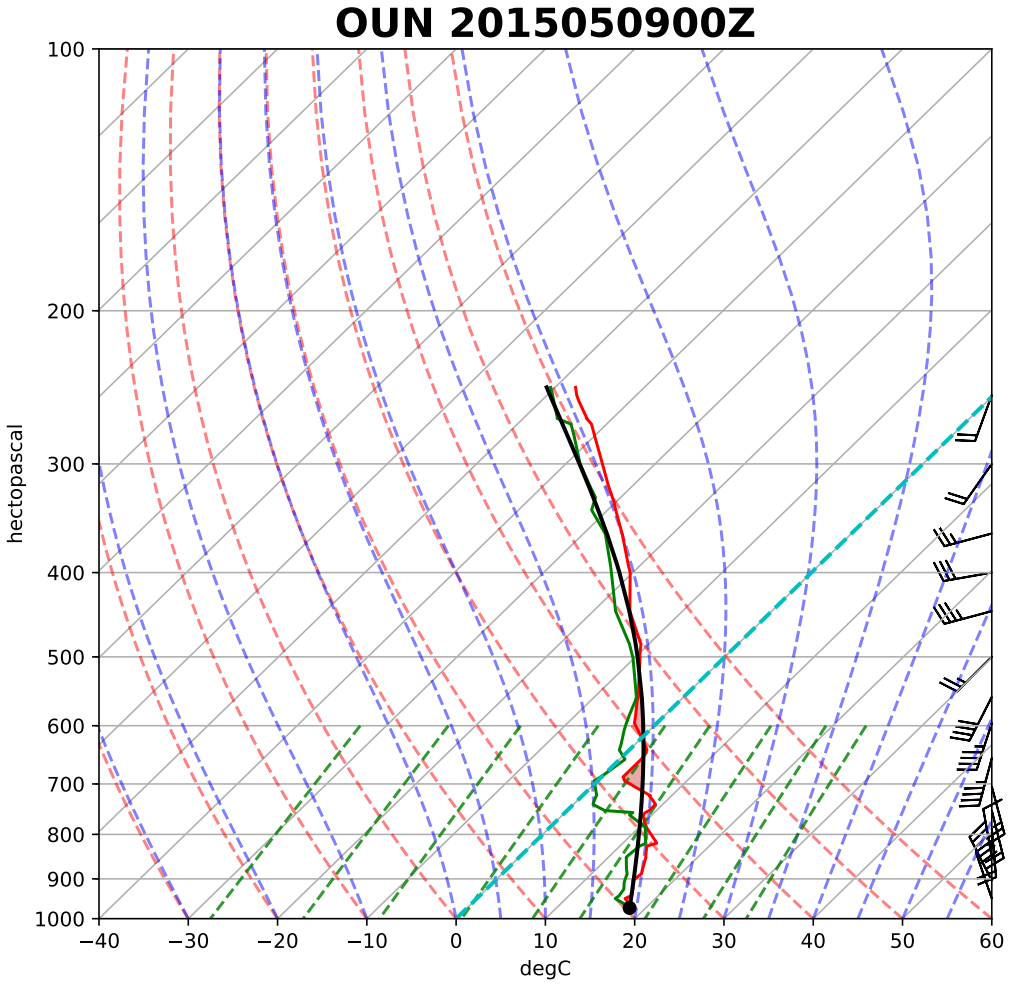

Figure 3.40: 2015050900Z OUN Sounding

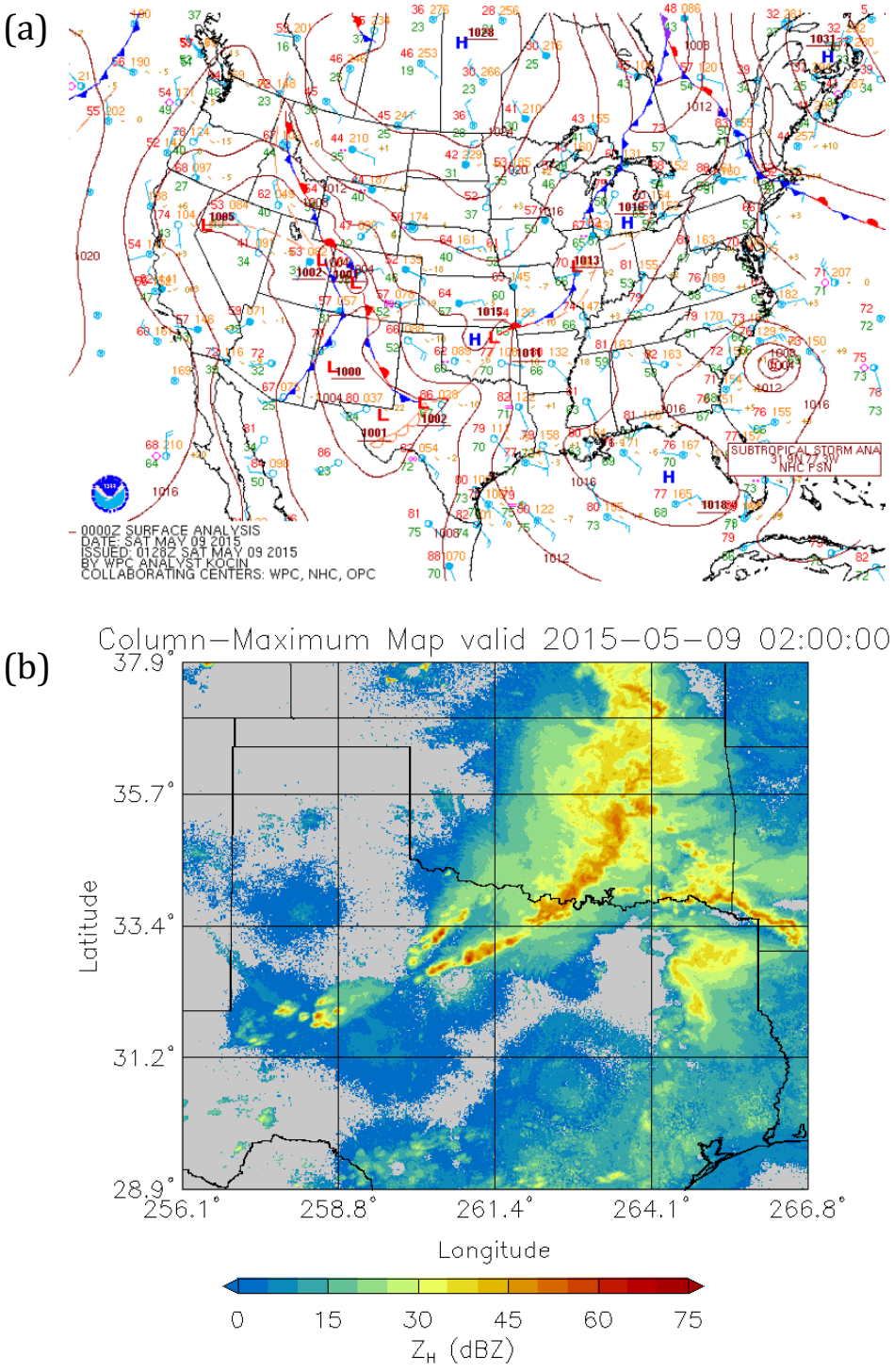

Figure 3.41: (a) 00 UTC WPC surface analysis on 9 May 2015. (b) Radar observations at 0200 UTC 9 May 2015.

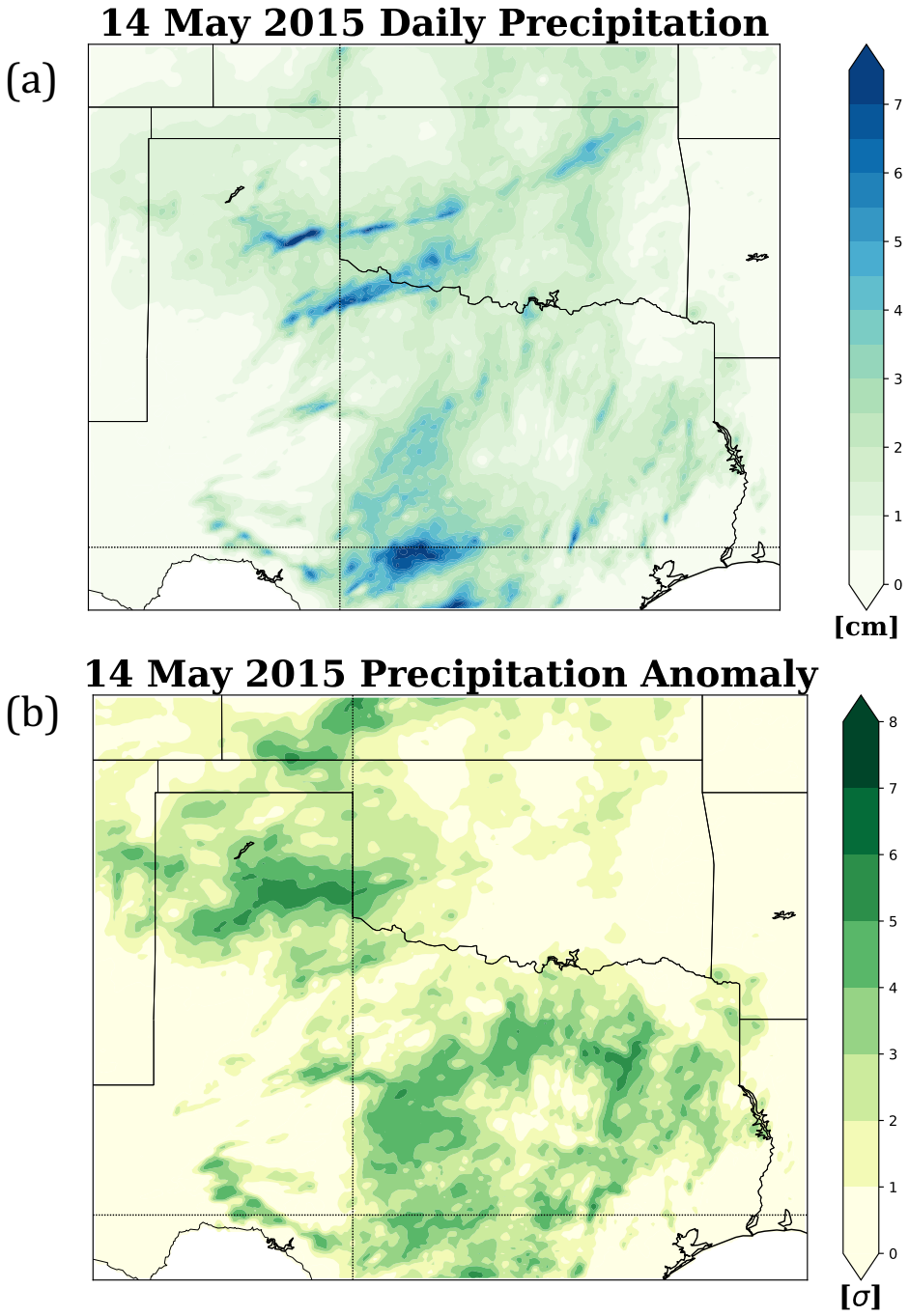

Figure 3.42: (a) The daily precipitation on 14 May 2015. (b) The daily precipitation anomaly on 14 May 2015.

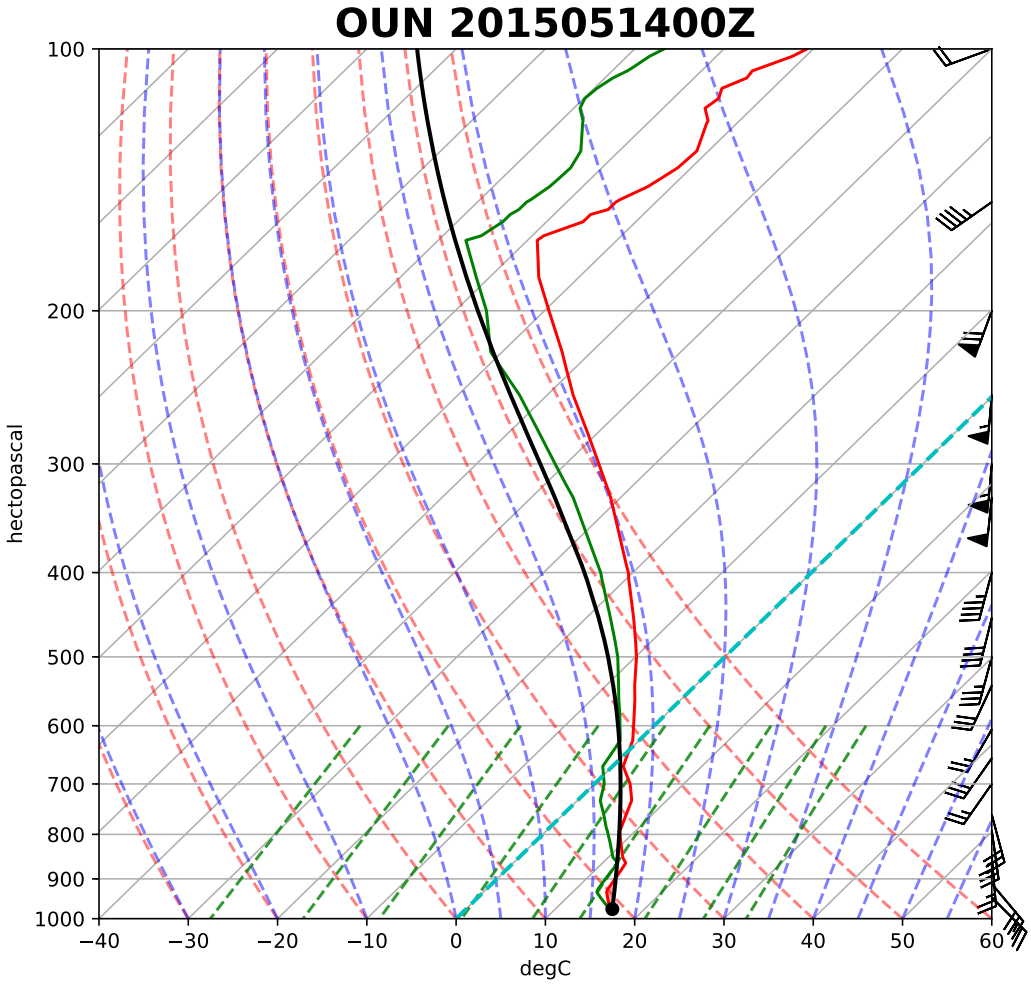

Figure 3.43: 2015051400Z OUN Sounding

(a)

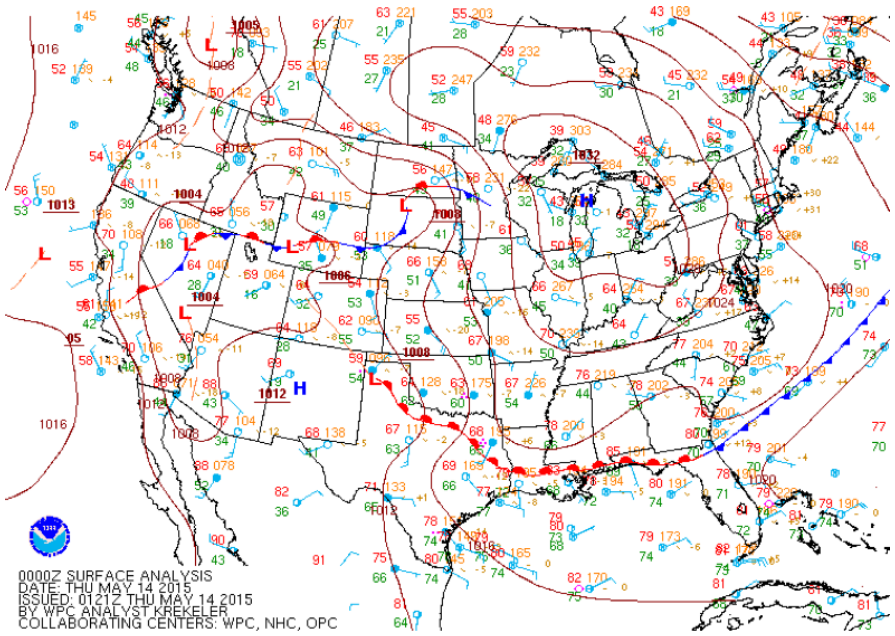

(b)

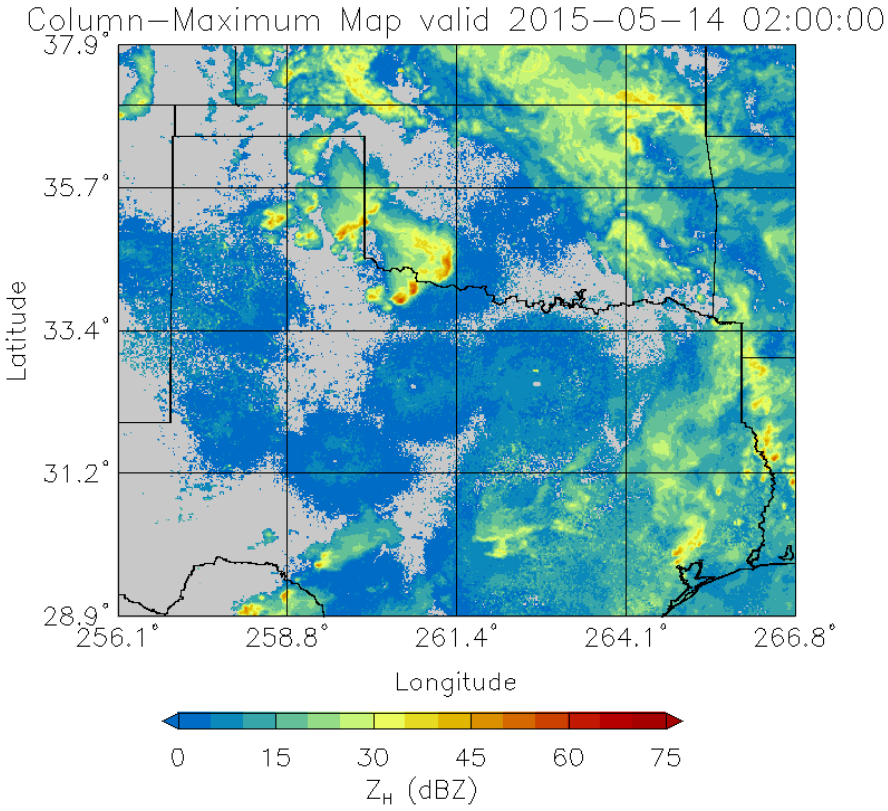

Figure 3.44: (a) 00 UTC WPC surface analysis on 14 May 2015. (b) Radar observations at 0200 UTC 14 May 2015.

displayed a cyclone across southeast Colorado with two boundaries: one across the Texas panhandle and Oklahoma and the other extending south on the Texas-New Mexico border. As shown via radar reflectivity (Fig. 3.47b), most precipitation was due to a large squall line.

3.6.5 29 May 2015

The second most significant precipitation day within the flash pluvial is 29 May 2015. This day saw localized precipitation as great at 12 cm, with broader areas exceeding 5 cm (Fig. 3.48a). While the greatest accumulations were south of the Red River and in north-central Texas, precipitation anomalies over 4 standard deviations were spread across much of southern Oklahoma and central Texas (Fig. 3.48b).

The 0000 UTC sounding from 29 May launched in Norman, OK (OUN) measured 2437 J/kg of CAPE, a large amount of CAPE (Fig. 3.49). The sounding measured precipitable water of 33.30 mm (1.31in), which exceeds the 75% moving average for this date, according to SPC sounding climatology. The WPC surface analysis from 0000 UTC 29 May showed a cyclone over southeast Colorado and northeast New Mexico (Fig. 3.50a). This is accompanied by a dry line that extended across eastern New Mexico. The 0200 UTC radar imagery showed a large linear system moving across Texas and southern Oklahoma, as well as a smaller system crossing from New Mexico into the Texas panhandle (Fig. 3.50b).

3.6.6 13 June 2015

The final, top-tier significant precipitation day prior to TD Bill was 13 June 2015, ranked tenth among the 95th percentile dates. This day impacted Oklahoma with many localized areas receiving between 4 to 10 cm of precipitation (Fig. 3.51a). This corresponded to widespread precipitation anomalies exceeding four standard deviations (Fig. 3.51b). The

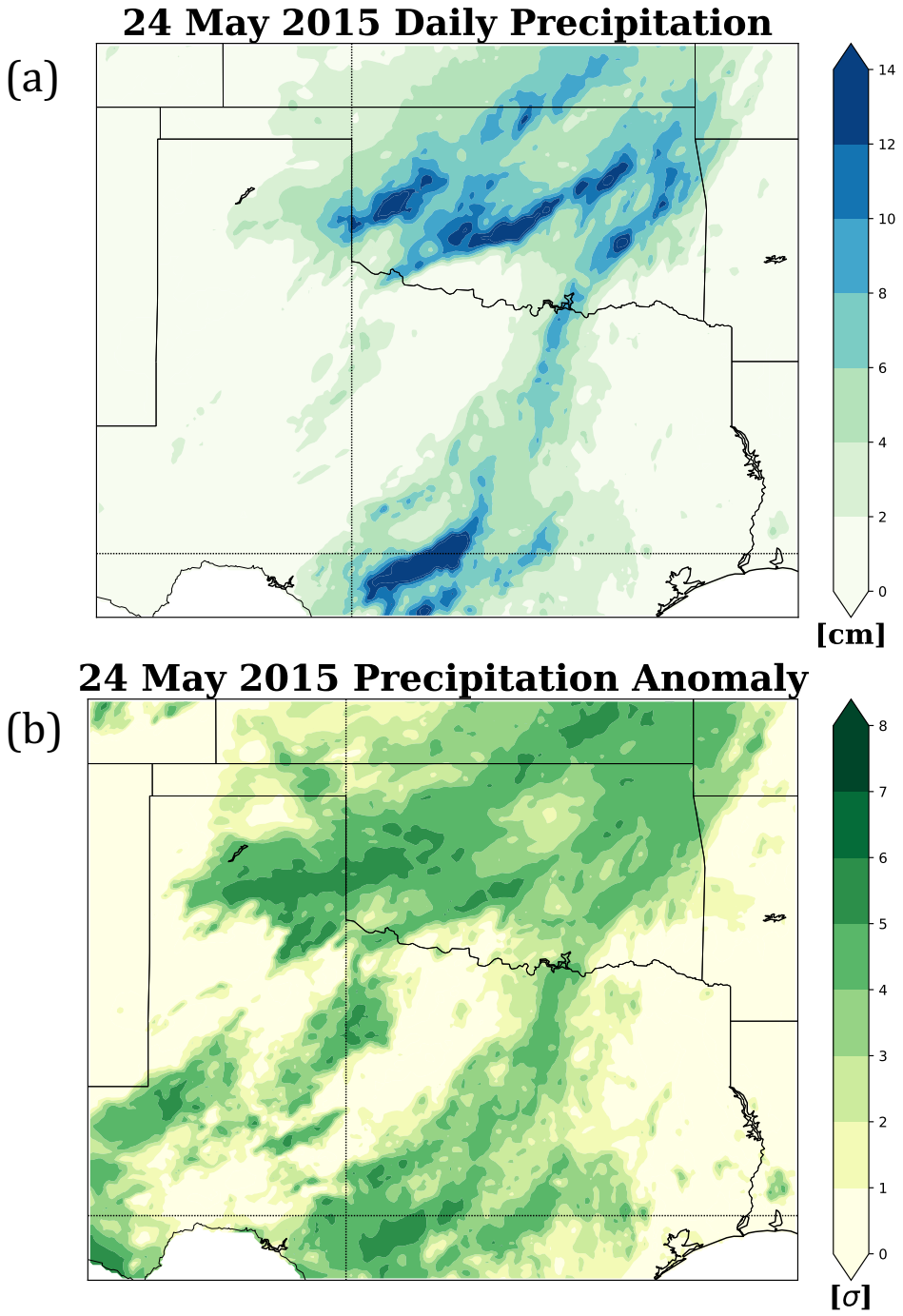

Figure 3.45: (a) The daily precipitation on 24 May 2015. (b) The daily precipitation anomaly on 24 May 2015.

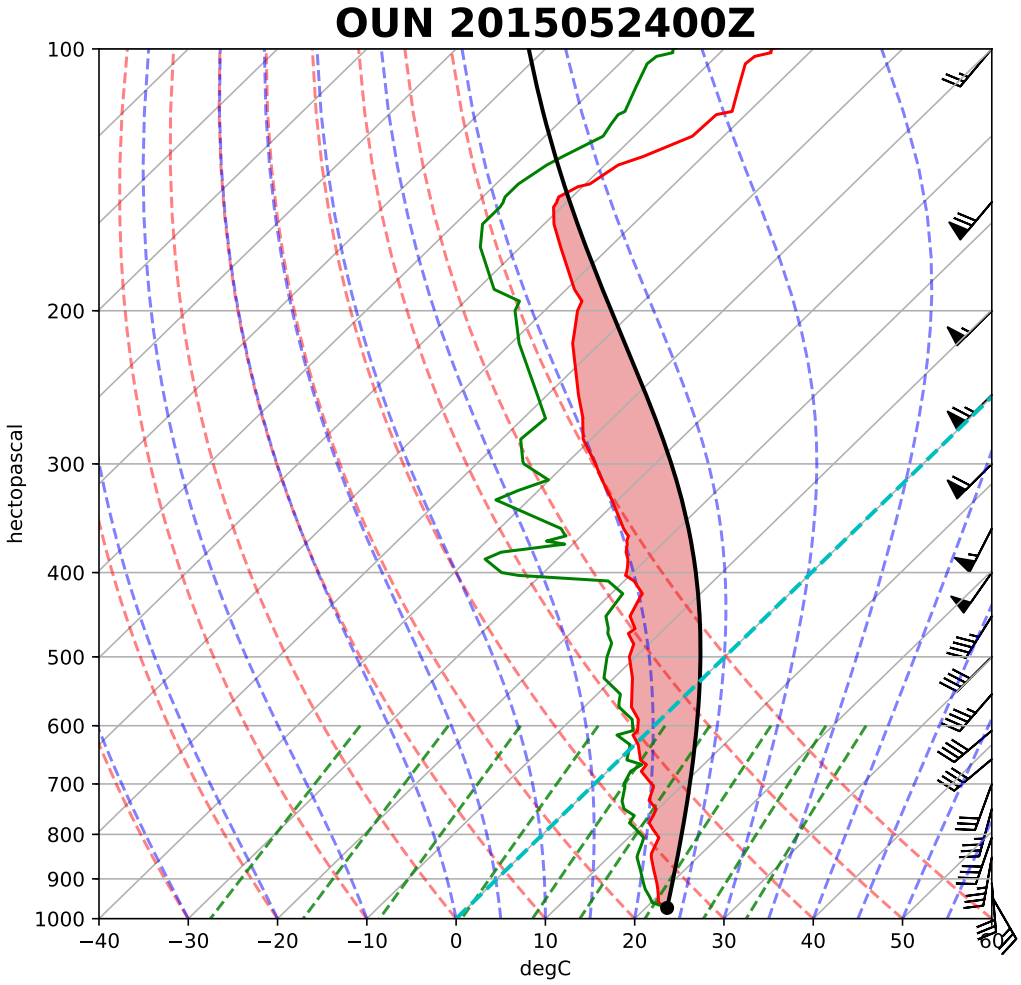

Figure 3.46: 2015052400Z OUN Sounding

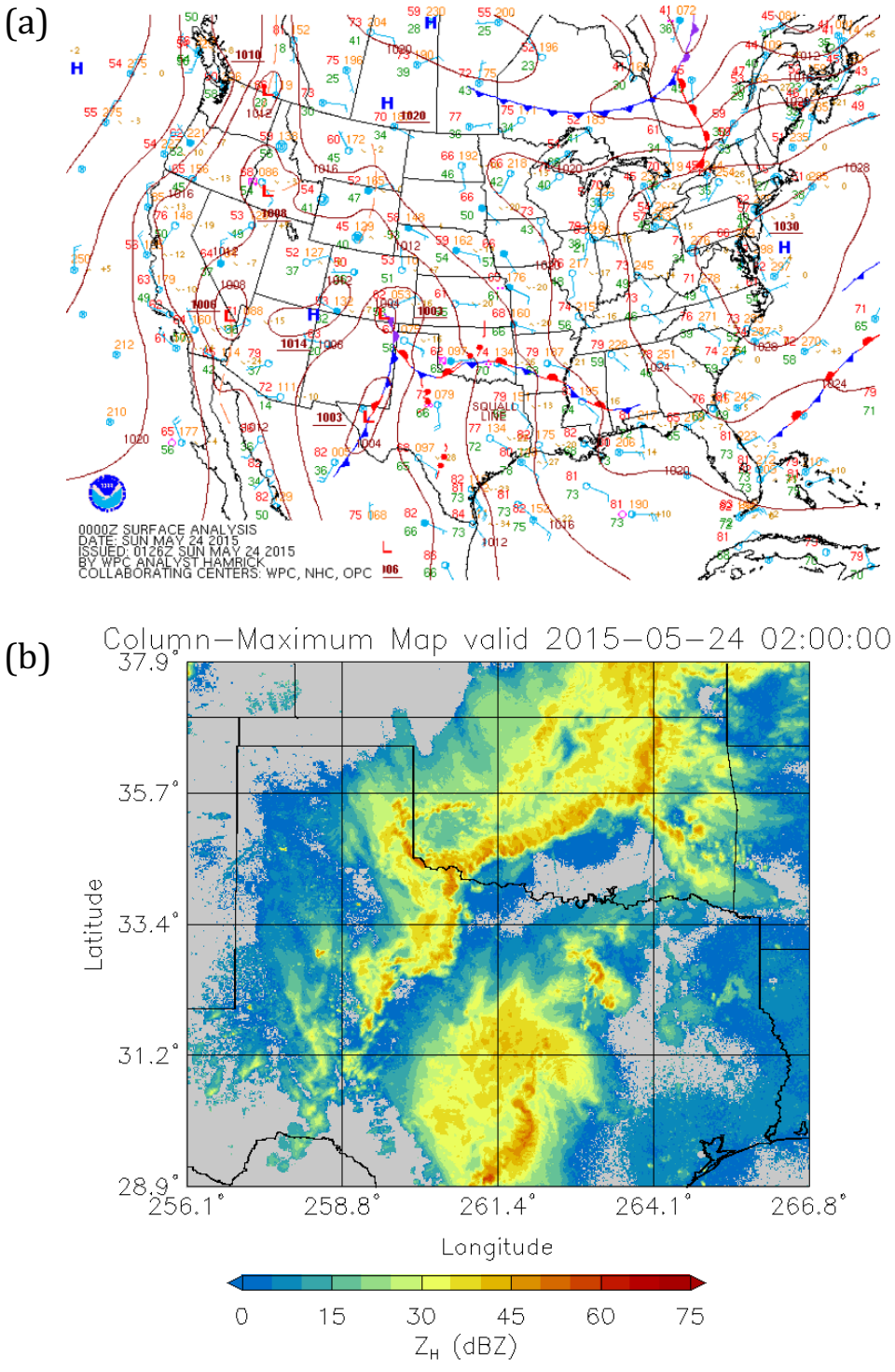

Figure 3.47: (a) 00 UTC WPC surface analysis on 24 May 2015. (b) Radar observations at 0200 UTC 24 May 2015.

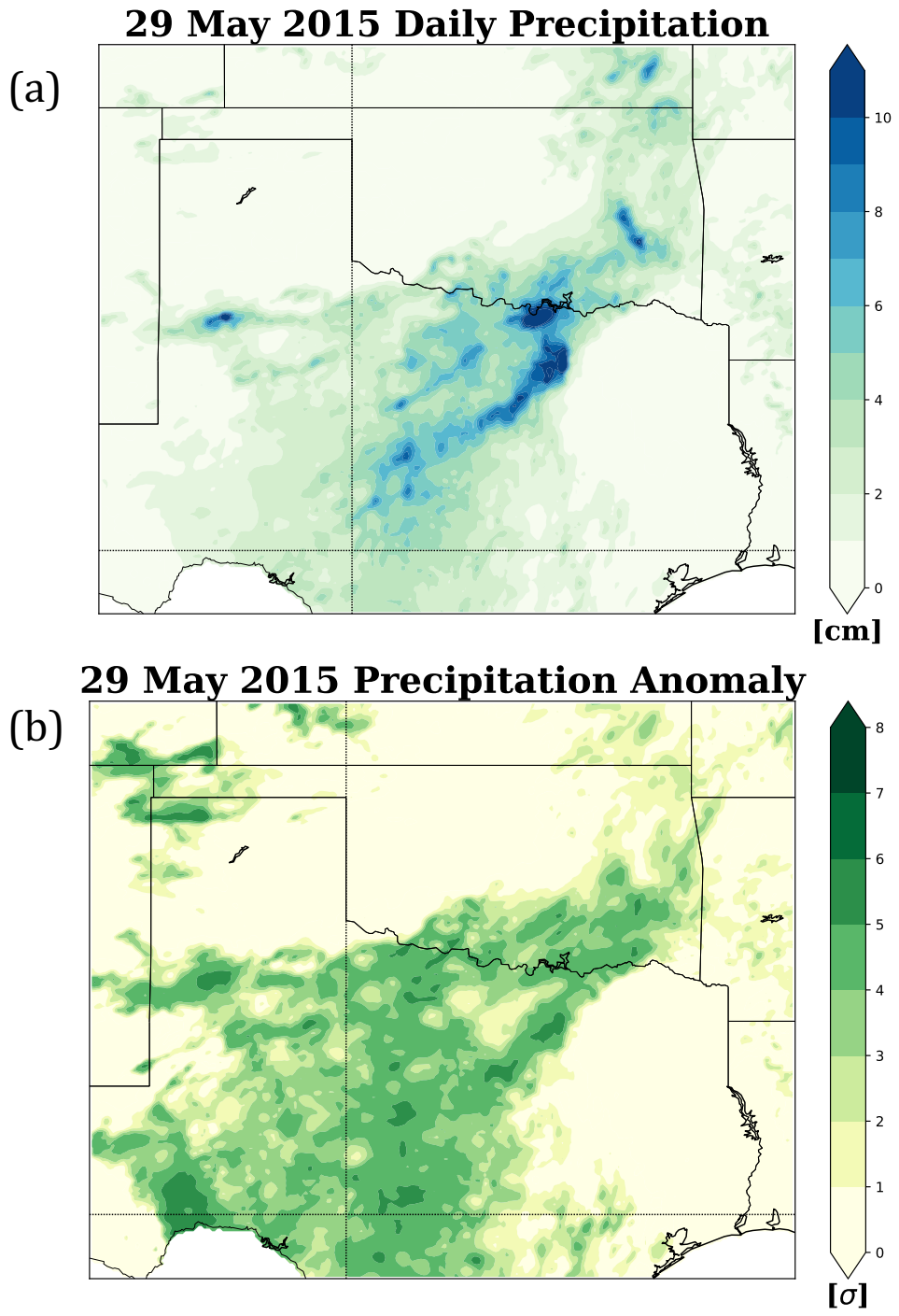

Figure 3.48: (a) The daily precipitation on 29 May 2015. (b) The daily precipitation anomaly on 29 May 2015.

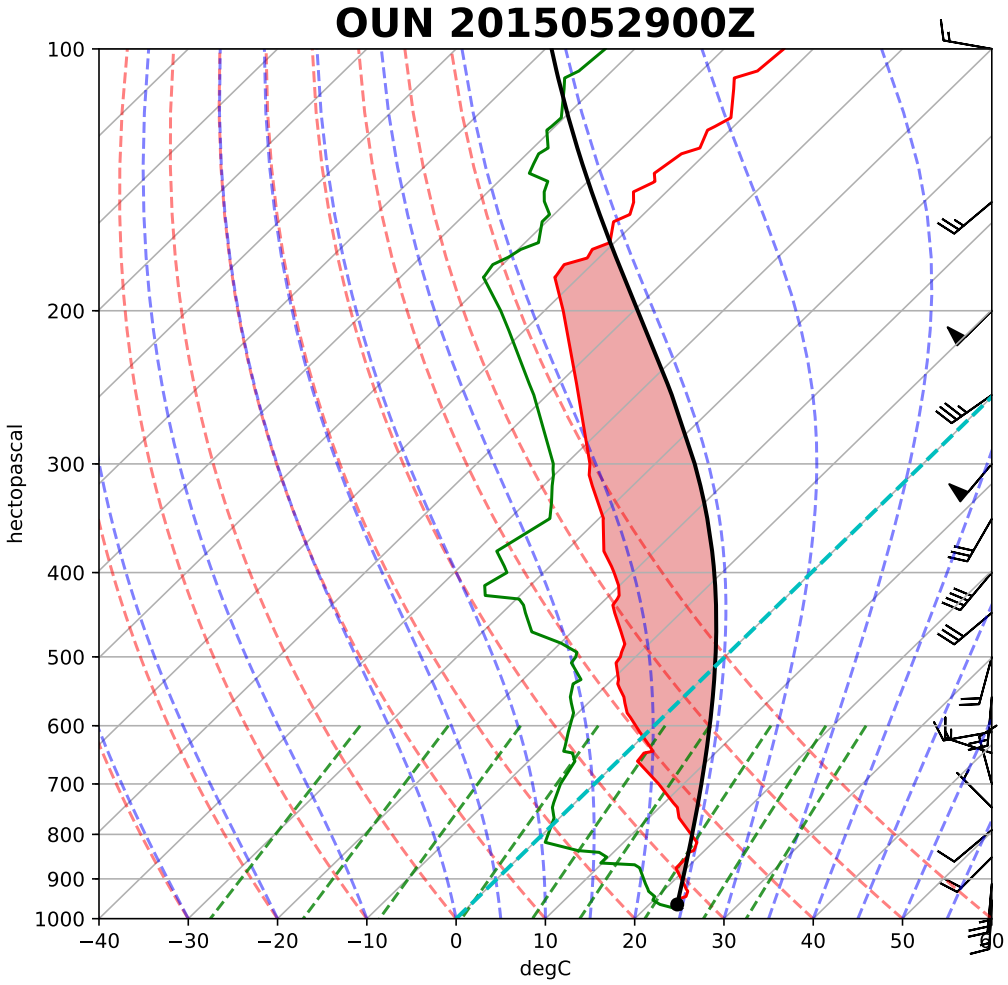

Figure 3.49: 2015052900Z OUN Sounding

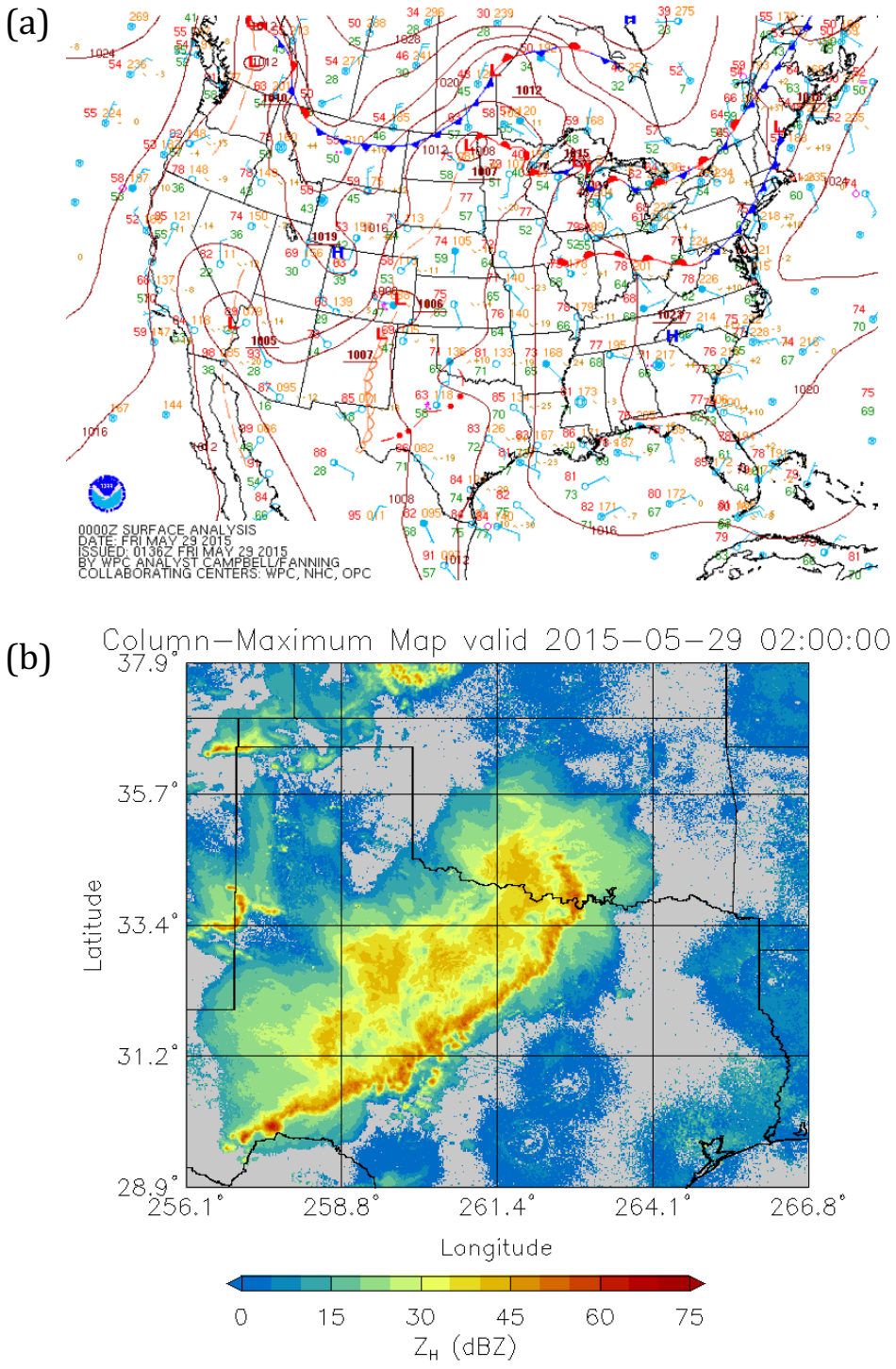

Figure 3.50: (a) 00 UTC WPC surface analysis on 29 May 2015. (b) Radar observations at 0200 UTC 29 May 2015.

Oklahoma City metropolitan area was at the epicenter of this event with the Mesonet stations at OKCE and NRMN yielding a majority of the rainfall occurring from 0300 UTC through 0900 UTC (Fig. 3.52).

The 0000 UTC sounding from 13 June launched in Norman, OK (OUN) displayed limited CAPE (671 J/kg; Fig. 3.53) with precipitable water observed of 36.51 mm (1.44 in); the latter exceeded the 75% moving average for this date, according to SPC sounding climatology. The WPC surface analysis at 1200 UTC for 12 June 2015 (Fig. 3.54a) displayed a cyclone over southwestern Texas with a cold front extending across the southern Texas panhandle through to northern Oklahoma. Discrete storms initiated 12 June along the Texas-New Mexico border and through the Texas panhandle. By early 13 June, these storms combined into a linear system across Oklahoma and northern Texas (Fig. 3.54b); this linear system was responsible for a large volume of the precipitation shown in Figure 3.51.

3.6.7 Tropical Depression Bill

Tropical Depression Bill (TD Bill) formed in the Gulf of Mexico near the Yucatan Peninsula and Belize due to the interaction between an upper level trough and surface low pressure (NHC). The tropical disturbance was steered northwest over the Gulf of Mexico through 14-15 June with a well defined circulation developing on 16 June (NHC). Bill reached tropical storm force winds prior to making landfall on Matagorda Island at 1645 UTC with 50 kt winds and central minimum in pressure at landfall of 997 hPa (NHC). The track of Bill is shown in Figure 3.55. TD Bill remained nearly stationary over the coast after landfall until it began accelerating northward towards Oklahoma on 17 June (NHC). Bill weakened to a tropical depression near Austin, TX and from the Dallas-Fort Worth metropolitan area through to Oklahoma City and Tulsa, TD Bill produced excessive precipitation. TD Bill yielded significant impacts with the Red River at Gainesville, TX reaching a record crest of 42.05 feet (NHC). TD Bill finally weakened on June 18 to a

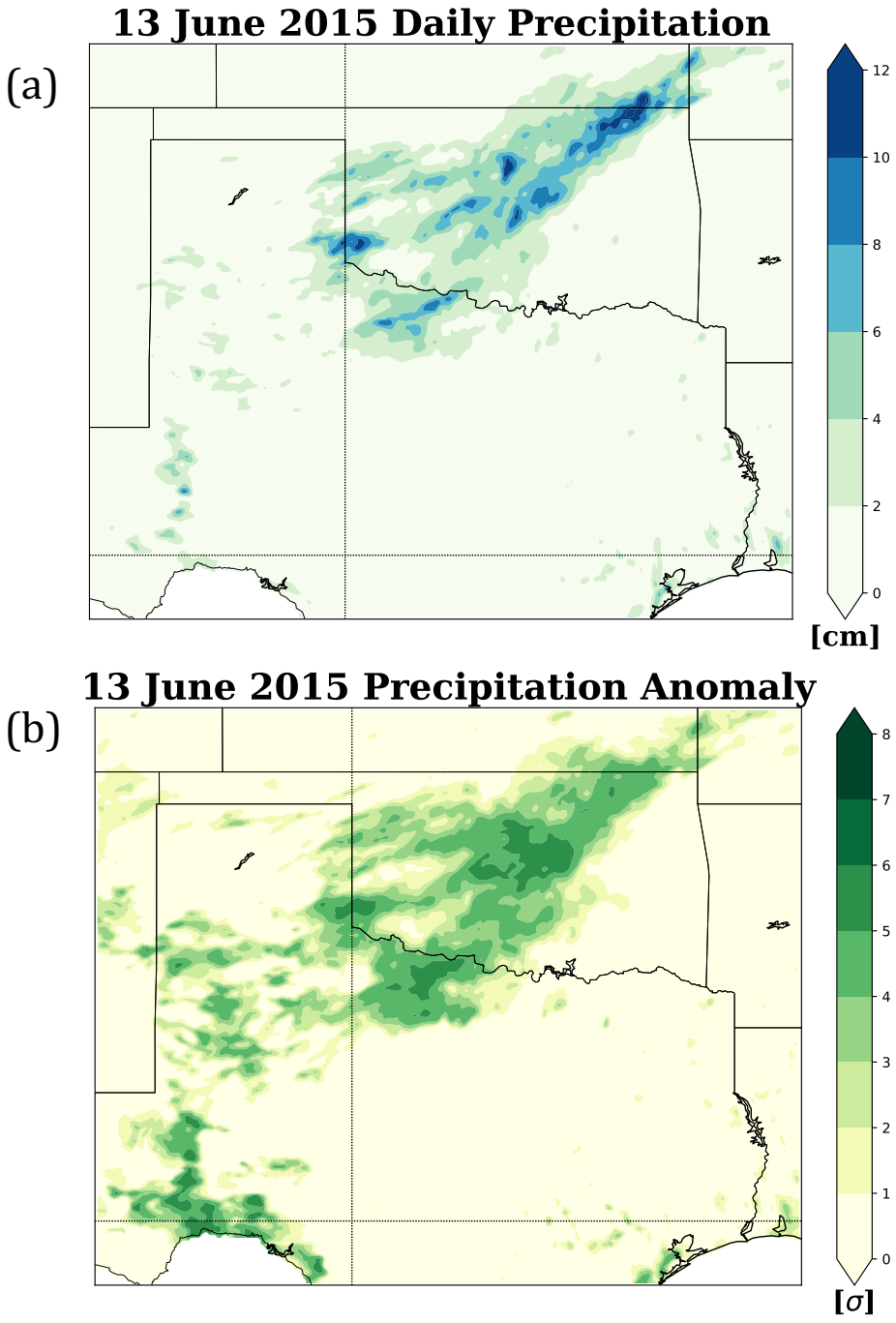

Figure 3.51: (a) The daily precipitation on 13 June 2015. (b) The daily precipitation anomaly on 13 June 2015.

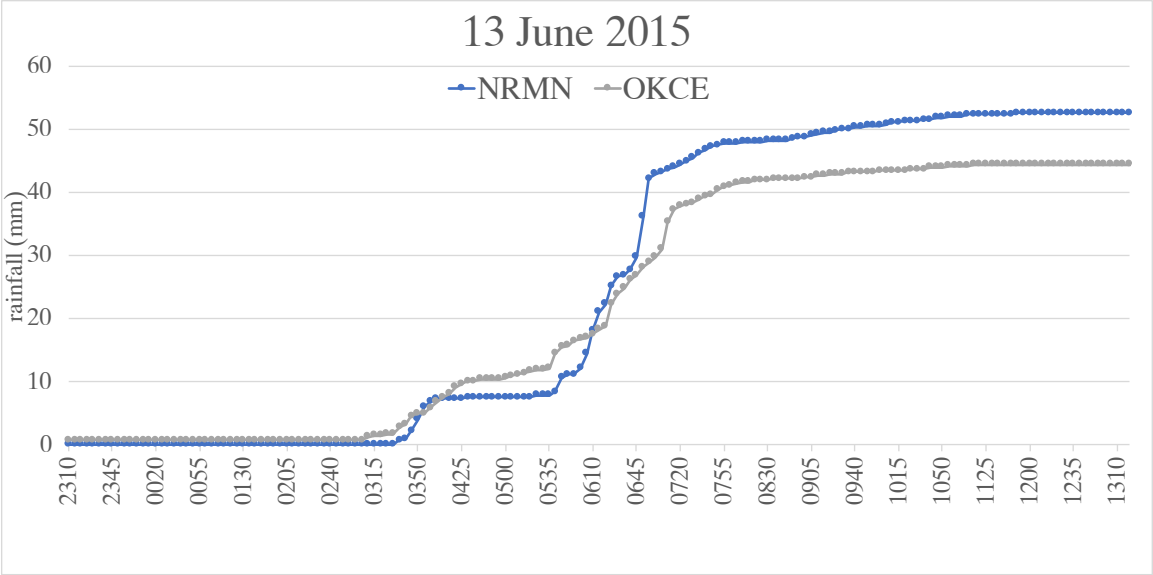

Figure 3.52: 12-13 June time series of precipitation at the NRMN and OKCE Mesonet sites.

remnant low southeast of Tulsa, OK (NHC); the National Hurricane Center cited the recent heavy rainfall across the SGP and wet soils as a reason for Bill maintaining tropical characteristics as far as 1000 miles inland. This "brown ocean effect" is similar to that seen in Tropical Storm Erin, in 2007 (NHC). The remnant circulation of Erin reached Oklahoma, where it strengthened and reached its peak winds and redeveloped an eyewall structure (Arndt et al. 2009; Evans et al. 2011). While Bill did not strengthen the way Erin did, it still retained the tropical appearance on radar (Fig. 3.56).

On 17 June Bill produced over 6 cm to central Texas and over 8 cm to southern Texas which corresponded to precipitation anomalies exceeding four standard deviations. Next, on June 18th a widespread area from the DFW metro to OKC metro observed over 8 cm of rainfall with areas exceeding 20 cm in southern Oklahoma (Fig. 3.57). As shown in OK Mesonet time series from stations in southern Oklahoma(Newport and Pauls Valley), locations experienced nearly constant rainfall from 1500 UTC on 17 June through 1500 UTC on 18 June 2015 (Fig. 3.58).

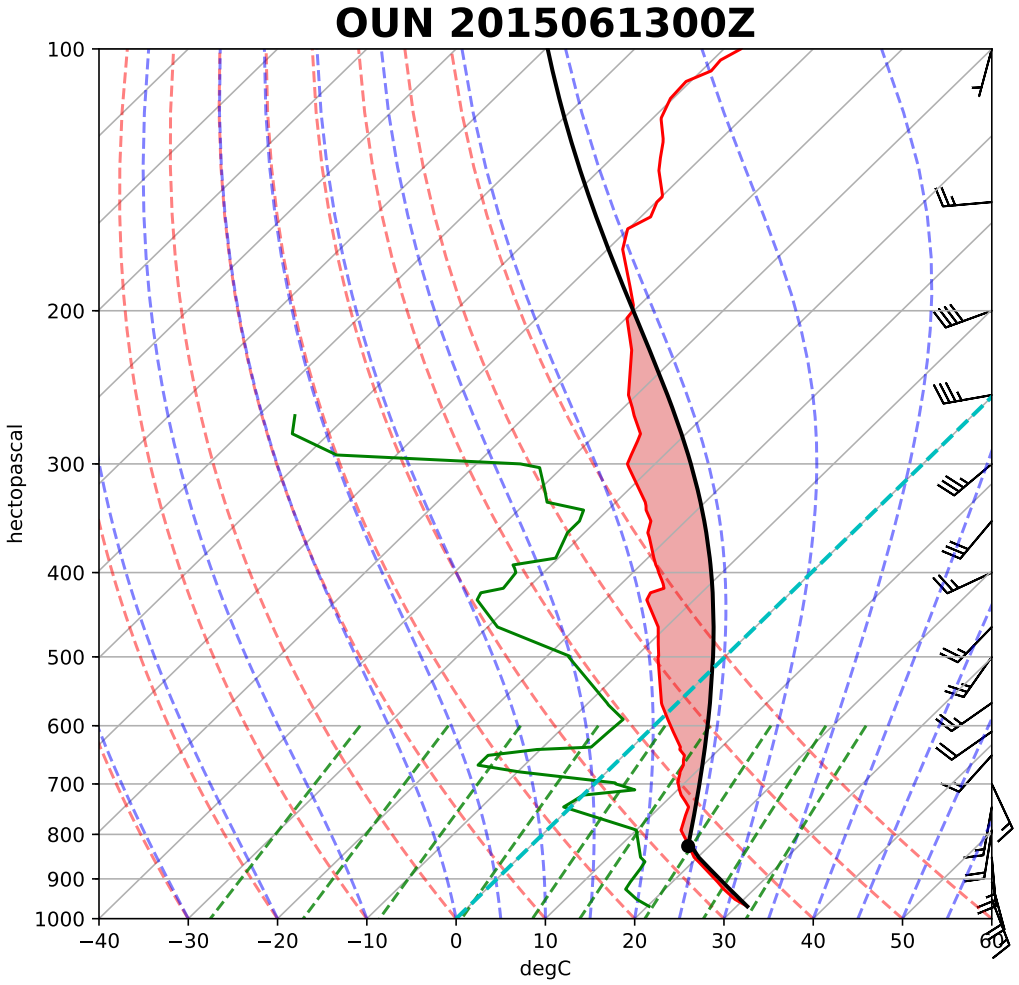

Figure 3.53: 2015061300Z OUN Sounding

(a)

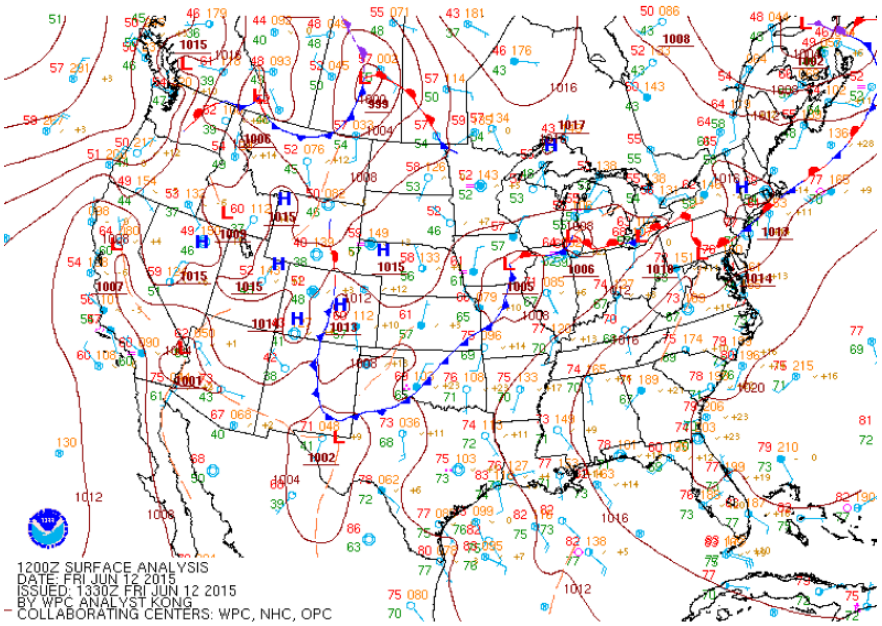

(b)

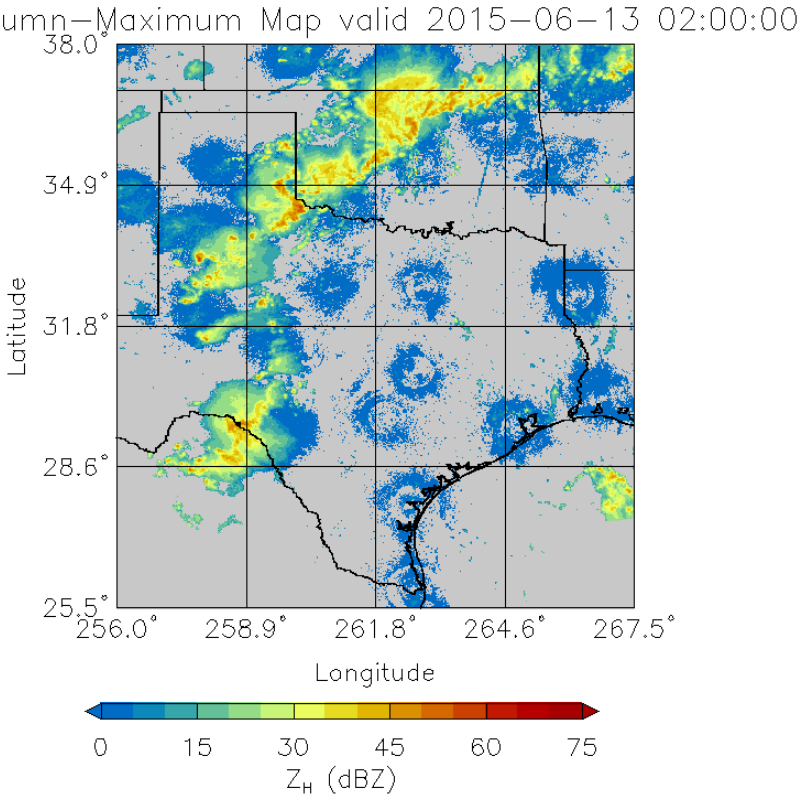

Figure 3.54: (a) 12 UTC WPC surface analysis on 12 June 2015. (b) Radar observations at 0200 UTC 13 June 2015.

A series of soundings launched in both Dallas/Fort Worth, TX and Norman, OK show a distinctly tropical atmosphere (Fig. 3.59). Each sounding from 1200 UTC on 16 June through 1200 UTC on 18 June display elongated, skinny CAPE, nearly saturated profiles, and high precipitable water values. Each of the soundings pictures in Figure 3.59 exhibit over 47 mm (1.85 in) of precipitable water, with three soundings exceeding 51 mm (2.00 in) of precipitable water (1200 16 June FWD, 0000 17 June FWD, and 1200 18 June OUN). All six upper air observations exceed the 90% moving average for the date, with two (1200 17 June OUN and 0000 18 June OUN) exceeding the daily maximum moving average for the dates according to SPC climatology.

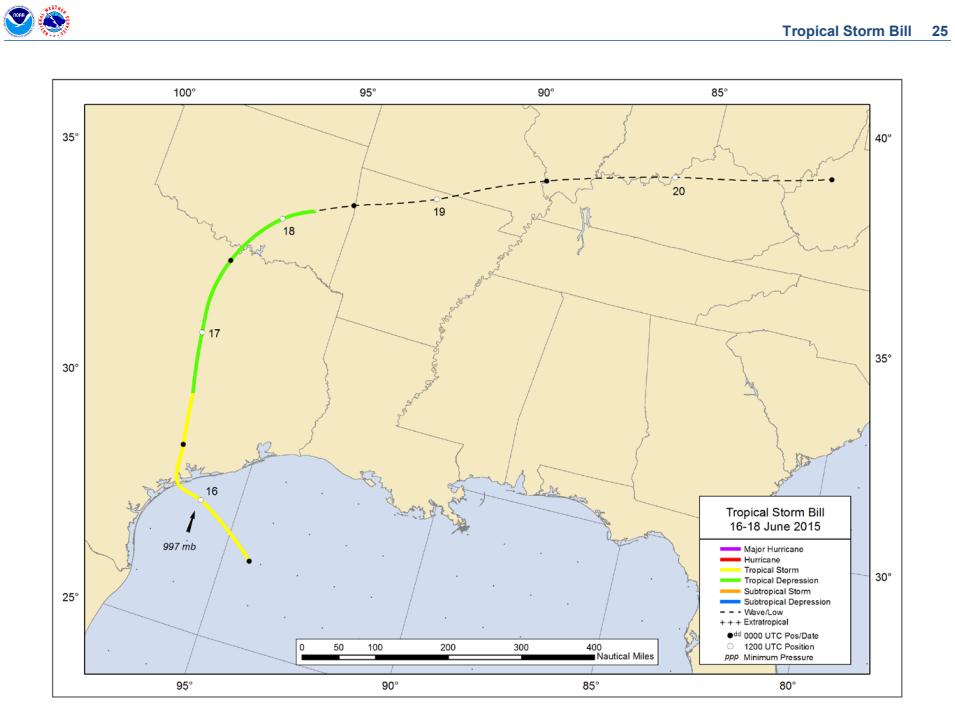

Figure 1. Best track positions for Tropical Storm Bill, 16-18 June 2015. Tracks over the United States and during the remnant low stage are partially based on analyses from the NOAA Weather Prediction Center.

Figure 3.55: Best track positions for Tropical Storm Bill, adapted from the NHC Tropical Cyclone Report (NHC).

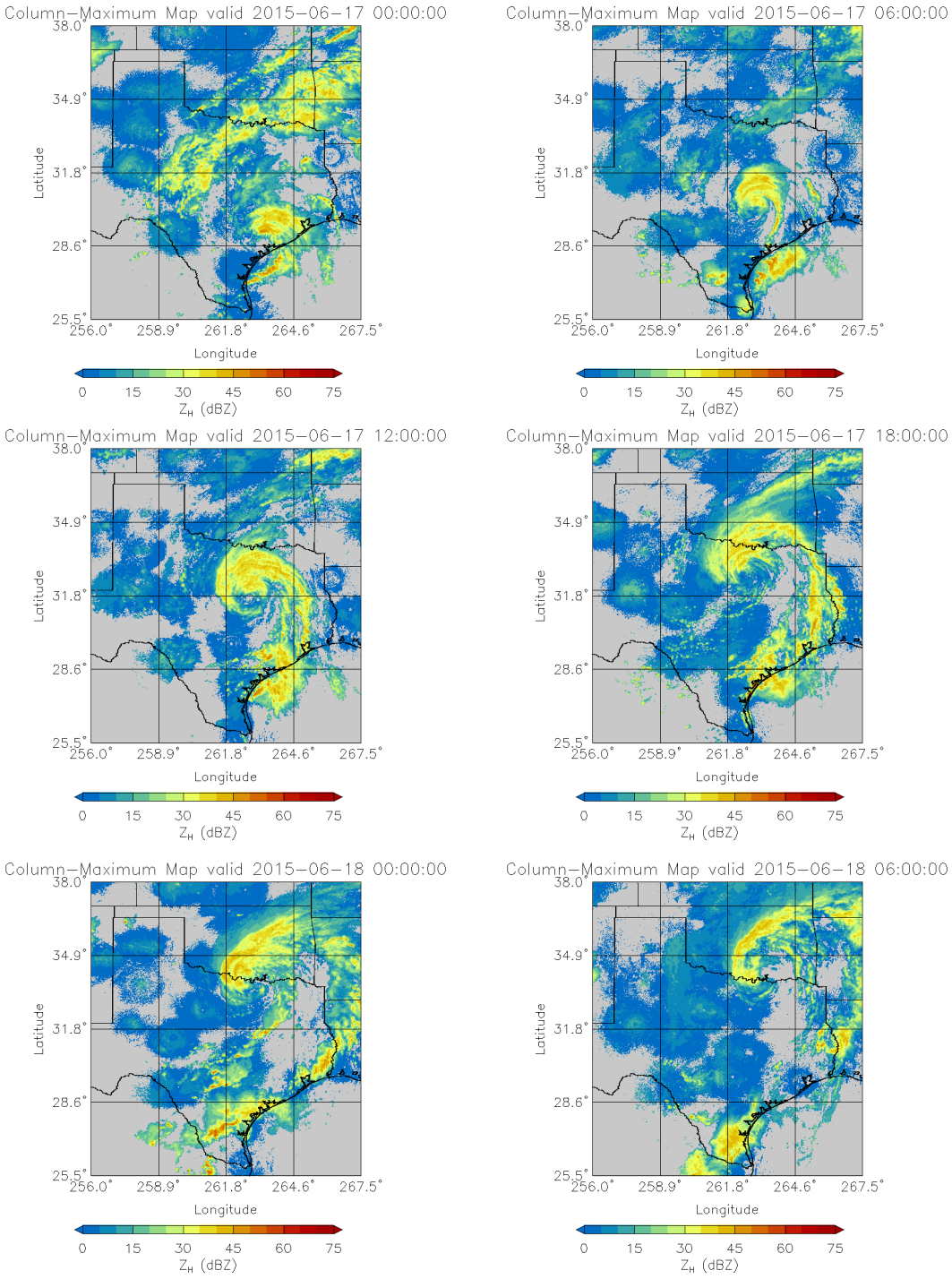

Figure 3.56: Radar observations every 6 hours from 0000 UTC 17 June through 0600 UTC 18 June.

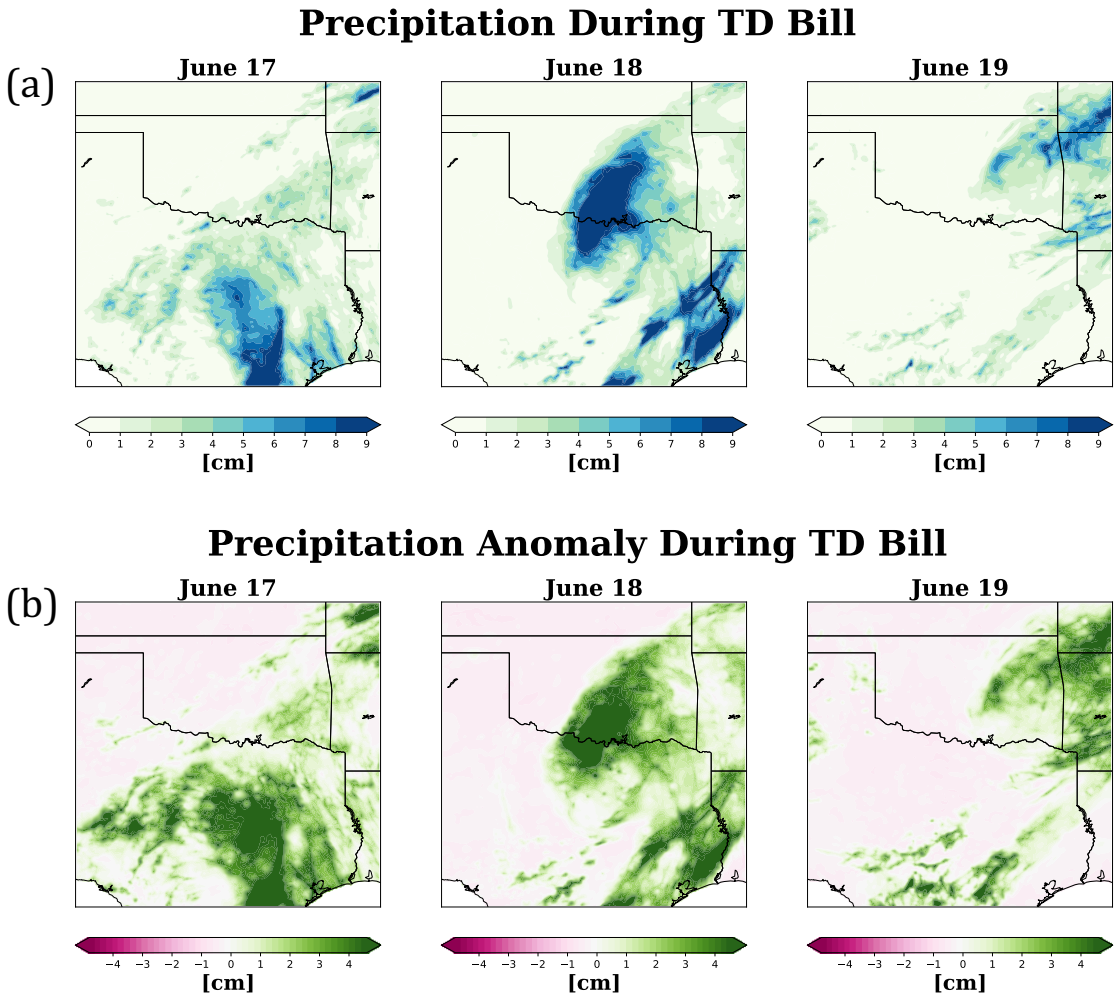

Figure 3.57: (a) The daily precipitation on 17 June, 18 June, and 19 June. (b) The daily precipitation anomaly on 17 June, 18 June, and 19 June

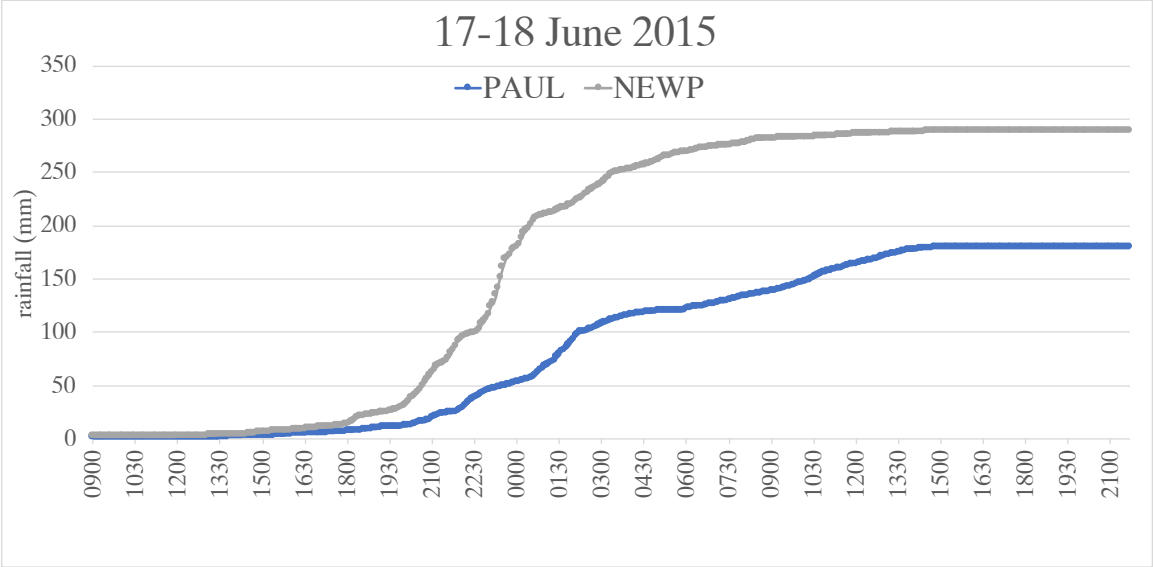

Figure 3.58: 17-18 June time series of precipitation at the PAUL and NEWP Mesonet sites.

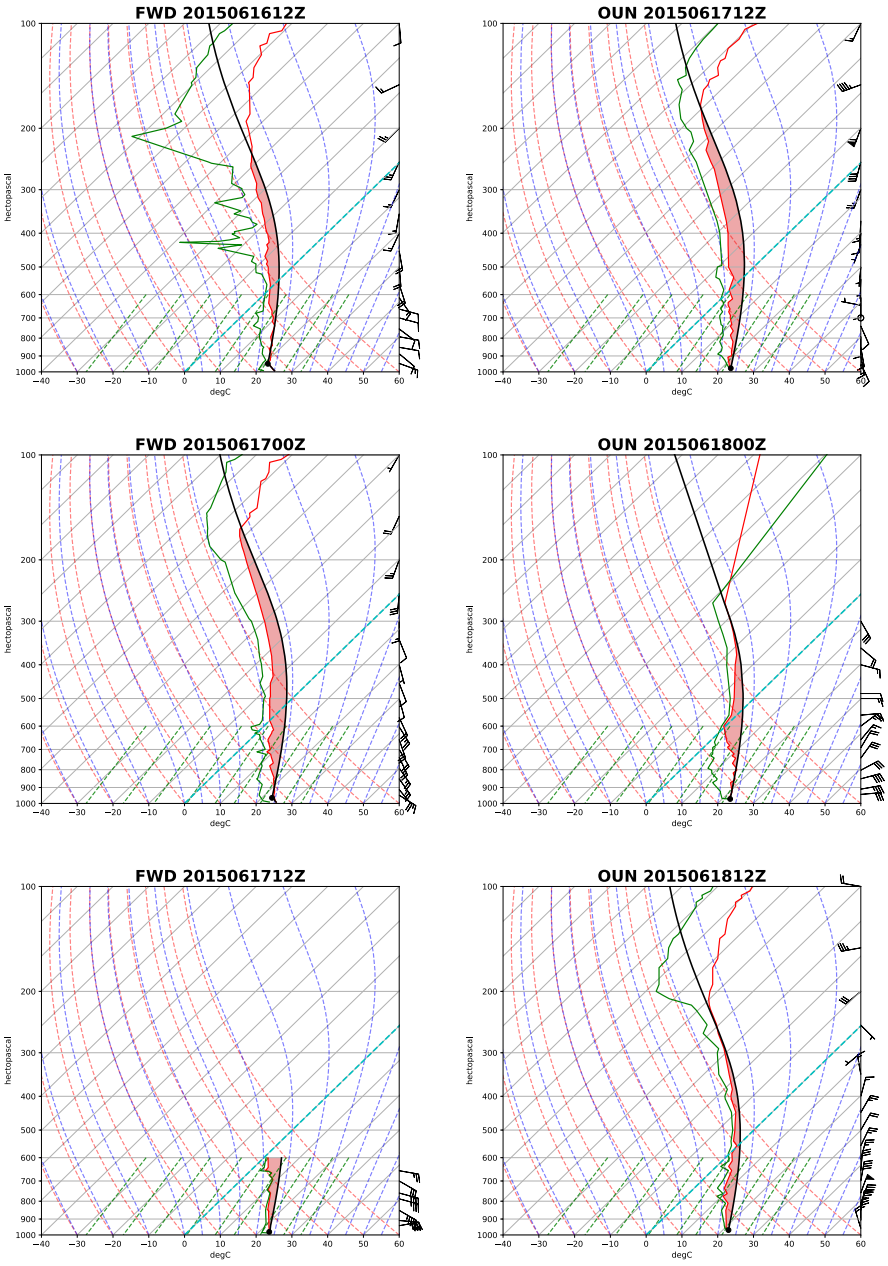

Figure 3.59: Upper air observations taken from both Dallas-Fort Worth (FWD) and Norman (OUN) while TD Bill was in Texas and Oklahoma. The FWD soundings are from 16 June 1200 UTC, 17 June 0000 UTC, and 17 June 1200 UTC. The OUN soundings are from 17 June 1200 UTC, 18 June 0000 UTC, and 18 June 1200 UTC. Each of the soundings exhibit over 47 mm (1.85 in) of precipitable water

Chapter 4

Summary and Conclusions

The period spanning May - June 2015 yielded exceptional rainfall and flooding within the SGP along with significant impacts to water resources due to a flash pluvial event. During the analysis of the 2015 flash pluvial event, the two primary areas were investigated including (1) the statistical significance of the precipitation and (2) critical atmospheric variables and patterns present during the event.

4.1 Statistical Significance of the 2015 Flash Pluvial

The primary result of testing the significance of the 2015 flash pluvial event is the definition of flash pluvial that can be applied to similar sub seasonal precipitation events. This study examined many methods of testing the significance on a range of temporal scales from monthly to daily. In light of the results of this study as well as literature on defining pluvial months (Christian et al. 2015; Flanagan et al. 2018), this work confirms the objective and mathematical definition that on a sub seasonal time scale, regions in excess of 80% above normal precipitation can be classified as impacted by a flash pluvial. This definition reflects previous work and well depicts the main areas impacted in the 2015 flash pluvial.

The 2015 flash pluvial demonstrated statistical significance for multiple environmental anomalies across numerous temporal scales. On the subseasonal scale, each of the two week periods yielded positive precipitation anomalies exceeding 1 standard deviation. Additionally, the entire study period included a wide region of positive precipitation anomalies whereby on a daily scale, each of the 95th percentile events included subscale regions exceeding 4 standard deviations of precipitation, anomalous accumulation of rainfall, and dangerous, damaging flooding events. Examining the significance of a flash pluvial on a range of time scale to assess its development over time sets forth a method to examine

similar events in this manner. By examining a variety of time scales ranging from the two month period to individual dates, it is possible to discern the rapid intensification of this event throughout early May. By tracing the evolution of this event, it can be easier to discern the evolution of similar flash pluvial events.

The spatial scale of the event demonstrated significance across a broad region of the SGP along with localized areas. The entire SGP domain included 10 distinct events (days) at the 95th percentile and over two thirds of the 1.75^{o} x 2.25^{o} regions had more than seven days exceeding the 95th percentile. The regions investigated by this method that saw the most frequent significant precipitation days were largely those encompassed in the region with 80% above normal precipitation. The frequency of significant precipitation days in a region also appears to be a reliable indicator of a flash pluvial.

The significance of the event extended beyond the rainfall into the soil moisture which lasted beyond the event and yielded persistent, elevated soil moisture at the deeper levels. This soil moisture was steadily depleted after the end of the flash pluvial event because of a slow transition back into drought conditions, though it marks a period of replenishment of moisture. The consideration of conditions before and after a flash pluvial event such as the May-June 2015 case is important for determining the long term impacts of sub seasonal events on the region. By investigating the conditions preceding and following the event, this study contributes a case study of a significant period of precipitation that is not a portion of persisting, annual pluvial. The drought that impacts the SGP before and after the flash pluvial makes the event unlike many other cases, and makes it an important case to add to the literature on extreme precipitation.

Examination of the most significant precipitation dates as individual cases illustrated that many of the significant precipitation dates included measured precipitable water in excess of either the 90% moving average or daily maximum of precipitable water according to the SPC sounding climatology. Sounding observations also illustrated similar, near-saturated profiles with elongated skinny CAPE. While very moist atmospheric profiles can

be expected in the study of precipitation events, the PWAT measurements in each of the case studies was highly significant and often in excess of the 90% moving average, centered around each case.

Further, radar observations also yielded similar storm modes with MCSs and large squall lines crossing the domain. This is a well established feature of significant precipitation events and pluvials on multiple time scales (Fritsch et al. 1986; Anderson and Arritt 1998; Anderson and Arritt 2001; Ashley et al. 2003, Haberlie and Ashley 2019). This work confirms the presence of MCSs as significant in sub seasonal precipitation events such as flash pluvials. Because MCSs and squall lines can significantly impact the annual rainfall (Fritsch et al. 1986; Anderson and Arritt 1998; Anderson and Arritt 2001; Ashley et al. 2003, Haberlie and Ashley 2019) the case studies confirmed that these critical features were present for numerous days with extreme precipitation.

4.2 Flash Pluvial Drivers

Composite and wave event analysis demonstrated that the spring of 2015 was very synoptically active. This was measured both in wave events impacting the SGP and strength of the low geopotential height anomaly seen in both the full period and criteria composites in the mid troposphere. The high synoptic wave activity is a feature examined in past literature, but not at the sub seasonal time scale of the 2015 flash pluvial. The identification of synoptic wave events in conjunction with sub seasonal extreme precipitation should be further investigated, though when combined with anomalous moisture, appears to be a signature of flash pluvial events.

The composites also yielded a strong subtropical jet extending into the southwestern US and into Texas. The presence of the upper level low and exit region of the jet in proximity to the SGP contributed to dynamic synoptic forcing of the persistent precipitation events. The presence of a cold surface temperature anomaly in the vicinity of the SGP suggests that surface fronts and boundaries played a role in the initiation of convection and precipitation

during this flash pluvial event. Additionally, the composite analyses included significant positive water vapor anomalies due to moisture flux off the Gulf of Mexico. This atmospheric moisture was a critical ingredient in producing the convective storms that impacted the region. The sources of the anomalous atmospheric moisture included low-level water vapor flux and atmospheric rivers. While atmospheric rivers were present and transporting moisture from both the Gulf of Mexico and Pacific ocean, the composites of IVT over the full period and significant days indicate that the Gulf of Mexico water vapor more strongly impacted the SGP moisture. The contribution of the moisture from the Gulf of Mexico was one of the defining features of this event. In studies of other flash pluvial events, it is important to determine the source of moisture. By understanding where the moist air mass is coming from, efforts to predict these extreme precipitation events can be improved.

The final analysis focused on precipitation efficiency. Many of the cases exhibited local areas of very high precipitation efficiency. The nontropically forced days in May yielded precipitation efficiency values on the same order of magnitude as those present in TD Bill. In light of the known flash flooding consequences of high precipitation efficiency convective storms, it was likely that enhanced precipitation efficiency contributed to the excessive precipitation events and flash pluvial as a whole.

4.3 Suggested Future Work

Going forward, additional analyses should be performed to (1) determine and examine similar past flash pluvial events and (2) to build a robust dataset of events to determine consistent drivers needed for predictability. At this stage, many facets of these events have yet to be explored including overall length of impact into later months. For example, flash drought events can lead to prolonged periods of drought or be eradicated by precipitation. Similar analyses of additional flash pluvial events can quantify how they impact later precipitation events and overall water resources.

Within the 2015 flash pluvial alone, further analysis into the microphysical processes of the precipitation events would determine how they contributed to the event. Additionally, one particular case from this study that would merit a more in depth analysis is TD Bill in the vein of TC Erin from 2007 (Arndt et al. 2008). Further work should specifically address the causes of the extreme rainfall during TD Bill and investigate any interactions this may have had with earlier precipitation events and antecedent soil moisture.

Bibliography

Anderson, C. J., and R. W. Arritt, 1998: Mesoscale Convective Complexes and Persistent Elongated Convective Systems over the United States during 1992 and 1993. *Monthly Weather Review*, **126 (3)**, 578–599, doi:10.1175/1520-0493(1998)126⟨0578:MCCAPE⟩2.0.CO;2, URL https://doi.org/10.1175/1520-0493(1998)126{\%}3C0578:MCCAPE{\%}3E2.0.COhttp://0.0.0.2.

Anderson, C. J., and R. W. Arritt, 2001: Mesoscale Convective Systems over the United States during the 1997–98 El Niño. *Monthly Weather Review*, **129 (9)**, 2443–2457, doi:10.1175/1520-0493(2001)129⟨2443:MCSOTU⟩2.0.CO;2, URL https://doi.org/10.1175/1520-0493(2001)129{\%}3C2443:MCSOTU{\%}3E2.0.COhttp://0.0.0.2.

Arndt, D. S., J. B. Basara, R. A. McPherson, B. G. Illston, G. D. McManus, and D. B. Demko, 2009: Observations of the Overland Reintensification of Tropical Storm Erin (2007). *Bulletin of the American Meteorological Society*, **90 (8)**, 1079–1094, doi:10.1175/2009BAMS2644.1, URL https://doi.org/10.1175/2009BAMS2644.1.

Ashley, S. T., and W. S. Ashley, 2008: Flood Fatalities in the United States. *Journal of Applied Meteorology and Climatology*, **47 (3)**, 805–818, doi:10.1175/2007JAMC1611.1, URL https://doi.org/10.1175/2007JAMC1611.1.

Ashley, W. S., T. L. Mote, P. G. Dixon, S. L. Trotter, E. J. Powell, J. D. Durkee, and A. J. Grundstein, 2003: Distribution of Mesoscale Convective Complex Rainfall in the United States. *Monthly Weather Review*, **131 (12)**, 3003–3017, doi:10.1175/1520-0493(2003)131⟨3003:DOMCCR⟩2.0.CO;2, URL https://doi.org/10.1175/1520-0493(2003)131{\%}3C3003:DOMCCR{\%}3E2.0.CO2.

Black, T. L., 1988: *The step-mountain, eta coordinate regional model : a documentation*. National Meteorological Center, Development Division, [Washington, D.C.].

Bowman, K. P., and C. R. Homeyer, 2017: GridRad - Three-Dimensional Gridded NEXRAD WSR-88D Radar Data. Research Data Archive at the National Center for Atmospheric Research, Computational and Information Systems Laboratory, Boulder, CO, URL https://doi.org/10.5065/D6NK3CR7, doi:10.5065/D6NK3CR7.

Brock, F. V., K. C. Crawford, R. L. Elliott, G. W. Cuperus, S. J. Stadler, H. L. Johnson, and M. D. Eilts, 1994: The Oklahoma Mesonet: A Technical Overview. *Journal of Atmospheric and Oceanic Technology*, **12 (1)**, 5–19, doi:10.1175/1520-0426(1995)012⟨0005:TOMATO⟩2.0.CO;2, URL https://doi.org/10.1175/1520-0426(1995)012{\%}3C0005:TOMATO{\%}3E2.0.COhttp://0.0.0.2.

Caruthers, A. L., 2017: Land Use Land Cover Change Effects on Southern Great Plains Precipitation. M.s. thesis, University of Nebraska-Lincoln, 96 pp.

Castillo, V., A. A. Gómez-Plaza, and M. Martínez-Mena, 2003: *The Role of Antecedent Soil Water Content in the Runoff Response of Semiarid Catchments: A Simulation Approach*, Vol. 284. Elsevier, 114–130 pp., doi:10.1016/S0022-1694(03)00264-6.

Changnon, S. A., 2001: Thunderstorm Rainfall in the Conterminous United States. *Bulletin of the American Meteorological Society*, **82 (9)**, 1925–1940, doi:10.1175/1520-0477(2001)082⟨1925:TRITCU⟩2.3.CO;2, URL https://doi.org/10.1175/1520-0477(2001)082{\%}3C1925:TRITCU{\%}3E2.3.COhttp://0.0.0.2.

Christian, J., K. Christian, and J. B. Basara, 2015: Drought and Pluvial Dipole Events within the Great Plains of the United States. *Journal of Applied Meteorology and Climatology*, **54 (9)**, 1886–1898, doi:10.1175/JAMC-D-15-0002.1, URL https://doi.org/10.1175/JAMC-D-15-0002.1.

Cook, B. I., R. Seager, and R. L. Miller, 2011: On the Causes and Dynamics of the Early Twentieth-Century North American Pluvial. *Journal of Climate*, **24 (19)**, 5043–5060, doi:10.1175/2011JCLI4201.1, URL https://doi.org/10.1175/2011JCLI4201.1.

Daly, C., 2006: Guidelines for assessing the suitability of spatial climate data sets. *International Journal of Climatology*, **26 (6)**, 707–721, doi:10.1002/joc.1322, URL https://doi.org/10.1002/joc.1322.

Daly, C., R. P. Neilson, and D. L. Phillips, 1994: A Statistical-Topographic Model for Mapping Climatological Precipitation over Mountainous Terrain. *Journal of Applied Meteorology*, **33 (2)**, 140–158, doi:10.1175/1520-0450(1994)033⟨0140:ASTMFM⟩2.0.CO;2, URL https://doi.org/10.1175/1520-0450(1994)033{\%}3C0140:ASTMFM{\%}3E2.0.COhttp://0.0.0.2.

Dee, D. P., and Coauthors, 2011: The ERA-Interim reanalysis: configuration and performance of the data assimilation system. *Quarterly Journal of the Royal Meteorological Society*, **137 (656)**, 553–597, doi:10.1002/qj.828, URL https://doi.org/10.1002/qj.828.

Dirmeyer, P. A., C. A. Schlosser, and K. L. Brubaker, 2009: Precipitation, Recycling, and Land Memory: An Integrated Analysis. *Journal of Hydrometeorology*, **10 (1)**, 278–288, doi:10.1175/2008JHM1016.1, URL https://doi.org/10.1175/2008JHM1016.1.

Dong, X., and Coauthors, 2011: Investigation of the 2006 drought and 2007 flood extremes at the Southern Great Plains through an integrative analysis of observations. *Journal of Geophysical Research: Atmospheres*, **116 (D3)**, doi:10.1029/2010JD014776, URL https://doi.org/10.1029/2010JD014776.

Doswell, C. A., H. E. Brooks, and R. A. Maddox, 1996: Flash Flood Forecasting: An Ingredients-Based Methodology. *Weather and Forecasting*, **11 (4)**, 560–581, doi:10.1175/1520-0434(1996)011⟨0560:FFFAIB⟩2.0.CO;2, URL https://doi.org/10.1175/1520-0434(1996)011{\%}3C0560:FFFAIB{\%}3E2.0.COhttp://0.0.0.2.

Evans, C., R. S. Schumacher, and T. J. Galarneau, 2011: Sensitivity in the Overland Reintensification of Tropical Cyclone Erin (2007) to Near-Surface Soil Moisture Characteristics. *Monthly Weather Review*, **139 (12)**, 3848–3870, doi:10.1175/2011MWR3593.1, URL https://doi.org/10.1175/2011MWR3593.1.

Federal Interagency Floodplain Management Task Force, 1992: Floodplain Management in the United States: An Assessment Report. Tech. rep., Federal Emergency Management Agency, Washington, D.C. URL https://www.fema.gov/media-library-data/20130726-1440-20490-2293/fema17.pdf.

Findell, K. L., and T. L. Delworth, 2010: Impact of Common Sea Surface Temperature Anomalies on Global Drought and Pluvial Frequency. *Journal of Climate*, **23 (3)**, 485–503, doi:10.1175/2009JCLI3153.1, URL https://doi.org/10.1175/2009JCLI3153.1.

Flanagan, P. X., J. B. Basara, J. C. Furtado, E. R. Martin, and X. Xiao, 2019: Role of Pacific Sea Surface Temperatures in United States Great Plains Pluvial Years. *Journal of Climate*, to appear.

Flanagan, P. X., J. B. Basara, J. C. Furtado, and X. Xiao, 2018: Primary Atmospheric Drivers of Pluvial Years in the United States Great Plains. *Journal of Hydrometeorology*, **19 (4)**, 643–658, doi:10.1175/JHM-D-17-0148.1, URL https://doi.org/10.1175/JHM-D-17-0148.1.

French, J., and K. Holt, 1989: Floods. *The Public Health Consequences of Disasters.*, M. Gregg, Ed., U.S. Department of Health and Human Services, Atlanta, GA, 69–78.

Fritsch, J. M., R. J. Kane, and C. R. Chelius, 1986: The Contribution of Mesoscale Convective Weather Systems to the Warm-Season Precipitation in the United States. *Journal of Climate and Applied Meteorology*, **25 (10)**, 1333–1345, doi:10.1175/1520-0450(1986)025⟨1333:TCOMCW⟩2.0.CO;2, URL https://doi.org/10.1175/1520-0450(1986)025{\%}3C1333:TCOMCW{\%}3E2.0.COhttp://0.0.0.2.

Guan, B., and D. E. Waliser, 2015: Detection of atmospheric rivers: Evaluation and application of an algorithm for global studies. *Journal of Geophysical Research: Atmospheres*, **120 (24)**, 12 514–12 535, doi:10.1002/2015JD024257, URL https://doi.org/10.1002/2015JD024257.

Guan, B., D. E. Waliser, and F. M. Ralph, 2017: An Intercomparison between Reanalysis and Dropsonde Observations of the Total Water Vapor Transport in Individual Atmospheric Rivers. *Journal of Hydrometeorology*, **19 (2)**, 321–337, doi:10.1175/JHM-D-17-0114.1, URL https://doi.org/10.1175/JHM-D-17-0114.1.

Gutmann, M. P., G. D. Deane, N. Lauster, and A. Peri, 2005: Two Population-Environment Regimes in the Great Plains of the United States, 1930–1990. *Population and Environment*, **27 (2)**, 191–225, doi:10.1007/s11111-006-0016-3, URL https://doi.org/10.1007/s11111-006-0016-3.

Haberlie, A. M., and W. S. Ashley, 2018: A Radar-Based Climatology of Mesoscale Convective Systems in the United States. *Journal of Climate*, **32 (5)**, 1591–1606, doi:10.1175/JCLI-D-18-0559.1, URL https://doi.org/10.1175/JCLI-D-18-0559.1.

Higgins, R. W., Y. Yao, E. S. Yarosh, J. E. Janowiak, and K. C. Mo, 1997: Influence of the Great Plains Low-Level Jet on Summertime Precipitation and Moisture Transport over the Central United States. *Journal of Climate*, **10 (3)**, 481–507, doi:10.1175/1520-0442(1997)010⟨0481:IOTGPL⟩2.0.CO;2, URL https://doi.org/10.1175/1520-0442(1997)010{\%}3C0481:IOTGPL{\%}3E2.0.COhttp://0.0.0.2.

Houze Jr., R. A., 2004: Mesoscale convective systems. *Reviews of Geophysics*, **42 (4)**, doi:10.1029/2004RG000150, URL https://doi.org/10.1029/2004RG000150.

IPCC, 2013: Climate Change 2013: The Physical Science Basis. Contribution of Working Group I to the Fifth Assessment Report of the Intergovernmental Panel on Climate Change. Cambridge University Press, Cambridge, UK, 1535, doi:10.1017/CBO9781107415324.

Janjić, Z. I., 1994: The Step-Mountain Eta Coordinate Model: Further Developments of the Convection, Viscous Sublayer, and Turbulence Closure Schemes. *Monthly Weather Review*, **122 (5)**, 927–945, doi:10.1175/1520-0493(1994)122⟨0927:TSMECM⟩2.0.CO;2, URL https://doi.org/10.1175/1520-0493(1994)122{\%}3C0927:TSMECM{\%}3E2.0.COhttp://0.0.0.2.

Jessup, S. M., and A. T. DeGaetano, 2008: A Statistical Comparison of the Properties of Flash Flooding and Nonflooding Precipitation Events in Portions of New York and Pennsylvania. *Weather and Forecasting*, **23 (1)**, 114–130, doi:10.1175/2007WAF2006066.1, URL https://doi.org/10.1175/2007WAF2006066.1.

Karl, T. R., J. M. Melillo, and T. C. Peterson, Eds., 2009: *Global Climate Change Impacts in the United States*. Cambridge University Press, New York, NY.

Krishnamurthy, L., G. A. Vecchi, R. Msadek, A. Wittenberg, T. L. Delworth, and F. Zeng, 2015: The Seasonality of the Great Plains Low-Level Jet and ENSO Relationship. *Journal of Climate*, **28 (11)**, 4525–4544, doi:10.1175/JCLI-D-14-00590.1, URL https://doi.org/10.1175/JCLI-D-14-00590.1.

Lee, S.-K., B. E. Mapes, C. Wang, D. B. Enfield, and S. J. Weaver, 2014: Springtime ENSO phase evolution and its relation to rainfall in the continental U.S. *Geophysical Research Letters*, **41 (5)**, 1673–1680, doi:10.1002/2013GL059137, URL https://doi.org/10.1002/2013GL059137.

Lorente-Plazas, R., T. P. Mitchell, G. Mauger, and E. P. Salathé, 2018: Local Enhancement of Extreme Precipitation during Atmospheric Rivers as Simulated in a Regional Climate Model. *Journal of Hydrometeorology*, **19 (9)**, 1429–1446, doi:10.1175/JHM-D-17-0246.1, URL https://doi.org/10.1175/JHM-D-17-0246.1.

Market, P., S. Allen, R. Scofield, R. Kuligowski, and A. Gruber, 2003: Precipitation Efficiency of Warm-Season Midwestern Mesoscale Convective Systems. *Weather and Forecasting*, **18 (6)**, 1273–1285, doi:10.1175/1520-0434(2003)018⟨1273:PEOWMM⟩2.0.CO;2, URL https://doi.org/10.1175/1520-0434(2003)018{\%}3C1273:PEOWMM{\%}3E2.0.COhttp://0.0.0.2.

Martínez-Mena, M., J. Albaladejo, and V. M. Castillo, 1998: Factors influencing surface runoff generation in a Mediterranean semi-arid environment: Chicamo watershed, SE Spain. *Hydrological Processes*, **12 (5)**, 741–754, doi:10.1002/(SICI)1099-1085(19980430)12:5⟨741::AID-HYP622⟩3.0.CO;2-F, URL https://doi.org/10.1002/(SICI)1099-1085(19980430)12:5{\%}3C741::AID-HYP622{\%}3E3.0.COhttp://2-f.

McPherson, R. A., and Coauthors, 2007: Statewide Monitoring of the Mesoscale Environment: A Technical Update on the Oklahoma Mesonet. *Journal of Atmospheric and Oceanic Technology*, **24 (3)**, 301–321, doi:10.1175/JTECH1976.1, URL https://doi.org/10.1175/JTECH1976.1.

Meehl, G. A., and H. Teng, 2007: Multi-model changes in El Niño teleconnections over North America in a future warmer climate. *Climate Dynamics*, **29 (7)**, 779–790, doi:10.1007/s00382-007-0268-3, URL https://doi.org/10.1007/s00382-007-0268-3.

Mesinger, F., and Coauthors, 2006: North American Regional Reanalysis. *Bulletin of the American Meteorological Society*, **87 (3)**, 343–360, doi:10.1175/BAMS-87-3-343, URL https://doi.org/10.1175/BAMS-87-3-343.

Metropolis, N., and S. Ulam, 1949: The Monte Carlo Method. *Journal of the American Statistical Association*, **44 (247)**, 335–341, doi:10.1080/01621459.1949.10483310, URL https://www.tandfonline.com/doi/abs/10.1080/01621459.1949.10483310.

Nieto, R., and Coauthors, 2005: Climatological Features of Cutoff Low Systems in the Northern Hemisphere. *Journal of Climate*, **18 (16)**, 3085–3103, doi:10.1175/JCLI3386.1, URL https://doi.org/10.1175/JCLI3386.1.

NOAA National Centers for Environmental Information (NCEI), 2015: Billion-Dollar Weather and Climate Disasters. URL https://www.ncdc.noaa.gov/billions/events/US/2014-2016.

NOAA National Weather Service Analyze Forecast and Support Office, 2015: Natural Hazard Statistics. URL https://www.nws.noaa.gov/os/hazstats.shtml.

NWS, 2006: Definitions and general terminology. *National Weather Service Manual 10-950*, **10 (950)**, 4, URL http://www.nws.noaa.gov/directives/sym/pd01009050curr.pdf.

NWS, 2010: Operations and Services Upper Air Program NWSPD 10-14. *National Weather Service Manual 10-1401*, **10 (1401)**, URL https://www.nws.noaa.gov/directives/sym/pd01014001curr.pdf.

Otkin, J. A., M. Svoboda, E. D. Hunt, T. W. Ford, M. C. Anderson, C. Hain, and J. B. Basara, 2017: Flash Droughts: A Review and Assessment of the Challenges Imposed by Rapid-Onset Droughts in the United States. *Bulletin of the American Meteorological Society*, **99 (5)**, 911–919, doi:10.1175/BAMS-D-17-0149.1, URL https://doi.org/10.1175/BAMS-D-17-0149.1.

Pederson, N., A. R. Bell, E. R. Cook, U. Lall, N. Devineni, R. Seager, K. Eggleston, and K. P. Vranes, 2012: Is an Epic Pluvial Masking the Water Insecurity of the Greater New York City Region? *Journal of Climate*, **26 (4)**, 1339–1354, doi:10.1175/JCLI-D-11-00723.1, URL https://doi.org/10.1175/JCLI-D-11-00723.1.

Ralph, F. M., P. J. Neiman, and R. Rotunno, 2005: Dropsonde Observations in Low-Level Jets over the Northeastern Pacific Ocean from CALJET-1998 and PACJET-2001: Mean Vertical-Profile and Atmospheric-River Characteristics. *Monthly Weather Review*, **133 (4)**, 889–910, doi:10.1175/MWR2896.1, URL https://doi.org/10.1175/MWR2896.1.

Rauber, R. M., J. E. Walsh, and D. J. Charlevoix, 2005: *Severe and Hazardous Weather: An Introduction to High-Impact Meteorology*. Kendall Hunt Publishing Company.

Schubert, S. D., M. J. Suarez, P. J. Pegion, R. D. Koster, and J. T. Bacmeister, 2008: Potential Predictability of Long-Term Drought and Pluvial Conditions in the U.S. Great Plains. *Journal of Climate*, **21 (4)**, 802–816, doi:10.1175/2007JCLI1741.1, URL https://doi.org/10.1175/2007JCLI1741.1.

Seager, R., Y. Kushnir, C. Herweijer, N. Naik, and J. Velez, 2005: Modeling of Tropical Forcing of Persistent Droughts and Pluvials over Western North America: 1856–2000. *Journal of Climate*, **18 (19)**, 4065–4088, doi:10.1175/JCLI3522.1, URL https://doi.org/10.1175/JCLI3522.1.

Smith, J. A., M. L. Baeck, J. E. Morrison, and P. Sturdevant-Rees, 2000: Catastrophic Rainfall and Flooding in Texas. *Journal of Hydrometeorology*, **1 (1)**, 5–25, doi:10.1175/1525-7541(2000)001⟨0005:CRAFIT⟩2.0.CO;2, URL https://doi.org/10.1175/1525-7541(2000)001{\%}3C0005:CRAFIT{\%}3E2.0.COhttp://0.0.0.2.

Smith, J. A., M. L. Baeck, G. Villarini, D. B. Wright, and W. Krajewski, 2013: Extreme Flood Response: The June 2008 Flooding in Iowa. *Journal of Hydrometeorology*, **14 (6)**, 1810–1825, doi:10.1175/JHM-D-12-0191.1, URL https://doi.org/10.1175/JHM-D-12-0191.1.

Stevenson, S., B. Fox-Kemper, M. Jochum, R. Neale, C. Deser, and G. Meehl, 2011: Will There Be a Significant Change to El Niño in the Twenty-First Century? *Journal of Climate*, **25 (6)**, 2129–2145, doi:10.1175/JCLI-D-11-00252.1, URL https://doi.org/10.1175/JCLI-D-11-00252.1.

Storm Prediction Center, 2015: Storm Prediction Center Sounding Climatology. URL https://www.spc.noaa.gov/exper/soundingclimo.

Sui, C.-H., X. Li, and M.-J. Yang, 2007: On the Definition of Precipitation Efficiency. *Journal of the Atmospheric Sciences*, **64 (12)**, 4506–4513, doi:10.1175/2007JAS2332.1, URL https://doi.org/10.1175/2007JAS2332.1.

Sun, Q., C. Miao, Q. Duan, H. Ashouri, S. Sorooshian, and K.-L. Hsu, 2018: A Review of Global Precipitation Data Sets: Data Sources, Estimation, and Intercomparisons. *Reviews of Geophysics*, **56 (1)**, 79–107, doi:10.1002/2017RG000574, URL https://doi.org/10.1002/2017RG000574.

Svoboda, M., and Coauthors, 2002: The Drought Monitor. *Bulletin of the American Meteorological Society*, **83 (8)**, 1181–1190, doi:10.1175/1520-0477-83.8.1181, URL https://doi.org/10.1175/1520-0477-83.8.1181.

Szewrański, S., J. Chruściński, J. Kazak, M. Świąder, K. Tokarczyk-Dorociak, and R. Żmuda, 2018: Pluvial Flood Risk Assessment Tool (PFRA) for Rainwater Management and Adaptation to Climate Change in Newly Urbanised Areas. MDPI, doi:10.3390/w10040386.

Trenberth, K. E., and C. J. Guillemot, 1996: Physical Processes Involved in the 1988 Drought and 1993 Floods in North America. *Journal of Climate*, **9 (6)**, 1288–1298, doi:10.1175/1520-0442(1996)009⟨1288:PPIITD⟩2.0.CO;2, URL https://doi.org/10.1175/1520-0442(1996)009{\%}3C1288:PPIITD{\%}3E2.0.COhttp://0.0.0.2.

Wang, S.-Y., W.-R. Huang, H.-H. Hsu, and R. R. Gillies, 2015: Role of the strengthened El Niño teleconnection in the May 2015 floods over the southern Great Plains. *Geophysical Research Letters*, **42 (19)**, 8140–8146, doi:10.1002/2015GL065211, URL https://doi.org/10.1002/2015GL065211.

Weaver, S. J., S. Baxter, and K. Harnos, 2016: Regional Changes in the Interannual Variability of U.S. Warm Season Precipitation. *Journal of Climate*, **29 (14)**, 5157–5173, doi:10.1175/JCLI-D-14-00803.1, URL https://doi.org/10.1175/JCLI-D-14-00803.1.

Wilks, D. S., 2006: *Statistical Methods In The Atmospheric Sciences*, Vol. 59. Academic Press, 467 pp., doi:10.1016/S0074-6142(06)80036-7.

Yeh, S.-W., and Coauthors, 2018: ENSO Atmospheric Teleconnections and Their Response to Greenhouse Gas Forcing. *Reviews of Geophysics*, **56 (1)**, 185–206, doi:10.1002/2017RG000568, URL https://doi.org/10.1002/2017RG000568.

Zhao, S., Y. Deng, and R. X. Black, 2016: A Dynamical and Statistical Characterization of U.S. Extreme Precipitation Events and Their Associated Large-Scale Meteorological Patterns. *Journal of Climate*, **30 (4)**, 1307–1326, doi:10.1175/JCLI-D-15-0910.1, URL https://doi.org/10.1175/JCLI-D-15-0910.1.

Zhu, Y., and R. E. Newell, 1998: A Proposed Algorithm for Moisture Fluxes from Atmospheric Rivers. *Monthly Weather Review*, **126 (3)**, 725–735, doi:10.1175/1520-0493(1998)126⟨0725:APAFMF⟩2.0.CO;2, URL https://doi.org/10.1175/1520-0493(1998)126{\%}3C0725:APAFMF{\%}3E2.0.COhttp://0.0.0.2.